Synthetic Circuits for Multicellular Spatial Patterning

Thesis by
Sheng Wang

In Partial Fulfillment of the Requirements for the
Degree of
Doctor of Philosophy

CALIFORNIA INSTITUTE OF TECHNOLOGY
Pasadena, California

2023
Defended May 23, 2023

Sheng Wang
ORCID: 0000-0002-4070-7313

ACKNOWLEDGEMENTS

While this might be a mundane beginning, much like most biology PhDs, my fascination and reverence for the complexity of biology started at a very young age. At that time, most of the biological research I encountered mainly consisted of observation, recording, and analysis. However, even then, I had a subtle intuition that the study of life sciences would undoubtedly necessitate a greater inclusion of mathematics and physics.

Therefore, when I first read the work conducted by my advisor, Michael Elowitz, I was profoundly captivated. The quantitative approach of synthetic biology research resonated completely with my vision for the future of biological studies.

What left me deeply impressed was his way of thinking during scientific discussions. He seemed to possess a magical ability to abstract inspiring ideas, seeing deeper insights within simple data and conclusions. Engaging in discussions with him was intellectually stimulating as he could discern patterns amidst the chaos, simplicity within complexity, and new perspectives when seemingly at an impasse.

Beyond the realm of science, what has truly amazed me over the years is his character. Michael is a kind and supportive mentor, sometimes so excellent that his praises appear inflated. Given that he never has negative comments, if he says "great" less than three times during a project discussion, it would imply that the results are average. However, I later realized that it was his absolute encouragement and tolerance that filled the lab with the most audacious ideas and fearless attempts. His emotional support and encouragement, more than just his academic guidance, helped me navigate through each difficult moment smoothly.

He provided immense support but never interfered excessively. The real-world academic environment is still more towards results-driven, but he created a utopia that encourages free exploration and learning from mistakes. It allowed us to focus on our research and enjoy ample support, free exploration, and a friendly environment. This made it possible for me to devote myself to an unknown and challenging research direction for a long time.

Another aspect of Michael that I admire is his passion for research. For him, being a professor is not merely a professional requirement but a lifestyle filled with enjoyment and dedication.

I also would like to extend my sincere gratitude to our collaborator Jordi Garcia-Ojalvo, who provided a wealth of guidance on the project, from the initial exploration of ideas to the final polishing of the paper. His countless hours and efforts are greatly appreciated. He, along with my advisor Michael, always seemed to be on the same wavelength, radiating positivity.

I would also like to express my gratitude to Pulin Li, who guided me when I first joined the lab. At that time, I did not have a specific preference for a particular project. During the rotation period, coincidentally, I worked with her on the study of synthetic multicellular spatial patterning with Sonic Hedgehog. Actually, the subsequent research on Turing patterns was inspired by this work. Since we have studied the positional information model with one morphogen, and then I was thinking about how to build a more complex system, and eventually, I turned my attention to the research of Turing patterns. Pulin is patient, methodical, and well-planned. She patiently guided me from basic experimental techniques to data analysis. During the years I worked with her, I felt significant growth.

I wish to express my appreciation to my research committee: Lea Goentoro, Markus Meister, and Richard Murray, for their guidance and support throughout my Ph.D. training. Their expertise and feedback were invaluable in shaping my research projects. I am grateful for this committee I chose.

My thanks also go to the summer students, rotation students, and junior graduate student I have worked with: Chibuikem Nwizu, Jerry Wang, Li-ang Yao, Yutian Li, Yunqing Wang, and Rongrong Du. Through our interactions, I have gained more experience in leading projects and collaborative work, and I've been exposed to a variety of research styles and life experiences that showed me the diverse possibilities of this field. I am thankful for their hard work and contribution, even if many explorations were later proven unfeasible.

I am grateful to my lab mates over the years, who not only offered selfless and sincere help, but also enriched my graduate life with colorful experiences and beautiful memories. Whenever I felt bored, I would seek out Mark, who could always bring interesting topics and laughter. When I needed some quiet time, I would sit at my station next to Kirsten, her presence providing a calming yet unintrusive companionship.

I especially want to thank the people who manage the lab: Jo Leonardo, James Linton, and Leah Santat. Innovation can often bring about chaos, but they magi-

cally maintained order in the lab while keeping it dynamic and innovative. I also appreciate the almighty James and Leah for their various assistance in the lab. Their generosity and professionalism have made "go find James or Leah" my subconscious choice when I feel helpless.

I am thankful for the friends that have appeared in my life over these years. Ronghui Zhu, as my roommate and lab colleague, with whom I have spent most of the hours of the day within twenty feet of distance for more than three years, I deeply appreciate all academic and life discussions and interactions with him. Also, Yitong Ma, who is meticulous in everything he does, and Xiaozhe Ding, who is careful and safe in all his undertakings, I am grateful for the time we spent together. There are simply too many friends to name individually. If I tried, this acknowledgment would be longer than the main text (given the time I've spent here). I am grateful for their companionship. They have given me the most important memories at Caltech, in the beautiful city of Pasadena, and on the leisurely sunny West Coast.

I want to thank my family: my father, Xianguang Wang, my mother, Guanghong Wang, and all my extended family members. My parents have subtly influenced me, imbuing me with an interest in exploration and a belief that the pursuit of life should not be solely materialistic. I want to thank my grandmother, who is already 86 years old this year but still loves to travel. Her positive attitude towards life has eased my worries about aging, showing me that age and mentality are not strongly correlated. I am grateful for the support and encouragement of my joyful family, which allows me to freely enjoy my graduate years, except for some weekends when they are having a barbecue and sharing photos while I am conducting my experiments on the other side of the earth.

Lastly, I want to express my gratitude to my cat, Ban Wang, who has kept me company since the Covid-19 pandemic. She often lounges in front of me, showing off the irregular patterns on her fur, which often inspires my spatial patterning research and also reminds me to get back to work.

ABSTRACT

Self-organized spatial periodic patterning mechanisms are responsible for the generation of repetitive structures, such as digits, vertebrae, and teeth, during multicellular development. Adopting a synthetic biology approach, we aim to unravel the core principles of multicellular spatial patterning by designing and reconstituting it in tissue-cultured cell lines.

The reaction-diffusion mechanism, as an established paradigm, has successfully elucidated and forecasted pattern formation across varying scales and species. However, the potential for reconstituting synthetic reaction-diffusion patterns using unconventional reaction-diffusion elements within mammalian cell cultures has been insufficiently explored, thus leaving a gap in our comprehension of how spatial periodic patterns could be generated.

The simplest reaction-diffusion systems are thought to necessitate a minimum of two morphogens to generate periodic patterns. In contrast, with the help of mathematical modeling, we illustrate that a simpler circuit, comprising only a single diffusible morphogen, can adequately produce long-range, spatially periodic patterns. These patterns propagate outward from transient initiating perturbations and remain stable after the disturbance is removed. Moreover, introducing an additional bistable intracellular feedback or operation on a growing cell lattice can enhance the robustness of the patterning against noise.

Concurrently, we reconstruct the Turing pattern in mammalian cell culture utilizing a bottom-up approach. We construct a synthetic circuit based on BMP4 and Activin signaling pathways in HEK293 cells. After validation of each circuit component, we exhibit the spatial pattern formation driven by a synthetic reaction-diffusion circuit within the mammalian cell line. This adaptable circuit facilitates us to adjust circuit parameters or implement various boundary conditions, thereby revealing the impact of these alterations on patterning dynamics.

Collectively, these findings lay the groundwork for the engineering of pattern formation in the nascent field of synthetic developmental biology.

PUBLISHED CONTENT AND CONTRIBUTIONS

Wang, Sheng, Jordi Garcia-Ojalvo, and Michael B Elowitz (Dec. 2022). "Periodic spatial patterning with a single morphogen." en. In: *Cell Syst* 13.12, 1033–1047.e7. DOI: 10.1016/J.CELS.2022.11.001.

S.W. participated in the conception of the project, solved and analyzed equations, prepared data, and wrote the manuscript.

Li, Pulin et al. (May 2018). "Morphogen gradient reconstitution reveals Hedgehog pathway design principles." en. In: *Science* 360.6388, pp. 543–548. DOI: 10.1126/science.aao0645.

S.W. participated in the conception of the project, conducted the experiments, and prepared data.

TABLE OF CONTENTS

LIST OF FIGURES

LIST OF TABLES

Chapter 1

INTRODUCTION

1.1 Spatial patterning in biology

Spatial patterning is a fundamental phenomenon in biology that involves the organization and distribution of biological structures and processes across various spatial scales. This can range from the subcellular level, such as the distribution of specific proteins or complexes within a cell, to the tissue and organism level, like the arrangement of distinct cell types within an embryo, and even to the community and ecosystem level, where organisms are distributed within a habitat.

These patterns are crucial for the proper functioning and organization of living systems, and disruptions in these patterns can lead to developmental defects (Ahmed et al., 2017; Subasioglu et al., 2015), disease (Muragaki et al., 1996; Quinonez and Innis, 2014), or ecological imbalance (Turner, 1989; Chen, Chi, and J. Li, 2020). Grasping the core principles and foundational logic of spatial patterning allows us to better understand, manipulate, and innovate various biological processes.

One fascinating example is the multicellular self-organized spatial patterning. This remarkable property emerges exclusively in multicellular systems that extend beyond a single cell, encompassing multicellular organisms or populations of single-cell organisms that coexist and function collectively. Multicellular organisms rely on self-organized spatial patterning to regulate development, tissue organization, and cellular coordination (Xavier da Silveira Dos Santos and Liberali, 2019; Wedlich-Söldner and Betz, 2018). In the case of populations of single-cell organisms, such as bacteria or yeast, self-organized spatial patterning can manifest as cooperative behavior, allowing the population to function as a whole. This may involve the formation of biofilms and the establishment of distinct microenvironments (Nunan et al., 2003; Ren et al., 2018).

This self-organization depends on the individual cell's ability to spatially send and receive signals, accurately interpret and respond differentially to these signals, and dynamically adapt to changes in their interactions with other cells (Xavier da Silveira Dos Santos and Liberali, 2019; Wedlich-Söldner and Betz, 2018). In practice, cells frequently communicate through various means, such as mechanical forces (Gordon et al., 2015; Chien, S. Li, and Shyy, 1998), secretion of signaling molecules (Briscoe

and Thérond, 2013; Rahman et al., 2015), or electrical signaling (Magee et al., 1998; Fromm and Lautner, 2007).

Delving deeper into its applications, one of the most prominent examples of self-organized spatial patterning in multicellular organisms is embryogenesis. This complex and highly dynamic process involves cells guided by intrinsic instructions, such as gene regulatory networks and extrinsic signals from neighboring cells. These signals play a critical role in directing proper spatial patterning, cell differentiation, and ultimately the formation of functional tissues and organs. Some key mechanisms underlying spatial patterning during development include the positional information mechanism (French flag model) (Wolpert, 1971) and reaction-diffusion systems (Turing patterns) (Turing, 1952).

1.2 Positional information mechanism

The positional information mechanism, often referred to as the French flag model, is a fundamental concept in developmental biology that explains how cells in a developing organism acquire their specific identities based on their positions within the tissue (Wolpert, 1971). This mechanism falls under the sender-receiver paradigm, which involves the exchange of signals between cells to drive coordinated developmental processes.

In this model, morphogens (signaling molecules) are secreted by sender cells and diffuse through the extracellular space or extracellular matrix, creating a concentration gradient across an extended region. Receiver cells detect the morphogen signal and interpret it in a dose-dependent manner, meaning that the cell's response to the signal is determined by the morphogen concentration it experiences. Based on specific morphogen concentration thresholds, cells will adopt distinct fates depending on their proximity to the sender cells. This process allows cells to generate spatial patterns based on their relative distance from the signal source.

While the positional information mechanism is effective for patterning tissues with a limited number of domains, it is less suited for generating multiple domains or spatial periodic patterns. There are several reasons for this limitation:

1. Additional concentration thresholds: Generating multiple cell fates requires the establishment of multiple concentration thresholds, which can be challenging to achieve when the difference between two thresholds is close to the biological

noise of the system. This can make it difficult for cells to reliably interpret the morphogen concentration and adopt the correct fate.

2. Increased complexity with additional morphogen species: Another strategy to pattern multiple domains is to incorporate more morphogen species that operate independently or cooperatively. However, this can dramatically increase the complexity of the system, making it more challenging to decipher the interactions and interdependencies between various morphogens and their effects on cell fate determination.

3. Despite these limitations, the positional information mechanism has been a foundational concept in understanding how cells acquire their spatial identities during development. Researchers continue to investigate the intricacies of this mechanism and explore alternative strategies for generating complex spatial patterns in developing tissues, including the use of reaction-diffusion systems and other self-organizing processes.

1.3 Reaction-diffusion mechanism

The reaction-diffusion mechanism is another self-organizing process that leads to the formation of patterns, particularly spatial periodic patterns (which can hardly achieve with the positional information mechanism), in various biological and chemical systems. In 1952, Alan Turing, a pioneering mathematician and computer scientist, proposed a simple mathematical model to explain the emergence of these patterns from a homogeneous tissue using only two diffusive signal molecules, or morphogens (Turing, 1952). This groundbreaking model laid the foundation for further understanding of pattern formation in developmental biology, chemistry, and other fields.

In Turing's model, there are two interacting morphogens: an activator and a repressor. The activator promotes the production of both itself and the repressor, while the repressor inhibits the production of both. The key to pattern formation in this model is that the repressor morphogen diffuses more rapidly than the activator. Within specific parameter ranges, this system can spontaneously form spatial patterns, which are now commonly referred to as "Turing patterns".

Following Turing's original work, researchers have expanded and refined the concept of the reaction-diffusion mechanism in several ways. These advancements include:

1. Incorporating more types of reaction kinetics: This has led to the develop-

ment of more complex and nuanced models that better represent the diverse array of interactions observed in biological and chemical systems (Gierer and Meinhardt, 1972; Schnakenberg, 1979).

2. Increasing the number of circuit components: By considering additional molecular species or cellular components, researchers have been able to model more intricate patterns and gain insights into the mechanisms driving the formation of these patterns (Scholes et al., 2019; Marcon et al., 2016).

3. Exploring various boundary conditions and initial conditions: By analyzing different spatial constraints and initial configurations, scientists have understood how these factors influence pattern formation and predict the resulting patterns under various circumstances (Cross and Hohenberg, 1993; Ben-Jacob et al., 1985).

These expansions and refinements of the reaction-diffusion mechanism have enabled a deeper understanding of how patterns form in nature and have led to practical applications in areas such as tissue engineering, material science, and the study of ecological systems. As a result, the reaction-diffusion mechanism has become a fundamental concept in the study of self-organization and pattern formation across multiple scientific disciplines.

Specifically, developmental biologists have used the concept of reaction-diffusion mechanisms to explain a variety of biological observations in living organisms. This theory posits that the patterning of tissues and organs during development is determined by the interplay between two opposing forces: the reaction of chemical signals that drive differentiation and the diffusion of those signals that spread their influence.

One of the most notable examples of reaction-diffusion mechanisms in action can be seen in the development of feather buds in birds (Jung et al., 1998). As the feathers begin to emerge, BMP4 and FDF4 are produced and diffuse outwards, guiding the growth and patterning of the feathers. This process is thought to be regulated by a series of genes that are activated or suppressed based on the concentration of the chemical signals.

Another example can be found in the branching of the lungs and kidneys (Warburton et al., 2000; Costantini and Kopan, 2010; Little, Combes, and Takasato, 2016). During embryonic development, these organs grow by a process known as branching

morphogenesis, where the organ bud splits and divides into smaller branches. This process is thought to be regulated by the interplay between chemical signals that promote branching and those that inhibit it.

Finally, the formation of digits and teeth can also be explained by reaction-diffusion mechanisms (Raspopovic et al., 2014; Kavanagh, Evans, and Jernvall, 2007). In these cases, chemical signals are produced in specific regions of the developing limb or jaw, and as they diffuse, they guide the differentiation and patterning of the developing tissue. The result is the formation of distinct digits or teeth, each with its own unique shape and size.

In conclusion, reaction-diffusion mechanisms are believed to play a crucial role in the development of a wide range of structures and organs, from animals to plants. However, due to the intrinsic defect of studying patterning in situ, no matter how detailed the model is proposed, these practices still have limitations in conclusively establishing the sufficiency of the underlying patterning circuit. Then, a bottom-up "build to understand" approach becomes necessary to answer this sufficiency question.

1.4 The bottom-up approach of synthetic biology

Synthetic biology is an interdisciplinary field that combines elements of biology, engineering, and computer science with the goal of designing and constructing novel biological systems, functions, and organisms. The primary goals of synthetic biology include understanding the fundamental principles of life, improving existing biological systems, and creating new applications that can address a wide range of challenges in areas such as medicine, agriculture, and environmental sustainability.

Synthetic biology, with its bottom-up approach of designing and constructing novel biological functions, systems, and organisms using well-characterized modules and basic elements, offers a unique perspective in the field of biology that resembles the engineering approach and provides several advantages over traditional biological study methodologies, including the following:

1. Isolated background: By designing and building biological systems from scratch or by modifying existing systems, synthetic biology allows researchers to study the components and interactions of a system in a controlled and isolated environment. This reduces the complexity of the system and minimizes interference from external factors, making it easier to determine the specific

roles and functions of individual components. This in turn facilitates a better understanding of the underlying biological mechanisms and principles.

2. Tunability: Synthetic biology enables researchers to precisely control the properties and behaviors of the biological systems they create. By altering specific components, such as genes or proteins, it is possible to modulate the expression levels, activities, or interactions within the system. This tunability allows scientists to explore a wide range of conditions and parameters, helping them to identify the optimal conditions for achieving a desired outcome, such as maximizing the production of a specific compound or minimizing the energy required for a particular process.

1.5 Multicellular synthetic biology and synthetic patterning

In the past 20 years, synthetic biology has started from designing, rewiring, and *de novo* constructing circuits intracellularly, including gene regulatory circuits and protein-based circuits (Elowitz and Leibler, 2000; Gardner, Cantor, and Collins, 2000; Gao et al., 2018; Moraga et al., 2017). Exploiting the capabilities of multicellular organization has the potential to significantly expand the functional capabilities of synthetic biology, enabling it to perform tasks that are challenging to accomplish within a single cell. This includes the ability to reproduce complex spatial-temporal dynamics observed during development. In this process, cell proliferation, migration, and differentiation are orchestrated through mutual signaling between cells and their local environment, resulting in a self-organized structure. Moreover, the phenomena observed at the multicellular level, such as self-organization, cannot be fully understood or predicted by examining the functions of individual cells in isolation. This suggests that the emergent properties of multicellular organization are more than just the sum of their parts. Consequently, the study and design of synthetic multicellular circuits are crucial in comprehending how organisms execute these complex tasks.

By advancing our understanding and ability to design synthetic multicellular systems, we will be able to harness and potentially replicate many of the processes and functions that are characteristic of multicellular organisms. This knowledge and these tools could open up new possibilities in a range of fields, from bioengineering to medicine. In application, synthetic organs will be the solution to the daily increasing shortage of organ donors and all side-effects of transplantation. With decades of effects, researchers have been able to generate almost all the types

of cells of the human body. Meanwhile, how to spatially organize multiple cells types in a designed manner still remains challenging. The ability to control spatial organization via designed and implemented circuits appears to be the most intuitive goal.

Meanwhile, synthetic patterning is still a young field with few studies and largely unsolved questions and challenges. In prior studies, investigators endeavored to construct circuits that direct spatial patterning via positional information mechanisms. The synthetic Shh system builds an isolated platform allowing researchers to study how morphogen modification and receptor feedback affect Shh signaling (P. Li et al., 2018). In Li's work, they build an Shh secretion cell line and an SHH reporter cell line. With spatial co-culture experiments, they are able to observe Shh secreted from senders forming a concentration gradient in the receiver region. The synNotch system was developed by designing a synthetic Notch-like receptor, which involved exchanging the extracellular recognition domain with the intracellular signaling domain (Morsut et al., 2016; Toda et al., 2018). Employing a Notch-like cell-cell interaction mechanism, the synNotch patterning circuit enables cells to communicate with and impact their immediate neighboring cells, resulting in the formation of well-ordered cellular fate layers.

Meanwhile, self-organized patterning via reaction-diffusion mechanism has been reported in both bacteria and mammalian systems (Karig et al., 2018; Sekine, Shibata, and Ebisuya, 2018). David Karig et al. worked with *E.coli* to reconstitute periodic patterns by using two quorum-sensing molecules as "morphogens" for the pattern formation on the growing biofilm (Karig et al., 2018). By wiring Nodal and Lefty natural signaling pathway to the Turing circuit in HEK293 cell culture, Ryoji Sekine et al. observed the dynamic of heterogeneity emerging and spatial pattern forming (Sekine, Shibata, and Ebisuya, 2018). However, the reaction-diffusion circuit in this work is based on two morphogens that have been reported working in pairs and creating Turing patterns in nature. The core reaction kinetics in their synthetic circuit is still the natural interactions where Nodal and Lefty compete for receptors. Thus, no experimental attempts have been made to advance this concept "self-organized patterning via reaction-diffusion mechanism" further, by constructing a synthetic reaction-diffusion circuit featuring two morphogens not previously documented within the same natural reaction-diffusion system.

1.6 Our research goal and strategy

Our objective is to employ a synthetic biology approach, combining mathematical modeling and experimental reconstitution techniques, to elucidate the core principles underlying reaction-diffusion-mediated spatial patterning in multicellular systems. By integrating computational simulations with experimental validation, we seek to gain a comprehensive understanding of the mechanisms that drive the formation of spatial patterns through reaction-diffusion processes, ultimately leading to the coordinated organization of multicellular structures.

Through the application of mathematical models, we will explore diverse circuit designs and a wide range of parameters that may influence pattern formation, not limited by the natural systems. These models will help us identify key factors that govern the emergence of distinct spatial patterns and generate testable hypotheses for experimental validation.

In parallel, we will perform experimental reconstitution, where we will reconstitute the reaction-diffusion systems in engineered cellular systems. This approach will enable us to manipulate and control individual components involved in patterning, allowing us to test the predictions generated by our mathematical models directly. By systematically altering specific factors and observing the resulting changes in pattern formation, we can gain valuable insights into the underlying principles of reaction-diffusion-mediated spatial patterning.

Ultimately, this integrated synthetic biology approach will enhance our understanding of the complex interplay between reaction-diffusion processes and multicellular spatial patterning, providing a solid foundation for future synthetic biology research and potential therapeutic applications in tissue engineering and regenerative medicine.

In Chapter 2, I will introduce our theoretical work on spatial periodic patterning using a single-morphogen reaction-diffusion circuit. We demonstrated that a reaction-diffusion circuit with only one diffusive component could generate regular spatial periodic patterns in a discrete system when given a spatially localized perturbation as the initial trigger. Additionally, we proposed two strategies to address the noise-sensitive issue in pattern formation and ensure regular pattern generation in a noisy environment.

In Chapter 3, I will present our experimental efforts to reconstitute the classical Turing pattern in mammalian cell culture. We interconnected two natural signaling

pathways, which have not been reported to function together in a natural reaction-diffusion system, to construct a synthetic reaction-diffusion circuit in wild-type HEK293 cell lines. We verified the diffusion coefficients of both morphogens, the orthogonality of the signaling pathways, and the functionality of each arm of our designed circuit. Ultimately, we demonstrated the pattern formation dynamics and the transformation of final patterns in response to adjustments in circuit parameters and various boundary conditions.

References

Ahmed, Humayun et al. (Nov. 2017). "Genetic Overview of Syndactyly and Polydactyly." en. In: *Plast Reconstr Surg Glob Open* 5.11, e1549.

Ben-Jacob, E et al. (Mar. 1985). "Pattern propagation in nonlinear dissipative systems." In: *Physica D* 14.3, pp. 348–364.

Briscoe, James and Pascal P Thérond (July 2013). "The mechanisms of Hedgehog signalling and its roles in development and disease." en. In: *Nat. Rev. Mol. Cell Biol.* 14.7, pp. 416–429.

Chen, Wanxu, Guangqing Chi, and Jiangfeng Li (Jan. 2020). "The spatial aspect of ecosystem services balance and its determinants." In: *Land use policy* 90, p. 104263.

Chien, S, S Li, and Y J Shyy (Jan. 1998). "Effects of mechanical forces on signal transduction and gene expression in endothelial cells." en. In: *Hypertension* 31.1 Pt 2, pp. 162–169.

Costantini, Frank and Raphael Kopan (May 2010). "Patterning a complex organ: branching morphogenesis and nephron segmentation in kidney development." en. In: *Dev. Cell* 18.5, pp. 698–712.

Cross, M C and P C Hohenberg (July 1993). "Pattern formation outside of equilibrium." In: *Rev. Mod. Phys.* 65.3, pp. 851–1112.

Elowitz, M B and S Leibler (Jan. 2000). "A synthetic oscillatory network of transcriptional regulators." en. In: *Nature* 403.6767, pp. 335–338.

Fromm, Jörg and Silke Lautner (Mar. 2007). "Electrical signals and their physiological significance in plants." en. In: *Plant Cell Environ.* 30.3, pp. 249–257.

Gao, Xiaojing J et al. (Sept. 2018). "Programmable protein circuits in living cells." en. In: *Science* 361.6408, pp. 1252–1258.

Gardner, T S, C R Cantor, and J J Collins (Jan. 2000). "Construction of a genetic toggle switch in Escherichia coli." en. In: *Nature* 403.6767, pp. 339–342.

Gierer, A and H Meinhardt (Dec. 1972). "A theory of biological pattern formation." en. In: *Kybernetik* 12.1, pp. 30–39.

Gordon, Wendy R et al. (June 2015). "Mechanical Allostery: Evidence for a Force Requirement in the Proteolytic Activation of Notch." en. In: *Dev. Cell* 33.6, pp. 729–736.

Jung, H S et al. (Apr. 1998). "Local inhibitory action of BMPs and their relationships with activators in feather formation: implications for periodic patterning." en. In: *Dev. Biol.* 196.1, pp. 11–23.

Karig, David et al. (June 2018). "Stochastic Turing patterns in a synthetic bacterial population." en. In: *Proc. Natl. Acad. Sci. U. S. A.* 115.26, pp. 6572–6577.

Kavanagh, Kathryn D, Alistair R Evans, and Jukka Jernvall (Sept. 2007). "Predicting evolutionary patterns of mammalian teeth from development." en. In: *Nature* 449.7161, pp. 427–432.

Li, Pulin et al. (May 2018). "Morphogen gradient reconstitution reveals Hedgehog pathway design principles." en. In: *Science* 360.6388, pp. 543–548. DOI: 10.1126/science.aao0645.

Little, Melissa H, Alexander N Combes, and Minoru Takasato (Oct. 2016). "Understanding kidney morphogenesis to guide renal tissue regeneration." en. In: *Nat. Rev. Nephrol.* 12.10, pp. 624–635.

Magee, J et al. (1998). "Electrical and calcium signaling in dendrites of hippocampal pyramidal neurons." en. In: *Annu. Rev. Physiol.* 60, pp. 327–346.

Marcon, Luciano et al. (Apr. 2016). "High-throughput mathematical analysis identifies Turing networks for patterning with equally diffusing signals." en. In: *Elife* 5.

Moraga, Ignacio et al. (May 2017). "Synthekines are surrogate cytokine and growth factor agonists that compel signaling through non-natural receptor dimers." en. In: *Elife* 6.

Morsut, Leonardo et al. (Feb. 2016). "Engineering Customized Cell Sensing and Response Behaviors Using Synthetic Notch Receptors." en. In: *Cell* 164.4, pp. 780–791.

Muragaki, Y et al. (Apr. 1996). "Altered growth and branching patterns in synpolydactyly caused by mutations in HOXD13." en. In: *Science* 272.5261, pp. 548–551.

Nunan, Naoise et al. (May 2003). "Spatial distribution of bacterial communities and their relationships with the micro-architecture of soil." en. In: *FEMS Microbiol. Ecol.* 44.2, pp. 203–215.

Quinonez, Shane C and Jeffrey W Innis (Jan. 2014). "Human HOX gene disorders." en. In: *Mol. Genet. Metab.* 111.1, pp. 4–15.

Rahman, Md Shaifur et al. (Apr. 2015). "TGF-β/BMP signaling and other molecular events: regulation of osteoblastogenesis and bone formation." en. In: *Bone Res* 3, p. 15005.

Raspopovic, J et al. (Aug. 2014). "Modeling digits. Digit patterning is controlled by a Bmp-Sox9-Wnt Turing network modulated by morphogen gradients." en. In: *Science* 345.6196, pp. 566–570.

Ren, Yijin et al. (May 2018). "Emergent heterogeneous microenvironments in biofilms: substratum surface heterogeneity and bacterial adhesion force-sensing." en. In: *FEMS Microbiol. Rev.* 42.3, pp. 259–272.

Schnakenberg, J (Dec. 1979). "Simple chemical reaction systems with limit cycle behaviour." en. In: *J. Theor. Biol.* 81.3, pp. 389–400.

Scholes, Natalie S et al. (Sept. 2019). “A Comprehensive Network Atlas Reveals That Turing Patterns Are Common but Not Robust.” en. In: *Cell Syst* 9.3, 243–257.e4.

Sekine, Ryoji, Tatsuo Shibata, and Miki Ebisuya (Dec. 2018). “Synthetic mammalian pattern formation driven by differential diffusivity of Nodal and Lefty.” en. In: *Nat. Commun.* 9.1, p. 5456.

Subasioglu, Aslı et al. (2015). “Genetic background of supernumerary teeth.” en. In: *Eur. J. Dent.* 9.1, pp. 153–158.

Toda, Satoshi et al. (July 2018). “Programming self-organizing multicellular structures with synthetic cell-cell signaling.” en. In: *Science*.

Turing, Alan Mathison (Aug. 1952). “The chemical basis of morphogenesis.” In: *Philos. Trans. R. Soc. Lond. B Biol. Sci.* 237.641, pp. 37–72.

Turner, Monica Goigel (Nov. 1989). “Landscape Ecology: The Effect of Pattern on Process.” In: *Annu. Rev. Ecol. Syst.* 20.1, pp. 171–197.

Warburton, D et al. (Mar. 2000). “The molecular basis of lung morphogenesis.” en. In: *Mech. Dev.* 92.1, pp. 55–81.

Wedlich-Söldner, Roland and Timo Betz (May 2018). “Self-organization: the fundament of cell biology.” en. In: *Philos. Trans. R. Soc. Lond. B Biol. Sci.* 373.1747.

Wolpert, L (1971). “Positional information and pattern formation.” en. In: *Curr. Top. Dev. Biol.* 6.6, pp. 183–224.

Xavier da Silveira Dos Santos, Aline and Prisca Liberali (Apr. 2019). “From single cells to tissue self-organization.” en. In: *FEBS J.* 286.8, pp. 1495–1513.

Chapter 2

PERIODIC SPATIAL PATTERNING WITH A SINGLE MORPHOGEN

2.1 Abstract

During multicellular development, periodic spatial patterning systems generate repetitive structures such as digits, vertebrae, and teeth. Turing patterning provides a foundational paradigm for understanding such systems. The simplest Turing systems are believed to require at least two morphogens to generate periodic patterns. Here, using mathematical modeling, we show that a simpler circuit, including only a single diffusible morphogen, is sufficient to generate long-range, spatially periodic patterns that propagate outward from transient initiating perturbations and remain stable after the perturbation is removed. Further, an additional bistable intracellular feedback or operation on a growing cell lattice can make the single-morphogen patterning robust to noise. Together, these results show that a single morphogen can be sufficient for robust spatial pattern formation, and should provide a foundation for engineering pattern formation in the emerging field of synthetic developmental biology.

2.2 Introduction

The fundamental question of how periodic spatial patterns emerge in multicellular organisms arises both in the context of natural developmental systems and in the emerging field of synthetic development, where researchers seek to engineer biological circuits that recapitulate fundamental aspects of multicellular development (Davies, 2008; Toda et al., 2018; Ebrahimkhani and Ebisuya, 2019). Understanding the minimal requirements to generate spatial patterning could provide insight into natural patterning processes, and offer a basis for engineering synthetic patterning circuits with minimal complexity.

Previous work has focused on three general paradigms for spatial periodicity (Schweisguth and Corson, 2019). First, studies of early embryonic development in *Drosophila* unveiled a far-reaching scenario for patterning based on positional information and hierarchical morphogen gradients (Briscoe and Small, 2015; Wieschaus, 2016). Second, at the other extreme, classic Turing patterning systems use interactions between two morphogens to spontaneously generate periodic spatial patterns (Kondo

and Miura, 2010). Finally, short-range alternating patterns can be produced by lateral inhibition mechanisms in which neighboring cells establish opposite fates through direct signalings, like those implemented by the Notch pathway (Collier et al., 1996; Sprinzak et al., 2011; Corson et al., 2017). While powerful, these three mechanisms may not, individually, be ideal for all purposes or may be more complex than necessary. For example, positional information-based mechanisms do not readily scale to pattern an arbitrarily extended region (Ben-Zvi, Shilo, and Barkai, 2011), potentially limiting their evolvability. In turn, classic Turing mechanisms require multiple morphogens and fine-tuning of key parameters (Marcon et al., 2016; Scholes et al., 2019), adding complexity for synthetic applications.

Finally, lateral inhibition patterns generally operate at small spatial length scales, comparable to that of the individual cell (Cohen et al., 2010; Hadjivasiliou, Hunter, and Baum, 2016). Natural systems undoubtedly combine these and other mechanisms to achieve more complex pattern formation capabilities (Green and Sharpe, 2015).

In natural contexts, periodic patterns are generated by a combination of 1) reaction-diffusion circuits operating within the developing tissue and 2) triggering signals that emerge from tissue boundaries. For example, digit patterning in the developing limb bud is set off by signals coming from the apical epidermal ridge (Raspopovic et al., 2014). Similarly, tooth patterning is thought to involve sequential activation of new primary enamel knots, through a mechanism that may involve both local morphogen dynamics and inputs from adjacent tissue (Kavanagh, Evans, and Jernvall, 2007). Feather patterning appears to similarly combine these mechanisms (Kavanagh, Evans, and Jernvall, 2007; W. K. W. Ho et al., 2019). These examples provoke the question of what minimal circuits are sufficient for periodic boundary-triggered patterning.

An ideal pattern-forming system would have several key characteristics: First, it should be triggered by signals from a localized adjacent region or boundary, to enable control of patterning. Second, the pattern would spatially propagate to fill an extended region of tissue. Third, to enable synthetic engineering, the system should be as simple as possible, utilizing a minimal number of components and interactions. The ideal system should further be robust to unavoidable fluctuations in cellular components.

Here, we introduce a remarkably simple mechanism for boundary-triggered spatial periodic patterns that uses a single morphogen. This architecture differs from

classical Turing systems in that the activator is confined to the cell in which it is synthesized, and cannot diffuse to other cells. It thus represents the limit of a classic Turing system when the mobility of the activator approaches 0. Unlike Turing systems, this circuit cannot, by itself, spontaneously produce consistent, well-defined long-wavelength patterns. However, when stimulated by an adjacent signal from a localized region, or boundary, it can produce spatially propagating periodic patterns in the levels of its components that self-sustain even after the initiating signal is removed. This single morphogen mechanism demonstrates how complex spatio-temporal patterns can arise from remarkably simple underlying circuit mechanisms, and provides a realistic design for synthetic developmental patterning systems.

2.3 A single morphogen is sufficient to form patterns on the spatial discrete lattice

Alan Turing's patterning circuit in his 1952 paper is one of the mathematically simplest models that can form patterns through diffusion-driven instability (Turing, 1952). The Turing circuit comprises two components that regulate their own production and/or degradation, and diffuse as morphogens (Figure 2.1A, upper left panel). Patterning occurs when the inhibitory morphogen has a larger diffusion coefficient than the activating morphogen, causing local activation and long-range inhibition (Figure 2.1A, left row) (Murray, 2001).

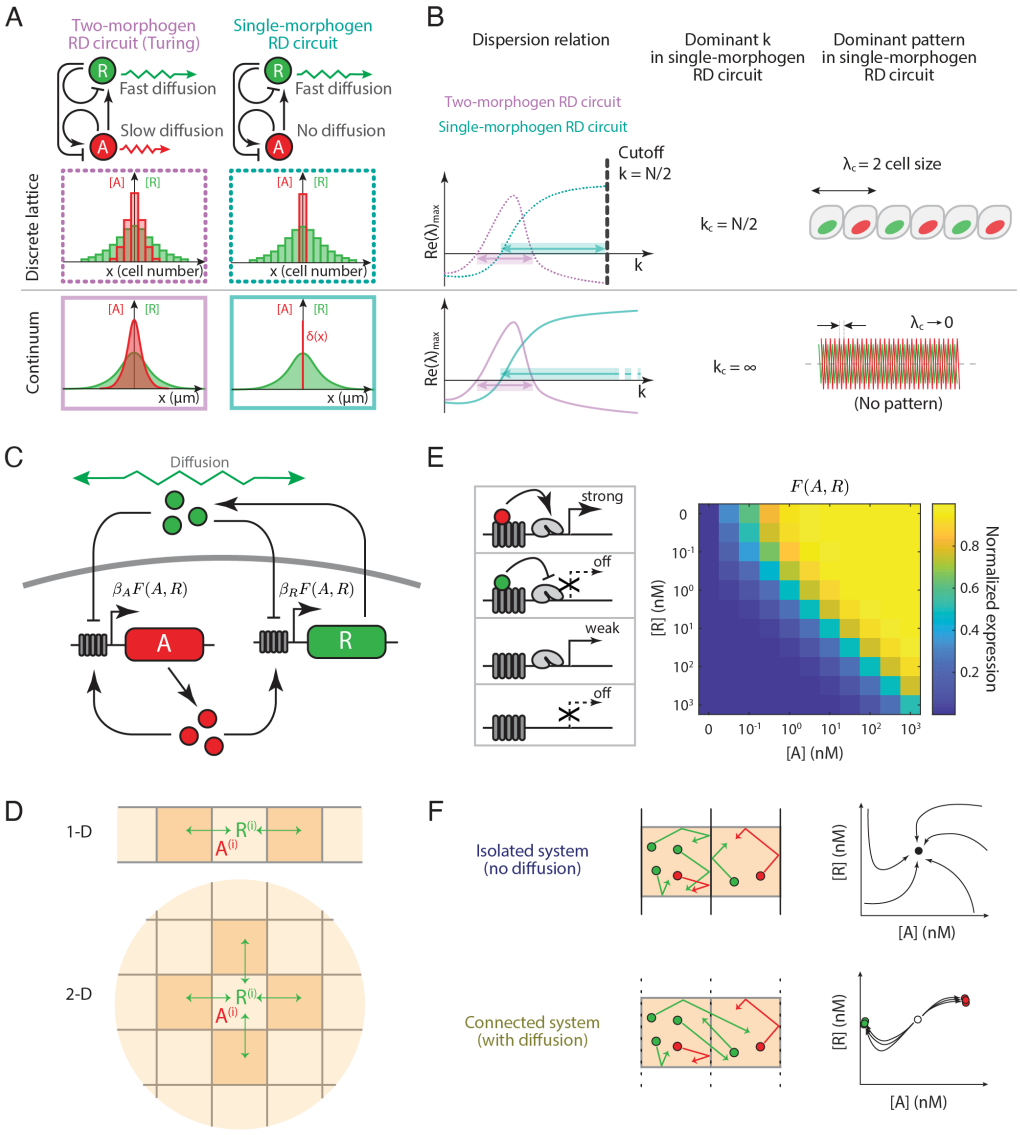

Figure 2.1: The lattice ODE simulation of a minimal single-morphogen reaction-diffusion circuit evaluates the pattern formation mechanism in discrete space.

(A) The single-morphogen reaction-diffusion circuit obeys the "local activation with long-range inhibition (LALI)" rule on the discrete lattice. Classical Turing circuit requires at least two diffusive species, while in the single-morphogen reaction-diffusion circuit, the repressor is the only component that could diffuse among the cells. In specific parameter regimes, the classical Turing mechanism could form patterns on both continuum and discrete lattice, though the power frequency selection is different in these two cases (Plahte, 2001). The patterning on discrete lattice provides the activator with at least two-cell size spatial period.

(B) The shortest wavelength on the discrete lattice determines the upper bound of the wavenumber for the single-morphogen reaction-diffusion circuit. Stability analysis reveals that once the single-morphogen reaction-diffusion circuit drives the patterning, the dominated wavenumber of the final pattern goes to infinity. This type of pattern, named "Type II Turing pattern" (Scholes et al., 2019), is purely a mathematical concept with no actual pattern in the physical world. Meanwhile, patterns on the discrete lattice intrinsically have the shortest wavelength as two-cell size, which sets a cutoff for wavenumbers and enables the reaction-diffusion patterning with a single morphogen.

(C) The minimal single-morphogen reaction-diffusion circuit contains two components driven by the same promoter, a non-diffusive activator upregulating both production and a diffusive repressor downregulating the production.

(D) The simulation executes on a chain (1-D) or a square lattice (2-D), where each lattice node directly contacts two or four neighboring nodes, respectively. The isolated system forbids diffusion of R among cells so that each lattice node is well separated. Meanwhile, the connect system allows free diffusion of R. i denotes the cell counts number in the lattice.

(E) The promoter integrates the upregulation from A and the downregulation from R in a ratiometric fashion. The model assumes four possible promoter binding states, polymerase + activator, polymerase + repressor, polymerase only, and empty cassette. The portion of the four states shaped by the A and R concentrations determines the promoter activity $F(A, R)$. The calculated titration matrix reveals that the promoter activity has a ratiometric relation of co-existing A and R.

(F) The simulation starts from the homogeneous state and ends up with stable patterns. In the isolated system where no diffusion is allowed among cells,

the lattice stays at its homogeneous steady-state. In the connected system, if a circuit is patternable, this steady-state should become unstable so that cells would bifurcate and evolve into heterogeneous patterns. Meanwhile, a non-patternable circuit is still stable under the connected system.

Since there is no lower bound for the diffusion coefficient of the activating morphogen, we wondered whether the system could support pattern formation in the limit of no activator diffusion at all, i.e. if the activator were confined to a single cell rather than diffusing as a morphogen. In continuous systems, the limit of no activator diffusion does not pattern due to the unbounded spectrum of high-frequency modes (Figure 2.1A, lower right panel). However, on a discrete lattice, cells expressing the non-diffusive activator exhibit local (same-cell) activation, while inhibiting cells in their extended neighborhood (Figure 2.1A, upper right panel). In this case, self-activation occurs on the scale of a single cell, providing a high-frequency cutoff (Figure 2.1B, upper left panel).

To understand whether such a discrete system could form robust patterns and, if so, what characteristics these patterns might have, we performed linear stability analysis of both discrete and continuous single-morphogen systems (Murray, 2001). We analytically computed the spatially homogeneous steady state of the system, and analyzed its stability to harmonic perturbations with varying wavenumber k (inversely related to the wavelength λ of the spatial perturbation, $k = 2\pi/\lambda$). To that end, we determined the eigenvalues of the system's Jacobian, focusing on the one with the largest real part, which we call the "dominant eigenvalue" in what follows. The dependence of the real part of the dominant eigenvalue on the wavenumber k is known as the dispersion relation (Murray, 2001). In a classic two-morphogen Turing system, the real part of the dominant eigenvalue takes on a maximum value at an intermediate wavenumber (Figure 2.1B, left panels, purple lines). By contrast, in a single-morphogen system, the resulting dispersion relation increases monotonically with increasing k (decreasing spatial period), as shown by the blue lines in the left panels of Figure 2.1B (Methods: Analytical study of the single-morphogen reaction-diffusion circuit in the continuum limit). This monotonic increase suggests that the resulting pattern should be dominated by perturbations with arbitrarily large spatial frequencies. In the continuous limit, this situation leads to physiologically unreasonable patterns, which involve infinitely small wavelengths (Figure 2.1B, lower right panel). However, a discrete lattice imposes a cutoff at a wavelength of two cell diameters (Figure 2.1B, upper left panel), and can thereby

support patterns involving alternating cell states (Figure 2.1B, upper right panel, Methods: Stability analysis of the single-morphogen reaction-diffusion circuit in a discrete lattice). Thus, a single-morphogen circuit that would not pattern in the continuous limit, could produce "fine-grain" alternating patterns on a lattice, similar to lateral inhibition patterns (Collier et al., 1996). Further, as we will see below, certain conditions, including particular initial perturbations, can further expand the spectrum of patterning behaviors to include longer wavelength patterns.

To gain more insight into particular realizations of single-morphogen reaction-diffusion systems, we considered a minimal, two-component regulatory system that could be constructed synthetically in a living cell using known genes and regulatory sequences (Figure 2.1C). In this system, an intracellular transcriptional activator denoted A, promotes its own production and that of a repressor, denoted R. The repressor, but not the activator, is assumed to be secreted and can diffuse from one cell to another to down-regulate production of both A and R in both its own cell and neighboring cells. In practice, this repressor could represent a composite of a diffusible morphogenetic protein and an intracellular transcriptional repressor that it activates through signaling (see Discussion). To simulate dynamics on a discrete cell lattice, we used ordinary differential equations (ODEs) to represent the dynamics within each cell, allowing R molecules to transfer from one cell to its neighbors (Figure 2.1D). With these assumptions, we obtain the following equations for the dynamics of the single-morphogen system on a discrete lattice:

$$\frac{\partial A_i}{\partial t} = \beta_A F(A_i, R_i) - \gamma_A A_i \tag{2.1}$$

$$\frac{\partial R_i}{\partial t} = \beta_R F(A_i, R_i) - \gamma_R R_i + D \sum_{j \in]i[}^{j} (R_j - R_i) \tag{2.2}$$

Here, β_A and β_R denote the maximal production rate of the activator and the repressor, respectively. γ_A and γ_R denote effective protein degradation and loss rates. D denotes the diffusion coefficient of the repressor. $]i[$ denotes the set of cells that directly contact cell i. Finally, to mathematically represent combinatorial regulation by the activator and repressor, we assume that the two regulators compete to bind to the same target DNA binding site, a relatively simple type of interaction that can be synthetically engineered (Phillips et al., 2012; Zhu et al., 2022). This results in the following dependence of target promoter activity on A and R concentration

(Figure 2.1E):

$$F(A,R) = \frac{(\frac{A}{K_A})^h + \kappa}{(\frac{A}{K_A})^h + (\frac{R}{K_R})^h + 1 + \kappa} \tag{2.3}$$

Here, κ quantifies the basal expression in the absence of activator and repressor, κ_A and κ_R respectively represent the concentrations required for half-maximal activation and repression, and h is a Hill coefficient that quantifies the ultrasensitivity of the response to either regulator. This production function $F(A, R)$ is assumed to affect the expression of both A and R.

We note that the alternative Gierer–Meinhardt reaction-diffusion kinetics (Meinhardt and Gierer, 1974), which is widely applied to model biological patterning formation, leads to similar results, albeit with additional patterning features (Figure 2.7, Methods: Patterning with Gierer–Meinhardt kinetics). Furthermore, systems with additional components or time delays are also compatible with this single-morphogen reaction-diffusion mechanism (Figure 2.9, Methods: Models with additional components or time delays).

A typical reaction-diffusion simulation starts from a homogeneous initial condition in which all cells are at the same value, equal to the steady-state for the case of no diffusion, D = 0 (Figure 2.1F, left), perturbed by small spatial fluctuations. As time progresses, diffusion can, under some circumstances, destabilize the spatially homogeneous initial state, leading to patterning. The simulation continues until the concentration profiles of all cells reach new steady-state values (Figure 2.1F, right).

We estimated model parameters (Methods: Parameter estimation, Parametric robustness analysis, Figure 2.10) and simulated the model on a square two-dimensional lattice, starting with a low level of random noise in the initial state (Figure 2.2A, Movie S1, Methods: Lattice ODE simulation). Concentrations of activator and repressor began diverging in different cells, eventually reaching two distinct states with high and low concentrations of A (Figure 2.2A). Spatially, these states formed a disordered "salt and pepper" pattern, with a wavelength of about 2 cell diameters, as expected from the dispersion relation (Figures 2.1B, 2.2B). Autocorrelation analysis showed that the diffusion coefficient defines the length scale of the final pattern (Figure 2.2C, Methods: Final stable pattern auto-correlation). In the low diffusion regime, the circuit generates checkerboard-like patterns (Figure 2.2C, upper two panels), while high diffusion rates produce irregular, low wavenumber patches of elevated A expression (Figure 2.2C, lower two panels). Further frequency power spectrum analysis confirmed the two regimes corresponding to the checkerboard-

like pattern and less regular patch pattern (Figure 2.2D). Together, these results show that the discrete single-morphogen system can spontaneously pattern with a diffusion-dependent wavelength.

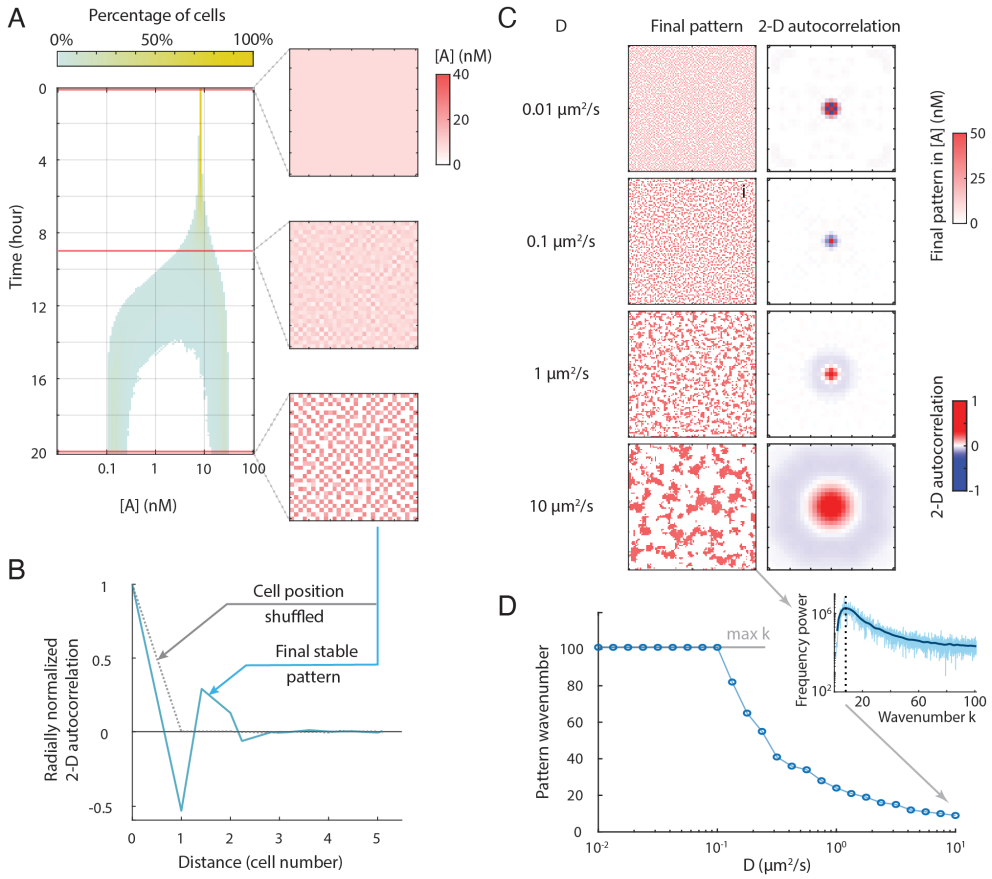

Figure 2.2: The single-morphogen reaction-diffusion circuit develops lateral inhibition patterns with global random noise as initial conditions.

(A) The identical lattice cells bifurcate during the simulation forming two distinct classes. The histogram of cell count percentage based on the activator concentration captures the dynamics of the bifurcation. The lattice system finally converges to a "salt and pepper" pattern.

(B) The final heterogeneous pattern is spatially autocorrelated. The blue curve presents the radially averaged 2-D autocorrelation of the final frame. The negative value at one cell distance reveals the lateral inhibition effect. As the control, random shuffling cell positions of the final pattern lose the spatial correlation (red curve).

(C) The diffusion coefficient of the repressor alters the range of the lateral inhibition zone. If the repressor diffuses slowly, the lateral inhibition intensively represses the adjacent cells. Meanwhile, with a large D, the adjacent neighbors show a positive correlation, and farther neighboring cells are repressed. Panels on the left show simulation results in a 100 x 100 zoom-in view of the original 200 x 200 lattice. The right panels show an origin-centered 31 x 31 submatrix of the 2D autocorrelation function. Autocorrelation values at long distances are close to zero, indicating that long-distance correlation is weak in this type of pattern.

(D) The wavenumber of the final pattern shows two types of dependence on the diffusion coefficient. Lower diffusion coefficients produce checkerboard patterns with wavenumber at the spatial frequency cutoff corresponding to two cell diameters. In the high diffusion regime, however, the final wavenumber decreases when the diffusion coefficient increases. The pattern wavenumber is defined as the spatial frequency with the highest power, as calculated from the spatial power spectrum (structure function), obtained from the Fourier transform of the 2-D autocorrelation function.

2.4 The single-morphogen reaction-diffusion circuit can generate stable, long-wavelength periodic patterns

Given the large range of wavenumbers for which the dispersion relation is positive, one could expect patterns with low wavenumbers to be stable, as long as they fall within the above-mentioned range of positive dispersion relation. We thus asked whether initial conditions could stabilize particular low wavenumber modes, and thereby establish well-defined spatial patterns. To that end, we first investigated the effect of point and line morphogen sources (Figure 2.3A, left). We simulated the same system (Figure 2.2A) as above, but transiently increased the concentration of

R to a higher value either in a single cell or a line of cells. These perturbations generated, respectively, either concentric rings or periodic lines of elevated activator expression (Figure 2.3A, right). The patterns exhibited several key features: First, they formed sequentially, as a front dynamically propagates away from the perturbation at a constant velocity, as shown in Figure 2.3B (orange arrow) and Movie S2 for the case of the line source (limitations on pattern propagation are discussed below). Second, in the final pattern, A and R exhibit in-phase periodic spatial oscillations (Figure 2.3C), as expected given that they are co-regulated by the same inputs (Figure 2.1C). Third, in contrast to standard Turing patterns in which spots of high activator concentration tend to rearrange to maximize distances from neighboring peaks, in this case, peak morphogen positions remained fixed throughout patterning (Figure 2.3B). Finally, once triggered, the dynamic patterning process is self-sustaining and continues to propagate even if the initiating perturbation is transient (Figure 2.3B, purple arrow).

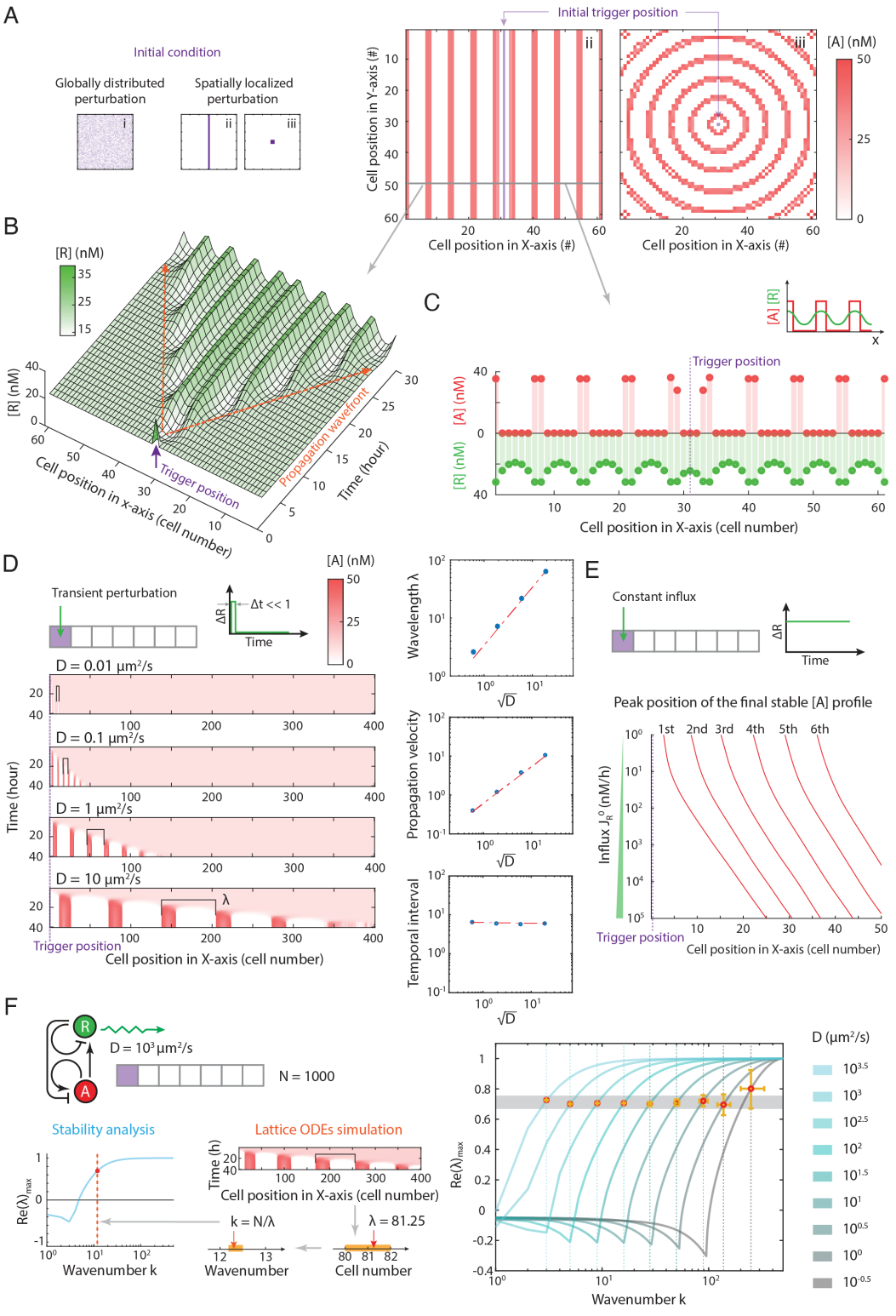

Figure 2.3: Spatially localized perturbation triggers low-wavenumber periodic patterns with the propagative dynamics.

(A) Spatially localized perturbation as initial condition provokes low-wavenumber regular patterns. The global noise triggers synchronized high-wavenumber patterns. Meanwhile, the perturbing at one cell or a line of cells would promote stripes patterns and circle patterns, respectively. The final wavenumber of stable patterns is notably lower than the ones of patterns triggered by global noise.

(B) This low-wavenumber pattern forms in a propagative fashion from the perturbation position. A uniform speed traveling wavefront provokes a series of low-wavenumber stripes to form with uniform time intervals. The established patterns stay unchanged in both position and amplitude.

(C) The concentration of the activator and the repressor in the final pattern stay in phase. The activator concentration profile behaves close to a binary style, while the repressor profile is more smooth and moderate.

(D) The diffusion coefficient determines the pattern wavelength. A lower diffusion coefficient produces shorter wavelength patterns. The pattern wavelength measured from simulations with various diffusion coefficients is proportional to the square root of the corresponding diffusion coefficient.

(E) The intensity of the constant repressor influx alters the phase of pattern stripes. The constant influx of repressors at the trigger position also induces propagative pattern formation. Increasing the influx level enlarges the distance from the trigger point to the first stripe. Meanwhile, the wavelength stays consistent.

(F) The dominated wavenumber measured from the final pattern is consistently lower than the wavenumber preference from stability analysis. The evaluation repeated with various D indicates the actual patterning dynamics do not choose the one with the highest tendency but the one with 70% of the maximum, which locates at the edge of the plateau reading from the dispersion relation curve. The orange region shows the error bar from the measurement.

All of these features can occur with a variety of perturbations, including reducing R, or increasing or decreasing A (Figure 2.8). Even perturbations whose amplitude is small compared to the initial state concentrations can be sufficient to generate the patterns in a deterministic setting (Figure 2.8). Similar results were also obtained on a hexagonal lattice (Figure 2.11A, Methods: Patterning on the hexagonal lattice and the rod-shaped lattice) or with anisotropic unit cells (Figure 2.11B,C). Analogous

patterns also form in three-dimensional systems (Figure 2.11D, Methods: Patterning in three-dimensional lattice). Together, these results indicate that transient spatially structured perturbations can initiate stable, periodic, long-wavelength patterns.

One of the most important features of patterns is their spatial periodicity. In our simulations, the wavelength of the single-morphogen pattern exhibited a square-root dependence on the diffusion coefficient, D, with larger diffusion coefficients producing larger intervals between adjacent stripes (Figure 2.3D, Methods: Pattern wavelength determination). This relationship can be understood from a dimensional argument: D, with units of $\mu m^2/s$, is the only parameter in the system whose dimensions include length. The velocity of pattern propagation is proportional to the square root of D for the same reason (Figure 2.3D, Methods: Pattern propagation speed determination). By contrast, the temporal interval between the formation of adjacent stripes is independent of D (Figure 2.3D).

In a biological context, the pattern-establishing perturbations could be generated by a group of "source" cells that produce the morphogen constitutively, as occurs with the sonic hedgehog morphogen in the developing neural tube (Dessaud, McMahon, and Briscoe, 2008; Alaynick, Jessell, and Pfaff, 2011; Briscoe and Small, 2015). To understand how these source cells impact patterning, we simulated the system with a constant influx of morphogen at a defined position (Figure 2.3E). Higher morphogen levels suppress the expression of A in correspondingly larger regions around the source, effectively pushing out the position at which periodic patterning begins (Figure 2.3E). When morphogen influx is stopped after patterning is established, the existing patterned region expands inward, effectively "filling in" the proximal spatial region without affecting the established phase (Figure 2.8B). Thus, morphogen production rates from source cells determine the phase of the final pattern, without affecting its period (Figure 2.3E). Taken together, these results indicate that a single-morphogen reaction-diffusion system, triggered by a spatially localized perturbation, can generate stable periodic patterns whose wavelength and phase can be controlled.

More generally, from the point of view of mode selection (Cross and Hohenberg, 1993), these dynamics suggest that transient perturbations can selectively amplify modes with intermediate wavenumbers despite the monotonically increasing dispersion relation, as shown in a simplified one-dimensional example (Figure 2.3F). This contrasts with the classic stationary-pattern formation scenario, in which the dispersion curve is only positive for intermediate wavenumbers (Figure 2.1B left, purple lines). In that case, the final wavenumber of the emerging pattern results from

the competition between the linear instability, the nonlinear terms, and the boundary conditions (Dee and Langer, 1983; Ben-Jacob et al., 1985; Murray, 2001). In our case, simulations revealed that the wavenumber of the spatial pattern corresponded to a dominant eigenvalue whose real part is about 70% of its maximum value (Figure 2.3F, right panel, gray shaded line).

2.5 Spontaneous single-morphogen pattern formation is sensitive to noise

We next asked if single-morphogen pattern formation is sensitive to stochastic fluctuations (noise) in circuit components (Kilfoil, Lasko, and Abouheif, 2009; Eldar and Elowitz, 2010) (Figure 2.4A). To quantify this sensitivity and understand how it impacts patterning, we considered a version of the circuit that could be implemented synthetically, in which A and R are co-expressed from a single promoter (e.g. using an internal ribosome entry site (IRES) or 2A ribosomal skip sequence). In this configuration, the expression of the two genes can fluctuate due to noise, in a largely correlated manner due to their co-transcriptional expression. We therefore assumed that the dominant source of the noise was extrinsic, comprising both static variation as well as dynamic, correlated variability in the expression of the two genes (Elowitz et al., 2002; Thattai and Oudenaarden, 2002; Raser and O'Shea, 2005). More specifically, we modeled expression noise using an Ornstein–Uhlenbeck process (Fox et al., 1988; Gillespie, 1996; Rohlfs, Harrigan, and Nielsen, 2013), which describes fluctuations with a standard deviation over time of σ, a standard deviation of mean expression across cells of η, and an autocorrelation time for fluctuations of τ (Figure 2.4B). These fluctuations are encapsulated in the random function $H(i,t)$, where i denotes the cell index, and t denotes time, to produce a modified set of circuit equations:

$$\frac{\partial A_i}{\partial t} = \beta_A^0 H(i,t) F(A_i, R_i) - \gamma_A A_i \tag{2.4}$$

$$\frac{\partial R_i}{\partial t} = \beta_R^0 H(i,t) F(A_i, R_i) - \gamma_R R_i + D \sum_{j \in]i[}^{j} (R_j - R_i) \tag{2.5}$$

Here, $H(i,t)$, the random time series for an individual cell, exhibits a normal distribution with mean $m_i =< H(i,t) >_t$ and variance σ^2. Mean expression levels are assumed to be normally distributed with mean 1 and variance η^2. The timescale of fluctuations, τ, is taken to be about 10 hours, comparable to the mRNA half-life, which sets a natural timescale for fluctuations.

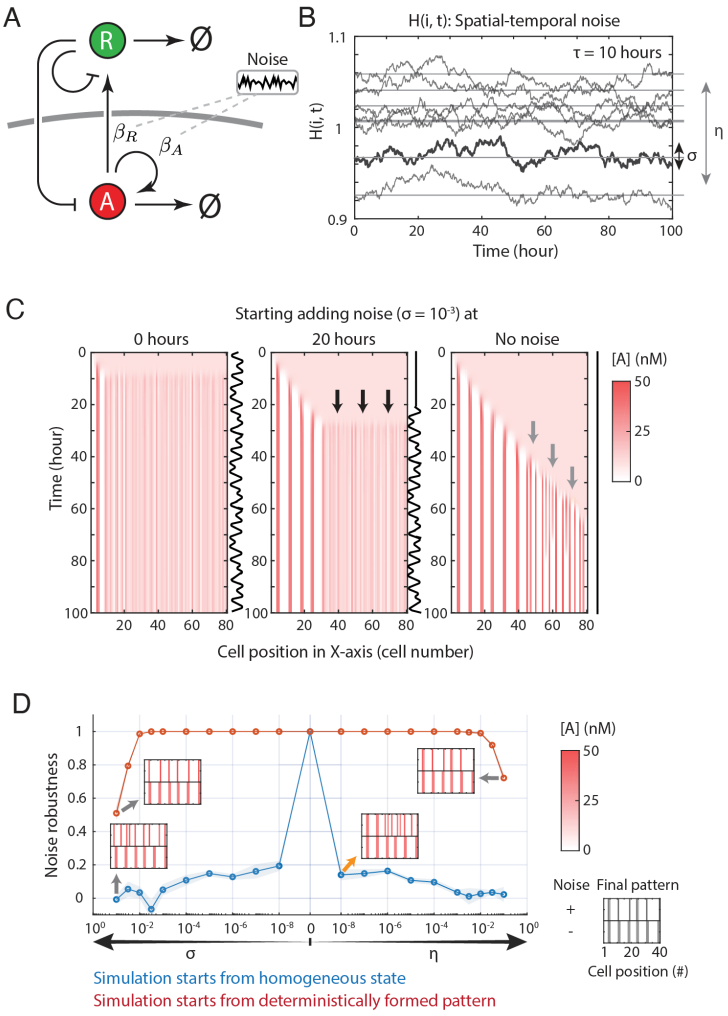

Figure 2.4: The propagation pattern is sensitive to noise during the formation process and is robust to noise once the pattern is established.

(A) The simulation of pattern formation in noisy conditions introduces noise in the production rate of both species. The noise in the simulation recapitulates the fluctuation in protein production in general.

(B) The dynamic noise represents the temporal fluctuation in a particular cell. Meanwhile, the static noise describes the heterogeneity among the cell population. The standard deviation quantifies the noise intensity, denoting σ and η, for the temporal dynamic noise and the static heterogeneity, respectively.

(C) The final pattern is sensitive to the timing of introducing noise. The simulations take place on a 1x100 lattice with reflective boundary conditions and transient perturbation on the left end. At time 0 hours or 20 hours, σ = 0.001 level of noise starts to add to the simulation. The kymograph shows the pattern formation dynamics averaging from 20 repeated simulations. The introduced noise causes cells far from the perturbation center to bifurcate, generating "salt and pepper" patterns and causing propagation failure (black arrows in middle panel). Note that even without introduced noise, there is some pattern regularity loss due to numerical errors in the simulation (gray arrows in right panel).

(D) The minimal single-morphogen reaction-diffusion circuit is sensitive to noise only during pattern formation. The spatial correlation of two final patterns with and without noise reveals the influence of noise and further indicates the circuit robustness to the noise. The simulations starting from the homogeneous state capture the pattern forming dynamics. Meanwhile, simulations with an established pattern as the initial condition reveal the pattern sustaining stage. During the patterning, the robustness score drops vastly even with a trace level of noise (orange arrow). The established pattern shows high robustness even with intensive noise.

In the presence of the noise sources described above, our simulations show that even small amplitudes of noise disrupted pattern formation (Figure 2.4C, Methods: Noise interpretation). In a one-dimensional system with stochastic fluctuations (σ = 0.001, η = 0), patterning was disrupted after formation of the first stripe (Figure 2.4C, left vs. right panel). Suspending noise until the middle of the simulation (t = 20 h) allowed more stripes to form, but pattern propagation was quickly blocked once the noise was present (Figure 2.4C, middle panel, black arrows). On the other hand, while noise prevented the formation of new stripes, it did not disrupt stripes that had already formed. These results indicate that noise can disrupt pattern

formation and cause propagation failure without destabilizing patterned regions. (Note that even in the noise-free condition, the pattern eventually loses regularity (Figure 2.4C, right panel, gray arrows) due to accumulated numerical errors in the simulation, reflecting the sensitivity of the system to noise.)

To quantify the ability of noise to disrupt pattern formation, we analyzed patterning across different values of σ and η. As a measure of noise robustness in pattern formation, we analyzed the spatial correlation between the steady state patterns with and without noise. Values near 1 indicate patterning is unaffected by noise, while values near 0 indicate the absence of periodic patterning at the expected frequency (Methods: Noise robustness quantification). With a homogeneous initial condition, the circuit was sensitive to noise during pattern formation (Figure 2.4D, blue line). Disruption increased with the amplitude of noise, but even extremely low values of σ and η were sufficient to at least partially disrupt patterning (Figure 2.4D, orange arrows). By contrast, if we initialized the system with a deterministically formed pattern, even larger values of noise, up to at least 10%, failed to disrupt it (Figure 2.4D, red line). These results were again consistent with the notion that noise disrupts patterning specifically in unpatterned regions and, more generally, could be understood in terms of the ability of noise-stimulated patterns to fill in previously unpatterned regions, but not penetrate regions in which the pattern is already formed (Figure 2.4C, middle panel).

2.6 An inhibition-release mechanism overcomes noise sensitivity

Based on the results above, and inspired by aspects of retinal patterning in Drosophila (Heberlein, Wolff, and Rubin, 1993), we reasoned that suppressing A and R expression in unpatterned regions could prevent their premature activation by noise, while preserving their ability to pattern in response to the advancing wave of pattern formation. To implement this behavior, we added an "inhibition release" mechanism to the A-R circuit, based on a hysteretic positive feedback loop (Figure 2.5A). More specifically, we incorporated an intracellular regulator, denoted M, which can exist in either an inactive (M) or active (M*) state. We assume three key interactions for M. First, the transition from the inactive M to active M* is stimulated by R in an ultrasensitive manner. Second, M* stimulates M activation, creating a positive, ultrasensitive, and bistable feedback loop. Third, M* inhibits A degradation, which is assumed to occur at an accelerated rate, and thereby boosts A protein levels. With these assumptions, in the appropriate parameter regimes, M* exhibits an ultrasensitive, hysteretic dependence on its input, R (Figure 2.5A, inset). Low levels of

M* lead to correspondingly low levels of A, which in turn ensures low levels of R production, maintaining the cell in a homogeneous (non-patterned) ground state (Figure 2.5B, purple). By contrast, when M* is high, stabilization of A allows the circuit to exhibit the pattern-forming behaviors described above, as the excited state (Figure 2.5B, orange). In this way, an advancing wave of R morphogen can convert M to its active form, progressively de-inhibiting the A-R circuit as it propagates (Figure 2.5C).

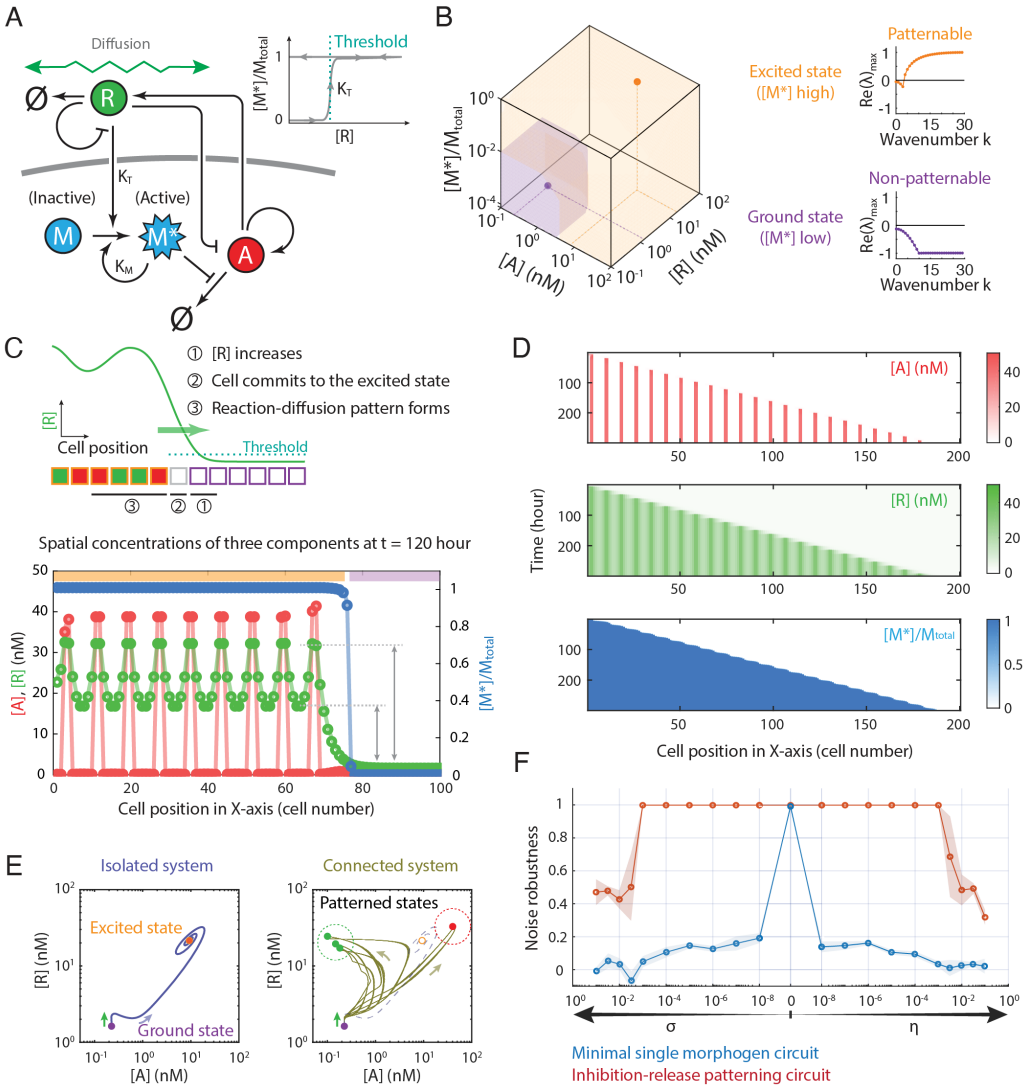

Figure 2.5: A bistable switch transiently stabilizing the patterning cells prevents the noise-triggered irregular bifurcation dynamics.

(A) Implementing this inhibition-release mechanism, we propose a three-component circuit that relies on an intracellular regulator (M) to temporarily stabilize pre-patterning cells. The third component has two forms: M* (active) and M (inactive). Only the active form could repress the degradation of A and restore its level in the cell. Meanwhile, both R and M* mediate the transition from M to M*. The ultra-sensitivity of R-mediated M activation ensures the M* level is either low or high.

(B) This inhibition-release circuit is bistable in the isolated system (no diffusion). The excited state is patternable while the ground state is non-patternable in the connected system. With proper parameters, the switch between two forms of M is designed to accomplish either stabilizing pre-patterning cells (ground state, purple) or releasing the inhibition to form patterns (excited state, orange).

(C) The patterned cells convert adjacent ground state cells and trigger new stripes in a propagative fashion. Initially, all cells stay in the ground state. The local increase of R converts the cell to the excited state. Reaction-diffusion pattern forms on these patternable cells. The high concentration of R from the region of patterned cells diffuses to their ground state neighbors and further converts them to be patternable. Three events, the repressor elevation in the ground state, the transition of the cell state from ground to excited, and the reaction-diffusion pattern formation on newly excited cells, occur in a synchronous sequential fashion. A snapshot of the concentration profiles from the simulation captures the detailed dynamics of the pattern formation, confirming our proposed dynamics in the model design.

(D) The inhibition-release circuit generates propagative periodic patterns, validated by the lattice ODE simulation. The simulation kymograph presents similar dynamics of A and R to the minimal single-morphogen reaction-diffusion circuit, where the periodic stripe pattern forms sequentially following the constantly propagated wavefront. Meanwhile, cells transform from the dormant to the active state, ahead of the wavefront swapping and patterning.

(E) In the connected system, cell trajectories bifurcate after being evicted from the ground state, bypassing the excited state. The phase portrait of the connected lattice system shows the populational behavior of bifurcation. If we provide perturbations (green arrows) to evict cells from the ground state in a connected system, instead of ending at a single stable steady-state as in an isolated system,

they end up with multiple stable states. All final states fall into two clusters, responding to a typical periodic pattern's bright (red dash circle) and dark regions (green dash circle).

(F) The inhibition-release circuit vastly increases the patterning robustness to either type of noise. Pattern formation simulations under such a paradigm at various noise intensities show better robustness to either type of noise than the minimal circuit. For minimal circuits, the regularity of the pattern is sensitive to even considerably low-level noise. Meanwhile, the inhibition-release circuit shows robustness to a wide range of both types of noise.

To test whether this circuit could prevent noise from triggering premature circuit activation, while still allowing pattern propagation, we simulated the system on a one-dimensional cell lattice (Figure 2.5C, 2.5D). We initialized the lattice with all cells in the homogeneous ground state (low M*), which is stable in the absence of external R. Production of R at the boundary triggered activation of M*, and consequent de-inhibition of the A-R circuit, in boundary-adjacent cells (Figure 2.5C). Since excited state cells produce R at a higher rate than ground state cells (Figure 2.5C, gray arrows), the R concentration gradient drove a net R flux towards more distal, inhibited cells, leading to a propagating front of M* activation (Figure 2.5C, 2.5D). Once de-inhibited in this way, the A-R circuit progressively developed periodic patterns of A and R concentration through a diffusion-driven bifurcation. Patterning occurred through three sequential stages: 1) elevation of the repressor, R, in the inhibited ground state, prior to its activation; 2) transition of the cell from the ground to the excited state by activation of M; and 3) reaction-diffusion pattern formation by the A-R circuit in the excited cells (Figure 2.5C). The third step resembled periodic stripe patterns following a propagating wavefront in the minimal A-R circuit (Figure 2.3). The effects of R diffusion can also be observed in the phase portrait (Figure 2.5E). Once cells are evicted from the inactive state, instead of ending at a stable excited state as in an isolated system, they exhibit multiple stable states as a consequence of the diffusion-driven bifurcation. Most importantly, all final states fall into two clusters, responding to the typical bright and dark regions of a periodic pattern (Figure 2.5C). Tuning the M activation threshold (K_T in the model) affects the propagation speed (Figure 2.12) by controlling the effective time delay before a cell converts from the ground state to the excited state in response to the propagating pattern. More specifically, with a higher threshold

value, ground state cells require a higher R level, and therefore a longer time to activate.

The inhibition-release mechanism makes patterning more robust to noise. We simulated the circuits with or without inhibition release at different noise intensities. Without inhibition release, even very low levels of noise were sufficient to disrupt patterning, as discussed previously (Figure 2.5F, blue line). With inhibition release, patterning remained robust across many orders of magnitude of noise strength that disrupted the simpler circuit (Figure 2.5F, red line). Taken together, these results show that single-morphogen reaction-diffusion can overcome the challenge of noise-induced spontaneous high-frequency patterns.

2.7 Growth-coupled patterning is robust to noise

A second mechanism that can make single-morphogen reaction-diffusion patterns robust to noise is through tissue growth. In many developmental systems, such as somitogenesis or intestinal crypt development, tissue patterning is closely coupled to growth (Schnell et al., 2002; Moreno and Kintner, 2004; Itzkovitz et al., 2012). In some cases, including intestinal crypts and apical meristems, progenitor cells at one location undergo repeated asymmetric divisions generating the rest of the tissue, which develops patterns as it is produced.

We reasoned that this sort of growth-coupled patterning could reduce the noise susceptibility of single-morphogen patterning. Assuming tissue growth occurs at a similar or slower rate compared to pattern propagation, newly formed tissue can immediately be patterned by adjacent, already patterned, tissue regions. The single-morphogen circuit could thus operate in a regime in which cells pattern immediately after division, and do not "wait" in a noise-sensitive state for a propagating front of patterned cells to reach them (Figure 2.6A).

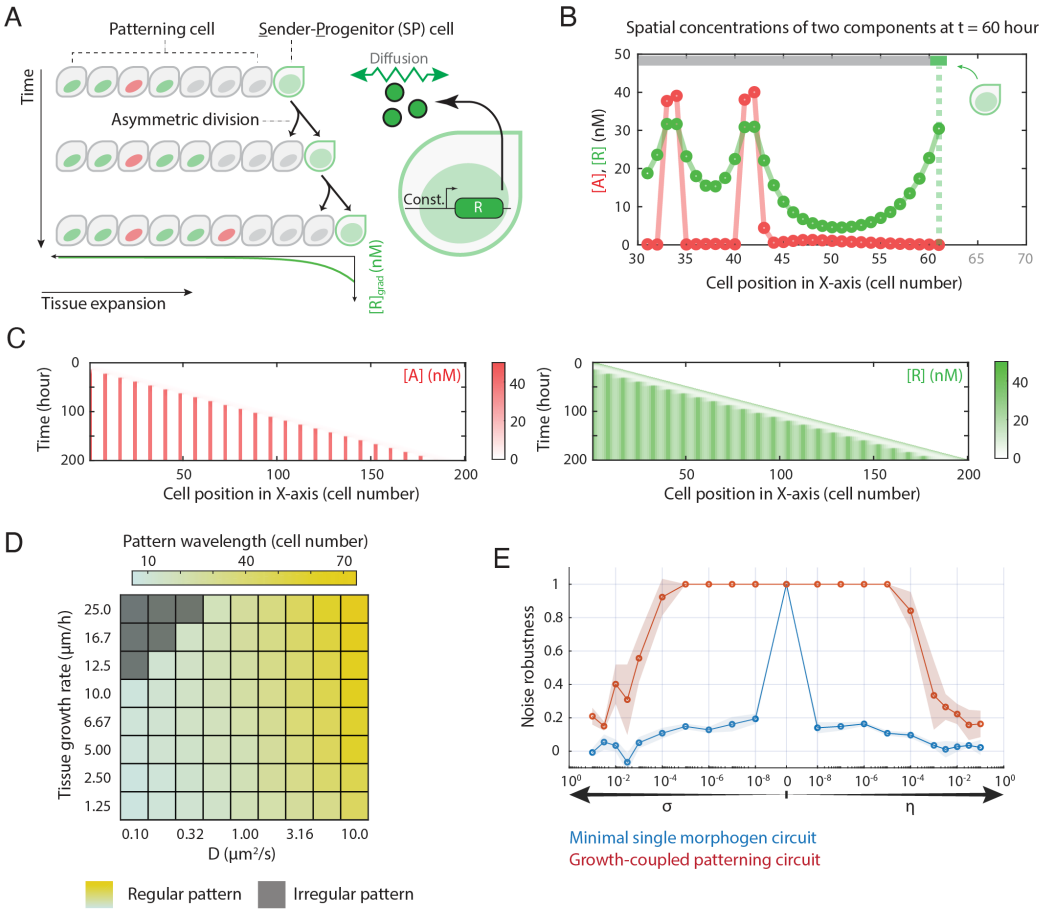

Figure 2.6: Coupling the tissue growth with the single-morphogen reaction-diffusion circuit increases the noise tolerance of pattern formation.

(A) The growth-coupled patterning model assumes a tissue growing in one dimension. All patterning cells with the minimal single-morphogen reaction-diffusion circuit originate from a specialized cell type, the sender-progenitor (SP) cell, which can asymmetrically divide, creating a patterning cell while keeping its number constant. The newborn cell appears between the SP and the elder patterning cell so that the entire tissue elongates as the consequence of cell division. Meanwhile, the SP cell stays at the tissue's elongation end and produces the repressor constantly. The Repressor gradient established by the SP cell stabilizes newborn patterning cells. $[R]_{grad}$ is the spatial concentration profile of the repressor gradient from the SP cell as an exponential decay function.

(B) The growth-coupled circuit forms periodic patterns on the actively growing tissue. The pattern formation process, initiated by the SP cell, takes place on the patterning cells. The new stripes emerge periodically near the growing center, where new patterning cells are produced. Meanwhile, the stabilized patterns on the mature pattering cells stay unchanged.

(C) The growth-coupled circuit generates periodic patterns on expanding tissue, validated by the lattice ODE simulation. The simulated kymograph presents similar dynamics of A and R to the minimal single-morphogen reaction-diffusion circuit. The propagation speed of pattern stripes is coupled with tissue growth rate.

(D) Both diffusion coefficient and tissue expansion rate scale the pattern wavelength. Besides the diffusion coefficient, the tissue expansion rate is the second spatial parameter in the model. A high expansion rate widens the wavelength. The diffusion coefficient is well-coupled with a wide range of tissue growth rates. Patterning circuits with small D fail to form regular stripes patterns on a fast-growing tissue. Each cell is assumed to have a size of 10 μm.

(E) The growth-coupled patterning circuit notably increases the noise robustness of the single-morphogen patterning. The noise interference test repeated with the tissue-growing paradigm shows significant improvement in noise robustness during the pattern formation stage. When the noise is beyond the tolerance, the robustness score drops faster for extrinsic noise than intrinsic noise.

To test whether tissue growth could allow robust single-morphogen patterning, we analyzed the minimal A-R patterning circuit on a growing cell lattice. We

designated a specialized sender-progenitor (SP) cell type that asymmetrically divides to generate a differentiated cell, which inserts itself between the SP and the products of the previous asymmetric divisions (Figure 2.6A). This simple toy model of tissue growth maintains a constant number of SP cells at one end of the tissue, while generating a linearly elongating lattice of patterning-competent cells. We assume that the differentiated cells express the full patterning circuit, and are therefore competent to form patterns. By contrast, the SP cell acts as a constitutive producer of the R repressor, establishing a concentration gradient from the tissue edge, whose length scale extends several cell diameters into the most recently generated cells (Figure 2.6A, Methods: Modeling growing tissue). In this scheme, the extracellular repressor emanating from the SP cell inhibits patterning in the proximal region (Figure 2.6B). However, as tissue growth progresses, individual cells eventually emerge from this inhibitory zone and can begin to pattern. Together, these features could allow growth-coupled patterning and avoid the disruptive effects of noise in pre-patterned cells.

To simulate deterministic growth-coupled patterning, we initialized the cell lattice with a single SP cell, and then periodically inserted newly differentiated cells directly adjacent to it (Figure 2.6B). In the differentiated cells, we simulated the same A-R circuit with the same parameter set analyzed above (Figure 2.3, 2.4), imposing reflective boundary conditions at both ends of the growing tissue. As anticipated, newborn cells initially expressed low levels of both A and R due to the production of R by the adjacent SP. Once a cell reached a distance from the SP, its A and R production rates switched to either a high state, in which both proteins were strongly expressed, or a low state, in which both were weakly expressed, depending on the states of the previous adjacent cells (Figure 2.6B). This led to periodic patterning (Figure 2.6B, 2.6C). Patterning proceeded indefinitely, and no defects were observed in this deterministic case for these parameters (Figure 2.6C). Further, growth-coupled patterning occurred across a broad range of values of diffusion coefficients and tissue growth rates (Figure 2.6D). These results show that coupling to growth can allow progressive patterning.

We next asked whether growth-coupled patterning could overcome the disruptive effects of noise. We simulated the system with the same growth dynamics, but systematically varied the levels of temporal and static noise, as discussed previously. Across a wide range of noise intensities, the growth-coupled system maintained predictable patterning for conditions that prevented periodic patterning in static

lattices (Figure 2.6E). In fact, both inhibition-release and growth-coupled allowed patterning in the presence of both types of noise (Figure 2.13). These results show that coupling to tissue growth can allow predictable patterning with a single morphogen in the presence of noise.

2.8 Discussion

Turing patterning is a classic concept in developmental biology. In this work, we investigated reaction-diffusion patterning using only a single diffusible morphogen — a regime that does not permit patterning under standard assumptions. Implemented on a discrete cell lattice, rather than in a continuous medium, this single-morphogen reaction-diffusion system can spontaneously generate patterns ranging from spatially alternating cell states to irregular, longer wavelength features (Figure 2.2). Motivated by the powerful roles that initial conditions and boundary conditions play in development (Murray, 2001; Hiscock and Megason, 2015), we considered their impact on patterning by this circuit. When stimulated by a point or line initial condition, the same circuit can generate propagating "stripes" that, once patterned, remain stable even if the initiating signal is removed (Figure 2.3). Transient initial conditions can thus control what types of single-morphogen circuits are capable of patterning.

In the single-morphogen system, low spatial frequency patterning modes must compete with the global attractor of high spatial frequency noise. Without mitigation, noise dominates, generally limiting the range and precision of the low-frequency patterns. More specifically, we found that noise was most disruptive when it had time to trigger high spatial frequency patterns that block the propagation pattern from the initiating boundary (Figure 2.4C). However, two remarkably simple, biologically plausible mechanisms are sufficient to ensure robust patterning.

On a static cell lattice, cells could circumvent noise-induced high-frequency patterns by "locking down" circuit activity until the propagating front of pattern formation approaches sufficiently to provide a high enough local concentration of morphogen to "unlock" the circuit. At that point, the adjacent cells are sufficiently well patterned to ensure the correct outcome for the cell in question. While this effect could be achieved in many ways, here we demonstrate how a relatively simple bistable switch, comprising a single positive autoregulatory factor, can provide this functionality, ensuring robust patterning (Figure 2.5).

In growing tissues, noise can be circumvented in a distinct manner, by limiting

patterning with tissue growth (Figure 2.6). In this regime, a set of progenitor cells elongate the tissue by self-renewing and differentiating into patterning cells. These newborn patterning cells immediately respond to the local environment to reach the appropriate state. In this case, cells spend little time in a noise-susceptible state where they are patternable, but not yet patterned. Hence, such a regime avoids the unwanted formation of high-frequency patterns.

How realistic are these assumptions? Mathematically, multicellular patterning systems are often imagined to first approach a transient homogeneous unstable state before cells diverge into distinct fates (Sprinzak et al., 2011; Raspopovic et al., 2014; Palau-Ortin et al., 2015; Onimaru et al., 2016). However, in natural development, patterning may more often proceed from a pre-patterned state that avoids the need for further symmetry breaking. In fact, many biological systems exhibit features that appear similar to those considered here. For example, in *drosophila* retinal development, the periodic patterning of ommatidia occurs dynamically in the wake of the morphogenetic furrow, as it sweeps across the eye disc, from posterior to anterior, over two days (Heberlein, Wolff, and Rubin, 1993). Cells located anterior to the morphogenetic furrow are unpatterned, while cells posterior to the morphogenetic furrow assemble into patterned ommatidia in a stepwise process. The progressive unlocking of patterning by the furrow is analogous to our inhibition-release model. We note, however, that this system relies on both the Hedgehog and Dpp signaling pathways, rather than a single morphogen, as analyzed here.

Patterning of the intestinal crypt provides an example of growth-coupled patterning (Gehart and Clevers, 2019). In this case, the columnar cells at the crypt base act as progenitor cells, dividing asymmetrically to produce a continually growing crypt with patterning of differentiated absorptive (high Notch signaling) or secretory (low Notch signaling) cells. Here, growth appears to play a role in unlocking competence for patterning. Further, Wnt ligands secreted by Paneth cells at the base of the crypt play a key morphogenetic role in inhibiting differentiation, although other diffusible signals also play roles in this system.

Finally, in plant development, apical meristem development involves a central zone of progenitor cells that divide and differentiate to replace cells in the peripheral and rib zones, which divide more rapidly and further differentiate (Nakajima and Benfey, 2002; Carles and Fletcher, 2003). Meanwhile, the shoot apical meristem also produces the signaling molecule auxin, preventing axillary buds, which initially locate in the leaf axil dormant, from undergoing shoot development because of the

apical dominance (Dun, Ferguson, and Beveridge, 2006; Kebrom, 2017). We note, however, that auxin signaling also involves efflux and influx carrier proteins that could generate more complex patterning dynamics than those modeled here.

The simplicity of single-morphogen patterning could make it ideal for the nascent field of synthetic development. As synthetic biology progresses from single-cell to multicellular systems, a key challenge is engineering cells that can establish their own spatial patterns. In this context, circuit architectures with minimal components and interactions, such as the single-morphogen patterning systems explored here, are critical. The entire single-morphogen reaction-diffusion circuit proposed here could be implemented with well-characterized components. For example, Gal4 or engineered zinc finger transcription factors (Khalil et al., 2012; Zhu et al., 2022) could serve as the activator, A. The repressive morphogen, R, could be implemented with the combination of a secreted diffusible signaling molecule and an intracellular repressor whose expression it activates. Sonic Hedgehog has been shown to form well-defined morphogenetic gradients in 3T3 cells, making it a candidate for the morphogen (Li et al., 2018). Other natural pathways such as BMP could also function in this way. Alternatively, synthetic small signaling molecules such as auxin (Liang, W. Q. Ho, and Crabtree, 2011; Ma et al., 2020), and variants of the synNotch system that allow morphogenetic patterning (Morsut et al., 2016) could enable the engineering of patterning systems orthogonal to natural pathways. Tet repressor variants could allow downstream negative regulation. To circumvent noise, the bistable switch (Figure 2.5) could be implemented with a self-stabilizing protease (Gao et al., 2018), synthetic phosphorylation systems (Mishra et al., 2021; Woodall et al., 2021), transcriptional autoregulation (Zhu et al., 2022), or RNA-level regulation (Levine et al., 2007; Morris and Mattick, 2014; Dykes and Emanueli, 2017), among other mechanisms. Finally, coupling patterning to tissue growth could be realized using spatially confined cell culture systems that restrict growth to elongated channels, as was shown for mammalian cells using the "mother machine" microfluidic system (Pearl Mizrahi et al., 2016; Potvin-Trottier et al., 2016).

Thus, we anticipate this circuit providing a feasible foundation for engineering synthetic pattern formation systems. Turing's remarkably general pattern-forming architecture is well known for the broad range of patterns it can generate. It is interesting to see how initial conditions, noise, and variations in circuit architecture jointly allow robust patterning in both natural and synthetic multicellular contexts.

2.9 Methods

Lattice ODE simulation

Framework To tie experiment and modeling closely, we use cell-lattice simulation to approximate experimental conditions. Depending on the geometry of the simulation, we run simulations on 1-D or 2-D. In the one-dimensional case, virtual cells in a finite length chain are connected with their left and right neighbors. In a two-dimensional case, cells are connected in a square lattice. For each cell, we assign one set of ODEs. Meanwhile, morphogen diffusion is realized by molecules transferring among adjacent cells.

Equilibrium simulation An initial concentration profile guess is assigned to all components. In the pre-equilibrium simulation, diffusion is turned off and the ODE systems in each virtual cell would evolve by themselves. The system eventually reaches the homogeneous steady state, in which all the cells have the same concentration profile in each circuit component.

Patterning simulation To start the pattern formation, we turn on the diffusion. A specific trigger, corresponding to the initial condition, creates a transient heterogeneous perturbation in the system. The simulation finishes once the pattern stops changing spatially and temporally.

Initial conditions Our simulations use two types of initial conditions, which lead to two types of patterning results and dynamics. All lattice nodes are subject to global random noise in the concentration of A (or R). The perturbation profile is generated by random sampling from a Gaussian distribution with zero mean and given standard deviation. The spatial localized initial condition only affects selected cells in the same fashion. The selected cells usually follow a certain geometry, either a single dot or a straight line. The pattern can be triggered by acting upon any of the two species, by increasing or decreasing its concentration for an arbitrary time window. Specifically, some tests involve a constant influx from a line of cells as the initial condition.

Boundary conditions We consider a square lattice of size $l \; x \; w$ for our simulations (in some cases the system is one-dimensional by setting $w = 1$). The simulation is repeated with two types of boundary conditions: reflective and periodic. The general features of the single-morphogen reaction-diffusion pattern are not affected by the choice of boundary condition.

Parameter estimation To better fit the biological context, we estimate model param-

Parameter Name	Parameter Description	Parameter value
β_A	Production rate of activator	100 nM/h
β_R	Production rate of repressor	80 nM/h
γ_A	Degradation rate of activator	1.5 $/h$
γ_R	Degradation rate of repressor	0.5 $/h$
D	Diffusion coefficient of morphogen	1 $\mu m^2/s$
K_A	Dissociation constant of activator	10 nM
K_R	Dissociation constant of repressor	10 nM
κ	Basal leakage of promoter	0.01
h	Hill coefficient of promoter	2

Table 2.1: Parameter list and estimated values in simulations

eters from BioNumbers (Milo et al., 2009) and from our own wet-lab experiments. The estimated parameter values are shown in Table 2.1. Our model assumes that the cell size is 10 μm x 10 μm x 10 μm, and we further deduce other parameter values from there.

Noise interpretation Our simulations consider two types of noise: temporal dynamic noise and static heterogeneity. Specifically, we generate the noise profile $H(i,t)|_{\eta,\sigma}$ with given σ and η ahead of the simulation. The temporal dynamic noise is denoted by $H(i,t)|_{\eta=0,\sigma}$and the static heterogeneity by $H(i,t)|_{\eta,\sigma=0}$. Initially, the noise randomizes the production rate of both species. Linear interpolation between time points in $H(i,t)|_{\eta,\sigma}$ is used when needed in the simulation. In the case where the noise starts to interfere with the simulation at a later time point, we reset the value of $H(i,t)|_{\eta,\sigma}$ to 1 during the noise-free time period.

Modeling growing tissue The lattice is initiated with two lines of cells. One line is the patterning cells, which have the complete single-morphogen reaction-diffusion circuit. The other line is sender-progenitor (SP) cells, which only constitutively produce the repressor. The "tissue growth" is realized by adding a new line of patterning cells between SP cells and the adjacent existing patterning cells every cell cycle T_{cyc}. In our model, the newborn patterning cells inherit R molecules associated with the mother cells, i.e., the initial concentration of R in a newborn cell is the same as that in the SP cell. The single-morphogen patterning circuit begins to operate immediately in newborn cells. We did not consider dilution in the model because the time-scale of R dynamics is faster than the timescale of cell division, allowing R levels to quickly re-equilibrate in SP cells after division. To realize cell growth in our model, the simulation "pauses" every T_{cyc} and extends the lattice by one cell. Thus, the tissue growth rate is defined as 1 cell /T_{cyc} in the later discussion

of this work.

Quantification and statistical analysis

Final stable pattern auto-correlation 2-D spatial auto-correlation, calculated by MATLAB function corr2() on the original 200 x 200 lattice simulation final frame, reveals lateral inhibition (Figure 2.2B, 2.2C). In the 1-D pattern, the auto-correlation function is calculated with the MATLAB function corr().

Pattern wavelength determination To measure the pattern wavelength, the MATLAB peak detection function identifies the peak positions from the auto-correlation profile of the 1-D simulation final frame. The measured wavelength is the average distance of two adjacent peaks.

Pattern propagation speed determination We locate the peak positions in the final pattern and then record the time when the activator in the corresponding cells crosses a threshold (10% above the steady state). The time series defines the propagation period. The propagation speed is the spacing between two peaks divided by the propagation period.

Noise robustness quantification To evaluate the noise robustness of a certain model, we run the pattern formation simulation with and without noise. The spatial correlation between the two final repressor profiles quantifies the similarity of the two patterns. If the correlation is near 1, we claim the model is robust to this particular level of noise. Otherwise, if the correlation is close to 0, the model is sensitive to noise. This test is repeated at various levels of noise (both temporal dynamic noise and static heterogeneity) in all three models, to evaluate the noise robustness in the three circuits.

2.10 Supplementary

Analytical study of the single-morphogen reaction-diffusion circuit in the continuum limit

The following analysis considers a two-component system, and the conclusion is valid for a multiple-component pattern. Given a single-morphogen patterning circuit

$$\frac{\partial A}{\partial t} = f(A, R) \tag{2.6}$$

$$\frac{\partial R}{\partial t} = g(A, R) + D\nabla^2 R \tag{2.7}$$

the necessary and sufficient condition to generate stable spatial patterns is that the Jacobian matrix stays stable without diffusion and becomes unstable for some

wavenumber k with diffusion. denoting J(k) as

$$J(k) = \begin{pmatrix} f_A & f_R \\ g_A & g_R - Dk^2 \end{pmatrix}, \tag{2.8}$$

where k is the wavenumber (k = 1, 2, 3, . . .). The eigenvalue is the solution of

$$(f_A - \lambda)(g_R - Dk^2 - \lambda) - f_R g_A = 0 \tag{2.9}$$

$$\lambda^2 - (f_A + g_R - Dk^2)\lambda + f_A g_R - f_R g_A - f_A Dk^2 = 0. \tag{2.10}$$

When k is large, the equation becomes,

$$\lambda^2 + Dk^2\lambda - f_A Dk^2 = 0. \tag{2.11}$$

Assuming $Re(\lambda_1) \leq Re(\lambda_2)$, then

$$\lambda_2 = \frac{-Dk^2 + \sqrt{D^2k^4 + 4f_A Dk^2}}{2} \tag{2.12}$$

$$= \frac{Dk^2}{2}(\sqrt{1 + \frac{4f_A}{Dk^2}} - 1) \tag{2.13}$$

$$= \frac{Dk^2}{2}[1 + \frac{1}{2}\frac{4f_A}{Dk^2} - \frac{1}{8}(\frac{4f_A}{Dk^2})^2 + \mathcal{O}(\frac{1}{k^6}) - 1] \tag{2.14}$$

$$= f_A - \frac{f_A^2}{Dk^2} + \mathcal{O}(\frac{1}{k^4}) \tag{2.15}$$

monotonically increases as the function of k when k is large.

Stability analysis of the single-morphogen reaction-diffusion circuit in a discrete lattice

Steady-state of the isolated system Given the lattice ODE of a single-morphogen patterning circuit, firstly we solve the steady-state without diffusion terms.

$$\frac{\partial A_i}{\partial t} = f(A_i, R_i) \tag{2.16}$$

$$\frac{\partial R_i}{\partial t} = g(A_i, R_i) + D\sum_{j\in]i[}^{j}(R_j - R_i) \tag{2.17}$$

$$f(A_i, R_i) = 0 \tag{2.18}$$

$$g(A_i, R_i) = 0 \tag{2.19}$$

The steady-state concentrations, denoted as A_0 and R_0, are valid for all lattice nodes.

Stability analysis on 1-D or 2-D discrete lattice Similar to the calculation in Plahte's work (Plahte, 2001), denoting C = [A_1, R_1, A_2, R_2, ... A_N, R_N], the linearized kinetics of the whole system near the steady-state is

$$\frac{\partial C}{\partial t} = (I_N \otimes J + Q \otimes B)C, \tag{2.20}$$

where

$$J = \begin{pmatrix} \frac{f}{\partial A} & \frac{f}{\partial R} \\ \frac{g}{\partial A} & \frac{g}{\partial R} \end{pmatrix}, \; B = \begin{pmatrix} 0 & 0 \\ 0 & 1 \end{pmatrix}.$$

Q is the matrix describing the connectivity of the lattice. For all diagonal elements, $Q_{ii} = -m$, where m is the number of cells directly connected with cell i. If diffusive molecules can directly transfer between cell i and cell j, $Q_{ij} = 1$. Otherwise, $Q_{ij} = 0$. If the connectivity matrix Q can be diagonalized with matrix U and U^{-1}, then we have

$$L = (U^{-1} \otimes I_2)^{-1}(I_N \otimes J + Q \otimes B)(U^{-1} \otimes I_2) \tag{2.21}$$

$$= \begin{pmatrix} J + q^{(1)}B & 0 & 0 & \dots & 0 \\ 0 & J + q^{(2)}B & 0 & \dots & 0 \\ 0 & 0 & J + q^{(3)}B & \dots & 0 \\ \vdots & \vdots & \vdots & \ddots & \vdots \\ 0 & 0 & 0 & \dots & J + q^{(N)}B \end{pmatrix}. \tag{2.22}$$

Since L is a block-diagonal matrix, which means

$$Eig(L) = \bigcup_{i \in \{1,2,\dots N\}} Eig(J + q^{(i)}B). \tag{2.23}$$

The whole lattice is stable, if and only if all of $J + q^{(i)}B$ are stable. Meanwhile, the lattice would be unstable as long as one of the $J + q^{(i)}B$ is unstable.

Connectivity matrix In our work, we study the patterning on both 1-D lattice and 2-D square lattice. In later analysis, we only demonstrate two analytical solutions from two specific boundary conditions. The simulation also repeats with other types of boundary conditions, which have no simple analytical solution for eigenvalues. The MATLAB code numerically solves the eigenvalues of the connectivity matrix from given boundary conditions in simulation.

Dispersion relation The 1-D dispersion relation, the maximum of the real part of the Jacobian eigenvalues as the function of wavenumber k, is symmetric since $q^{(k)} = q^{(N-k)}$. In the Dispersion curve, we only show the left half, from $k = 0$ (isolated system) to $k = N/2$.

Parameter Name	Parameter Description	Parameter value
k_1	Basal production of activator	0.1
k_2	Degradation rate of activator	1
k_3	Production rate of activator	1
k_4	Production rate of repressor	1
k_5	Degradation rate of repressor	1
D_A	Diffusion coefficient of activator	0
D_R	Diffusion coefficient of repressor	3

Table 2.2: Parameter list and estimated values in the Gierer-Meinhardt model simulations

Patterning with Gierer–Meinhardt kinetics

The Gierer-Meinhardt model (Gierer and Meinhardt, 1972) is a well-studied reaction-diffusion patterning system that has been evaluated in many simulation studies (Ruan, 1998; Iron, Ward, and Wei, 2001; Sun, Wang, and Wu, 2017). Here we demonstrate the mechanism behind the single-morphogen patterned propagative periodic patterns is also valid with Girrer-Meinhardt kinetics. The Girrer-Meinhardt kinetics are

$$\frac{\partial A}{\partial t} = k_1 - k_2 A + k_3 \frac{A^2}{R} + D_A \nabla^2 A \tag{2.24}$$

$$\frac{\partial R}{\partial t} = k_4 A^2 - k_5 R + D_R \nabla^2 R, \tag{2.25}$$

where k_1, k_2, k_3, and k_4 are circuit parameters. Setting $D_A = 0$, we simulated the non-dimensionalized system with values in Table 2.2 for other parameters.

Simulation on a square lattice with the same initial triggers as in the main model showed similar patterns (Figure 2.7A). This periodic pattern also forms in a propagative fashion (Figure 2.7B).

Models with additional components or time delays

Separating the morphogen and the transcriptional repressor In the model analyzed in the main text, the protein R has two distinct functions: acting as a morphogen that can transmit signals from one place to another, and acting as a repressor that can down-regulate A expression. Biologically, these two functions are more likely to be implemented by distinct proteins. To analyze this more realistic scenario, we considered an expanded three-component model, in which the activator (A) and the repressor (R) are two transcription factors functioning intracellularly, while a new morphogen "ligand" (L) can diffuse among cells and transmit signals. The promoter integrates inputs from A and R to control the expression of A and L. Once secreted

Parameter Name	Parameter Description	Parameter value
β_A	Production rate of activator	100 nM/h
β_R	Production rate of repressor	80 nM/h
β_L	Production rate of morphogen	80 nM/h
γ_A	Degradation rate of activator	0.4 $/h$
γ_R	Degradation rate of repressor	0.6 $/h$
γ_L	Degradation rate of morphogen	0.6 $/h$
D	Diffusion coefficient of morphogen	1 $\mu m^2/s$
K_A	Dissociation constant of activator	10 nM
K_R	Dissociation constant of repressor	10 nM
K_L	Dissociation constant of singling	10 nM
κ	Basal leakage of promoter	0.01
κ_2	Basal leakage of signaling promoter	0.01
h	Hill coefficient of promoter	2
h_2	Hill coefficient of signaling promoter	2

Table 2.3: Parameter list and estimated values in the three-component model simulations

from the cell, the extracellular L can diffuse and signal to upregulate R expression via a cognate signaling pathway, which is not explicitly modeled. In this case, we have the following PDEs (Figure 2.9A):

$$\frac{\partial A}{\partial t} = \beta_A((A/K_A)^h + \kappa)/((A/K_A)^h + (R/K_R)^h + 1 + \kappa) - \gamma_A A \tag{2.26}$$

$$\frac{\partial R}{\partial t} = \beta_R((L/K_L)^(h_2) + \kappa_2)/((L/K_L)^(h_2) + 1 + \kappa_2) - \gamma_R R \tag{2.27}$$

$$\frac{\partial L}{\partial t} = \beta_L((A/K_A)^h + \kappa)/((A/K_A)^h + (R/K_R)^h + 1 + \kappa) - \gamma_L L + D\nabla^2 L \tag{2.28}$$

This model contains extra parameters. β_L, γ_L, are the production and degradation rates of the morphogen ligand L. κ_L, h_2, κ_2 describes the production dependence of intracellular R to the L level. In this three-component model, we assigned physiological values (Table 2.3) to these parameters and ensured the parameter set was in the patternable regime.

Simulations of this model on the standard cell lattice produce similar patterns to those observed in the more minimal circuit (Figure 2.9B).

Incorporating time delays in the regulatory system In cells, key regulatory functions such as transcription, translation, secretion, and signaling can involve substantial time delays of minutes to hours. These time delays could potentially impact the

ability of the circuit to generate patterns. Moreover, compared to the activator, the diffusible repressor is expected to have a longer delay, because it must be secreted and then sensed by a corresponding signaling pathway. We therefore introduced two time-delay constants, one for each arm of the circuit, denoted τ_A and τ_R, with $\tau_A < \tau_R$. With these additions, the system can be modified to the following set of delay differential equations:

$$\frac{\partial A}{\partial t} = \beta_A F(A(t-\tau_A), R(t-\tau_R)) - \gamma_A A(t) \tag{2.29}$$

$$\frac{\partial R_i}{\partial t} = \beta_R F(A(t-\tau_A), R(t-\tau_R)) - \gamma_R R(t) + D\nabla^2 R(t) \tag{2.30}$$

Here, the notation $A(t-\tau_A)$ and $R(t-\tau_R))$ represents the value of A or R at a time of τ_A or τ_R time units in the past. We simulated pattern formation dynamics with various time delays spanning a physiological range from 10 minutes to 10 hours, while fixing all other parameters (Figure 2.9C). Incorporating the time delay maintained patterning but slowed down its spatial propagation (Figure 2.9C). If only introducing a time delay in the repression arm, the time delay eventually destroyed pattern propagation and replaced it with temporal oscillations (Figure 2.9D). Similar phenomena have been described previously by (Gelens, Anderson, and Ferrell, 2014; Bailles, Gehrels, and Lecuit, 2022). They demonstrated that a time delay only in the repression arm leads to oscillations of the activator-repressor system. In a combinatorial evaluation of the two delay terms, we also found that the system with greater time delay in two regulation arms has a lower tolerance to time delay difference (Figure 2.9E). Together, these results show that the two-component patterning circuit discussed in this work can function under reasonable parameter values when expanded to a three-component system, or when explicit time delays are included.

Parametric robustness analysis

Understanding how patterning depends on parameter values is critical for engineering synthetic pattern formation and for understanding the constraints on natural patterning. We performed two analyses of parametric robustness: First, we evaluated the robustness of the system to perturbations of the basal parameter set (Methods: Parameter estimation, Table 2.1) used in this work. Second, we compared the robustness of the single-morphogen patterning circuit to that of a corresponding classical Turing circuit (by setting $D_A > 0$) for the same parameter values.

Variation of basal parameters We analyzed parametric robustness using an ap-

proach described previously (Scholes et al., 2019; Landge et al., 2020). We analyzed system behavior across a multi-dimensional grid in parameter space, and calculated the percentage of grid nodes that allow the pattern to form. Our minimal model has nine parameters. We first focused on the four that can most readily be tuned experimentally: the production and degradation rates of both activator and repressor. We created a 4-D grid varying each parameter over a 100-fold range, from 0.1 to 10 times its initial value, in logarithmic steps (Methods: Parameter estimation, Table 2.1). The patternable regime occupied about 8% of this scanned 4-D parameter space (Figure 2.10A). We also scanned each parameter individually, while fixing the values of the others (Figure 2.10B orange bars above each plot). This analysis showed the range of robustness for each parameter.

Comparison to classical Turing patterning We also compared the sensitivity of the single morphogen system to that of a classical two-morphogen Turing model. In the Turing system, we take the same parameter values from the single morphogen system (in which $D_R = 1\ \mu m^2/s$) and set the diffusion coefficient of A equals $0.1\ \mu m^2/s$ (D_A/D_R = 1:10). The stability analysis reveals 3.1% of the available parameter space can generate patterns. This value is nearly three times smaller than the patterning region exhibited by the single-morphogen patterning circuit (8%). In a more systematic analysis (Figure 2.10B), we evaluated the D_A, the diffusion coefficient of A, from 0.001 $\mu m^2/s$ to 1 $\mu m^2/s$. This value was chosen to be greater than 0 but still lower than the R diffusion coefficient (1 $\mu m^2/s$), consistent with the known requirement for standard Turing patterning. The patternable regimes are getting narrower when $D_A > 0$ in all single parameter scans (Figure 2.10B). These results suggest that, at least in these regimes, the single-morphogen patterning circuit can operate with comparable parameter robustness as the classical Turing circuit.

Patterning dynamical behaviors varying in parameter space We also performed simulations to investigate how the patterning dynamical behaviors vary in parameter space. The patterning dynamics are mainly affected by two patterning criteria: 1) The Jacobian of the isolated system is stable; 2) the Jacobian of the multicellular connected system is unstable for some wavenumber (Figure 2.10C). Regimes satisfying both criteria are the patternable regime, where the single-morphogen mechanism we discussed is valid (Figure 2.10C, panel ii, iii, v). Meanwhile, regimes only satisfying criteria 1 always stay homogeneous statically (Figure 2.10C, panel i, vi). However, interestingly, regimes only satisfying criteria 2 starts from temporal oscillation and forms spatial patterns in a propagative fashion (Figure 2.10C, panel iv). Similarly,

we performed simulations varying all other parameters one at a time (Figure 2.10D). In general, increasing β_A, γ_R, and K_R increases the activator level and increasing β_R, γ_A, K_A, and h decreases the activator level. Moreover, patterns tend to have shorter wavelengths when the activator level is high.

Patterning on the hexagonal lattice and the rod-shaped lattice

Besides the square lattice, the single morphogen patterning mechanism is comparable with other isotropic lattices. Meanwhile, an anisotropic lattice, which is equivalent to an isotropic lattice with anisotropic diffusion coefficients, would rescale the patterns in corresponding directions. Here, we demonstrate that on the hexagonal lattice, the circuit recurs the same pattern features (Figure 2.11A, left). The upper panels in Figure 2.11A below show where the initial condition was applied. The final stable patterns (Figure 2.11A, lower panels) and formation dynamics are similar to the simulation results from the square lattice. Next, we investigate an anisotropic cell lattice that has rod-shaped (length: width $\neq$ 1) cells (Figure 2.11B, left). The patterning dynamics from this lattice are similar to previous ones, however, because of the anisotropy, patterns elongate in the cells' major axis (Figure 2.11B, middle and right). Simulations performed on the rod-shaped (ratio 3:1) cell lattice clearly reveal that the pattern wavelength is anisotropic in two propagation directions (Figure 2.11C, upper panels). Furthermore, the scaling of wavelength is dependent on the length:width ratio of the lattice cell. Figure 2.11C lower panels show patterns from a less anisotropic lattice (rod-shape, length: width = 2). The pattern in the x-axis is less "stretched" compared to the one from the ratio 3:1 cell lattice.

Patterning in a three-dimensional lattice

This single-morphogen reaction-diffusion circuit forms patterns in 3-D. We simulated pattern formation in a 3-D cubic lattice, where cells are allowed to signal their six directly adjacent neighbors. Simulating with the same set of parameters used in the 2-D case, spatially localized perturbations (Figure 2.11D, upper panels) still triggered pattern formation in 3 dimensions (Figure 2.11D, lower panels). A point source at the origin generates sequentially propagating concentric "shells" of activation (Figure 2.11D, left column). Meanwhile, a 1D perturbation (a line of cells) triggers concentric cylindrical patterns, and a 2D perturbation (a sheet of cells) triggers propagating parallel planes of patterning (Figure 2.11D). The spatial periodicity is similar in 3-D to the period obtained for the analogous perturbation in 2-D.

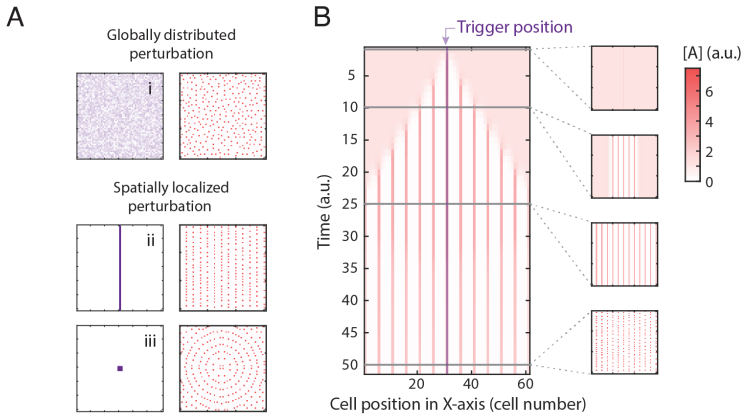

Figure 2.7: Single-morphogen reaction-diffusion circuit with Gierer–Meinhardt kinetics also generates propagating spatial patterns.

(A) Simulations of the single morphogen model on a 61 x 61 cell lattice with Gierer–Meinhardt kinetics, as described in Supplementary. Here, we show three types of initial conditions: i) global random noise, ii) a line, and iii) a point. The Gierer–Meinhardt kinetics generate similar patterns to those observed with the main circuits analyzed in this paper, although additional bifurcations (stripe breaks up into spots perpendicular to the propagation direction) can occur.

(B) Patterns propagate from the linear initial trigger. Simulations showed similar pattern propagation dynamics, but different from those in Figure 2.3 in that they also exhibited further bifurcations.

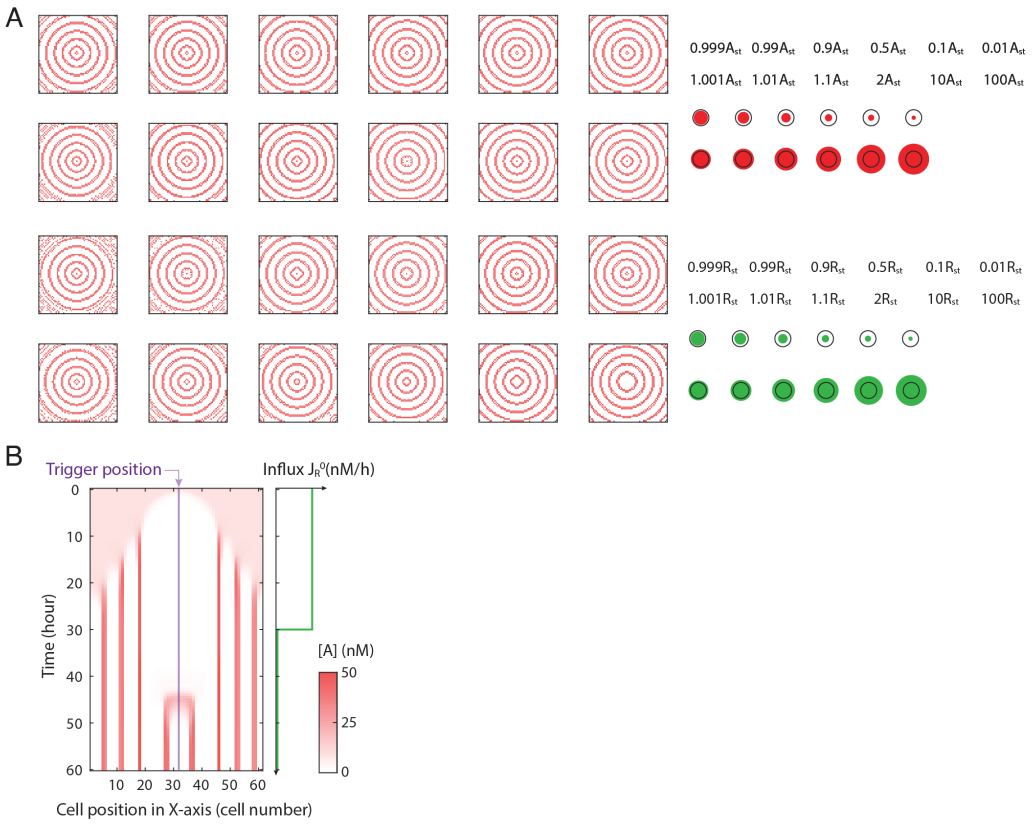

Figure 2.8: Pattern initiation is capable with a wide range of perturbations.

(A) A transient perturbation at the center in [A] or [R] profile can both initiate the ring pattern formation. In the test, the perturbed concentration varies from 0.01x to 100x of the original steady state values. In all cases, the system is able to form patterns, with changes in the phase of the patterns.

(B) Removal of morphogen influx causes pattern stripes to "fill in" the empty space. The constant influx of R creates an inhibition zone for the peaks of the activator. Parallel stripes form on both sides at distance and propagate further. Once R influx stops, the inhibition zone dampens. New stripes form in the empty space with proper distance.

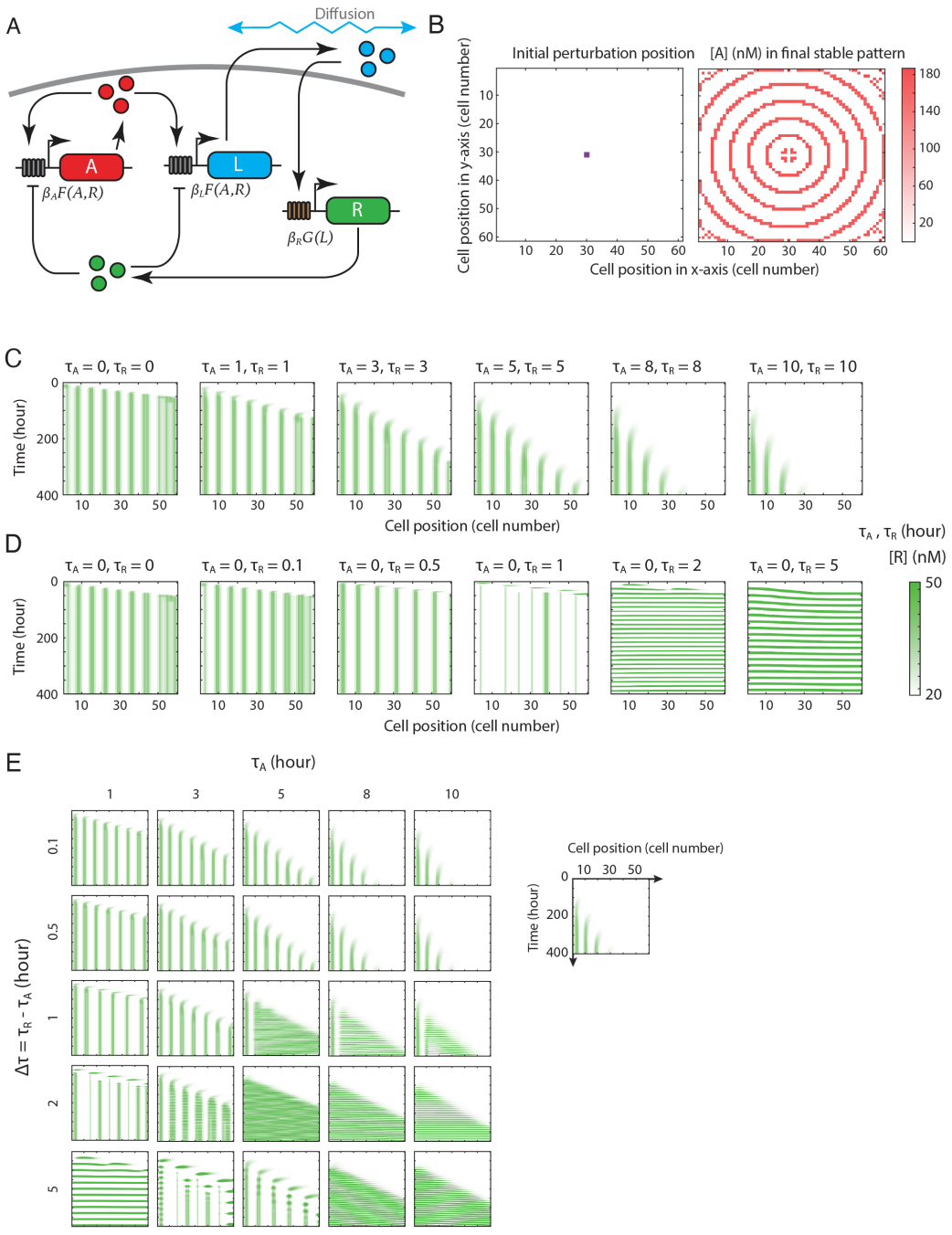

Figure 2.9: Single-morphogen reaction-diffusion mechanism is expandable to models with additional components or time-delay.

(A) In a more realistic model, the dual functions of the repressor in the minimal model are realized by an intracellular repressor and a morphogen. The activator (A) and the repressor (R) are two transcription factors functioning intracellularly, while a new morphogen "ligand" (L) can diffuse among cells and transmit signals. The promoter integrates inputs from A and R to control the expression of A and L.

(B) The three-component model can form propagative spatial periodic patterns. With certain parameters (Methods: Models with additional components or time delays) and proper initial condition, the expanded model forms "ring" patterns.

(C) The time-delayed model has good tolerance to the time-delay which is applied equally in both regulation arms within a physiological range. With the 10 hours' time-delay, the pattern stripes still form while the propagation speed slows down.

(D) The model is sensitive to the time-delay difference of the two regulation arms. If the time-delay is above one hour, this single-morphogen circuit produces temporal periodic patterns rather than the spatial periodic patterns.

(E) The single-morphogen model has lower tolerance to time-delay difference with greater time-delay in two regulation arms.

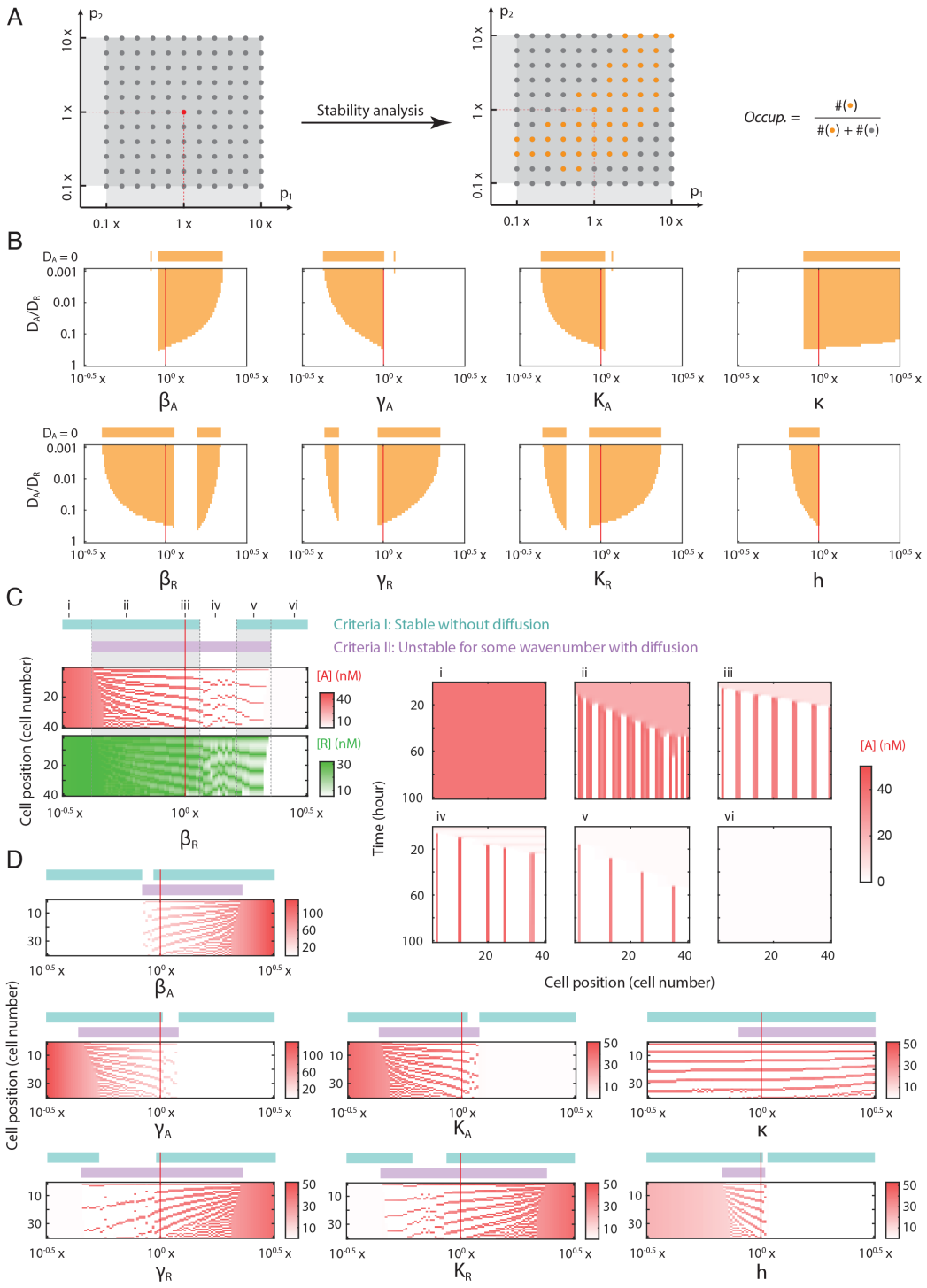

Figure 2.10: Parametric analysis reveals the patternable regime of the single-morphogen reaction-diffusion model.

(A) Stability analysis on the high-dimensional grid in parameter space surrounding the basal parameter set reveals the patternable regime. The patternable domain is quantified as the percentage of patternable parameter sets in the entire searched grid.

(B) Varying each individual parameter, the patternable regime of a single-morphogen circuit is greater than a corresponding classic two-morphogen circuit. For each value of D_A (horizontal line) stability analysis shows the patternable regime (orange) when varying a particular parameter (X-axis) and fixing all others. The first line presents the single-morphogen circuit ($D_A/D_R = 0$). The other lines show classic two-morphogen circuits with varying values of D_A ranging from 0.0001x D_R (0.0001 $\mu m^2/s$) to 1x D_R (1 $\mu m^2/s$).

(C) The patterning dynamics and final spatial concentration profiles shift when varying each individual parameter. The orange and purple bars show the regimes satisfying each of the two patterning criteria: 1. The Jacobian matrix of this system is stable without diffusion; 2. The Jacobian matrix is unstable for some wavenumber with diffusion. The overlap regime (gray shade) is patternable (also refers to Figure 2.10B, orange region). Lower panels stitch 1-D simulation results (vertical, triggered from top) with different values of β_R. In general, increasing β_R lowers the concentration of both components and increases the pattern wavelength. Right panels present the pattern formation dynamics with six given β_R values. Panel i and vi satisfied criteria 1, showing homogenous static concentration profiles. Panel ii, iii, and v satisfied both criteria and formed propagative spatial patterns, which followed the single-morphogen reaction-diffusion patterning mechanism discussed in this work. Panel iv only satisfied criteria 2 and showed a new pattern mechanism, where a propagative wavefront converts a temporal oscillation into spatial periodic patterns. Instead of staying at a steady state, the whole system undergoes temporal oscillation without diffusion. Once the trans-signaling is allowed and the proper initial trigger is applied, the wavefront propagates and converts oscillation into spatial patterns. This interesting mechanism is not discussed in this work.

(D) A similar analysis for other parameters shows how dynamic behavior varies in the corresponding parameter space.

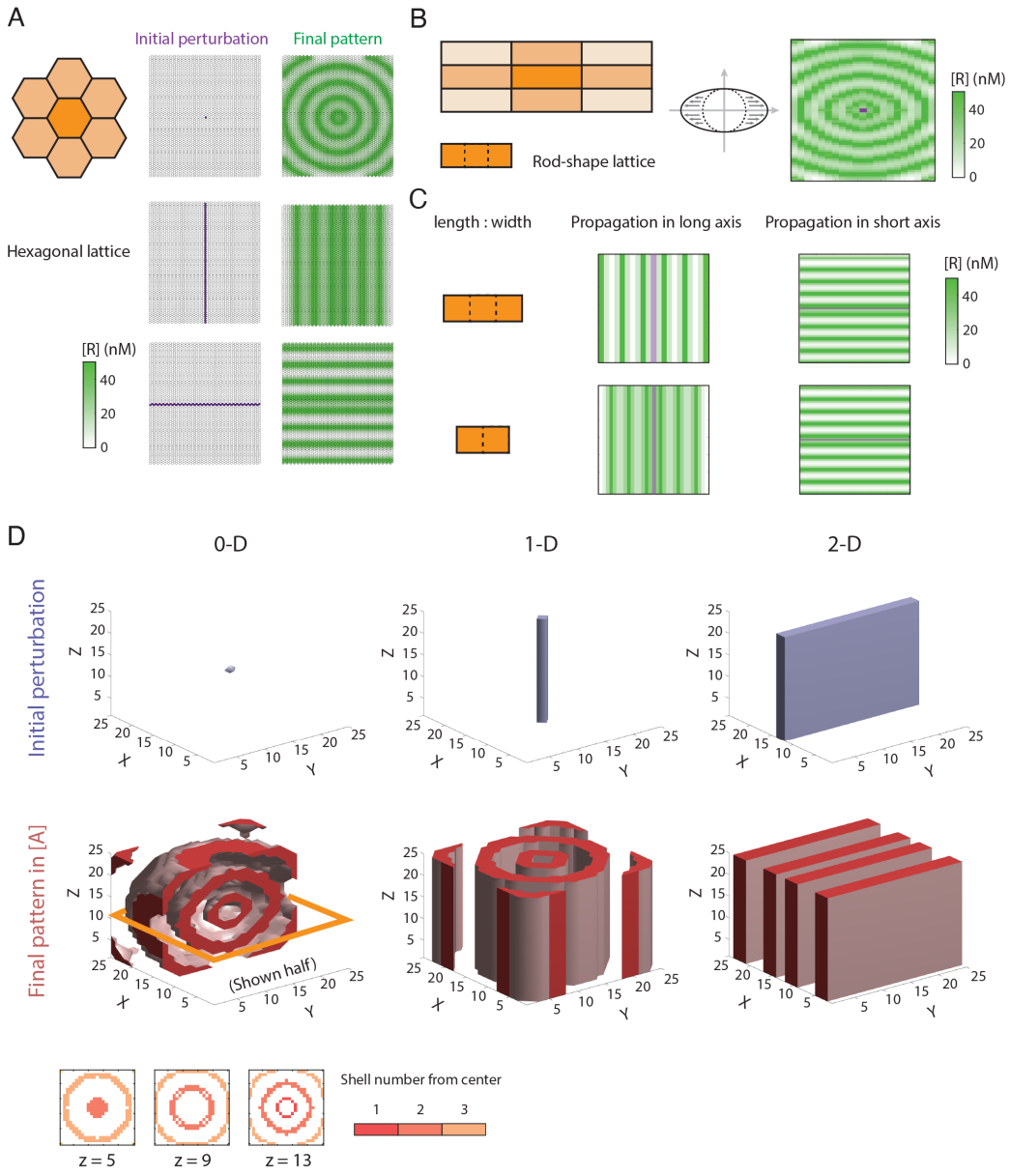

Figure 2.11: The single-morphogen system can pattern on hexagonal lattices and rod-shaped lattices, as well as 3-D lattices.

(A) In a hexagonal lattice, where each lattice node has six adjacent neighbors, the single-morphogen patterning circuit can form rings and stripes patterns.

(B) The single-morphogen patterning circuit forms “stretched” patterns on rod-shaped lattices.

(C) The length: width ratio of a rod-shaped lattice cell affects the “stretching” effects of the final patterns. Vertical stripes patterns have longer wavelengths generated from more elongated cells, while the horizontal stripes patterns are not affected.

(D) The 3-D simulations start from point, line, and plane initial perturbations (upper panels) and produce corresponding types of patterns (lower panels). To visualize 3-D patterns, the final patterns only show cells with the activator concentration higher than an arbitrary level (here we set [A] > 1 nM) in red and hide the rest. In the sphere pattern (left column), three plane cross sections (z = 5, 9, 13 cell number) show the concentric “shells”, colored by each layer of shells (from inner layer to outer layer, red to yellow).

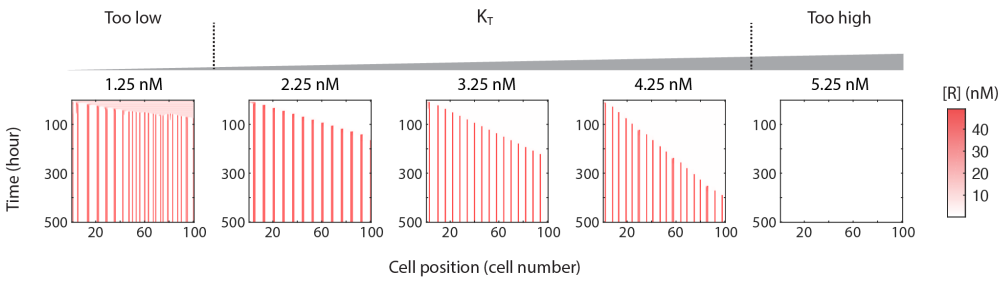

Figure 2.12: The M activation threshold K_T affects pattern propagation speed in the inhibition-release model.

(A) If K_T is too small, the final stable pattern is similar to the one from minimal circuit (regularity loss), which indicates that the inhibition-release mechanism is not active. If K_T is too large, since the threshold is too high to have the trigger wavefront to flip the cell state, no pattern will form.

(B) In the valid regime, the higher K_T slows down the propagation speed by increasing the effective time delay before a cell converts from the ground state to the excited state.

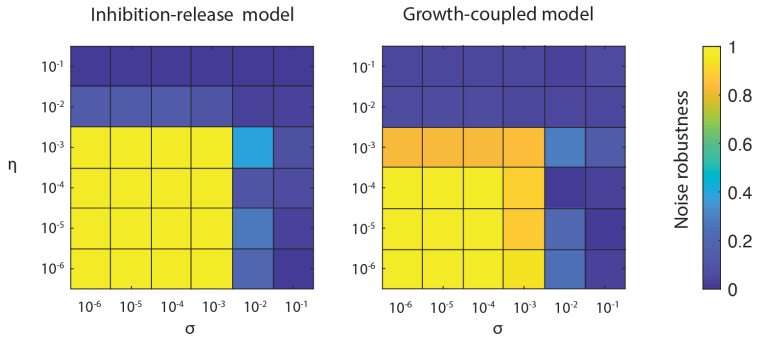

Figure 2.13: The intrinsic (dynamic) and extrinsic (static) noise degrade patterning in a roughly independent manner.

Both inhibition-release and growth-coupled models allow patterning in the presence of either or both types of noise.

References

Alaynick, William A, Thomas M Jessell, and Samuel L Pfaff (July 2011). "SnapShot: spinal cord development." en. In: *Cell* 146.1, 178–178.e1.

Bailles, Anaıs, Emily W Gehrels, and Thomas Lecuit (May 2022). "Mechanochemical Principles of Spatial and Temporal Patterns in Cells and Tissues." en. In: *Annu. Rev. Cell Dev. Biol.*

Ben-Jacob, E et al. (Mar. 1985). "Pattern propagation in nonlinear dissipative systems." In: *Physica D* 14.3, pp. 348–364.

Ben-Zvi, Danny, Ben-Zion Shilo, and Naama Barkai (Dec. 2011). "Scaling of morphogen gradients." en. In: *Curr. Opin. Genet. Dev.* 21.6, pp. 704–710.

Briscoe, James and Stephen Small (Dec. 2015). "Morphogen rules: design principles of gradient-mediated embryo patterning." en. In: *Development* 142.23, pp. 3996–4009.

Carles, Cristel C and Jennifer C Fletcher (Aug. 2003). "Shoot apical meristem maintenance: the art of a dynamic balance." en. In: *Trends Plant Sci.* 8.8, pp. 394–401.

Cohen, Michael et al. (July 2010). "Dynamic filopodia transmit intermittent Delta-Notch signaling to drive pattern refinement during lateral inhibition." en. In: *Dev. Cell* 19.1, pp. 78–89.

Collier, J R et al. (Dec. 1996). "Pattern formation by lateral inhibition with feedback: a mathematical model of delta-notch intercellular signalling." en. In: *J. Theor. Biol.* 183.4, pp. 429–446.

Corson, Francis et al. (May 2017). "Self-organized Notch dynamics generate stereotyped sensory organ patterns in Drosophila." en. In: *Science* 356.6337.

Cross, M C and P C Hohenberg (July 1993). "Pattern formation outside of equilibrium." In: *Rev. Mod. Phys.* 65.3, pp. 851–1112.

Davies, Jamie A (June 2008). "Synthetic morphology: prospects for engineered, self-constructing anatomies." en. In: *J. Anat.* 212.6, pp. 707–719.

Dee, G and J S Langer (Feb. 1983). "Propagating Pattern Selection." In: *Phys. Rev. Lett.* 50.6, pp. 383–386.

Dessaud, Eric, Andrew P McMahon, and James Briscoe (Aug. 2008). "Pattern formation in the vertebrate neural tube: a sonic hedgehog morphogen-regulated transcriptional network." en. In: *Development* 135.15, pp. 2489–2503.

Dun, Elizabeth Ann, Brett James Ferguson, and Christine Anne Beveridge (Nov. 2006). "Apical Dominance and Shoot Branching. Divergent Opinions or Divergent Mechanisms?" en. In: *Plant Physiol.* 142.3, pp. 812–819.

Dykes, Iain M and Costanza Emanueli (June 2017). “Transcriptional and Post-transcriptional Gene Regulation by Long Non-coding RNA.” en. In: *Genomics Proteomics Bioinformatics* 15.3, pp. 177–186.

Ebrahimkhani, Mo R and Miki Ebisuya (Oct. 2019). “Synthetic developmental biology: build and control multicellular systems.” en. In: *Curr. Opin. Chem. Biol.* 52, pp. 9–15.

Eldar, Avigdor and Michael B Elowitz (Sept. 2010). “Functional roles for noise in genetic circuits.” en. In: *Nature* 467.7312, pp. 167–173.

Elowitz, Michael B et al. (Aug. 2002). “Stochastic gene expression in a single cell.” en. In: *Science* 297.5584, pp. 1183–1186.

Fox, R F et al. (Dec. 1988). “Fast, accurate algorithm for numerical simulation of exponentially correlated colored noise.” en. In: *Phys. Rev. A Gen. Phys.* 38.11, pp. 5938–5940.

Gao, Xiaojing J et al. (Sept. 2018). “Programmable protein circuits in living cells.” en. In: *Science* 361.6408, pp. 1252–1258.

Gehart, Helmuth and Hans Clevers (Jan. 2019). “Tales from the crypt: new insights into intestinal stem cells.” en. In: *Nat. Rev. Gastroenterol. Hepatol.* 16.1, pp. 19–34.

Gelens, Lendert, Graham A Anderson, and James E Ferrell Jr (Nov. 2014). “Spatial trigger waves: positive feedback gets you a long way.” en. In: *Mol. Biol. Cell* 25.22, pp. 3486–3493.

Gierer, A and H Meinhardt (Dec. 1972). “A theory of biological pattern formation.” en. In: *Kybernetik* 12.1, pp. 30–39.

Gillespie, D T (Aug. 1996). “Exact numerical simulation of the Ornstein-Uhlenbeck process and its integral.” en. In: *Phys. Rev. E Stat. Phys. Plasmas Fluids Relat. Interdiscip. Topics* 54.2, pp. 2084–2091.

Green, Jeremy B A and James Sharpe (Apr. 2015). “Positional information and reaction-diffusion: two big ideas in developmental biology combine.” en. In: *Development* 142.7, pp. 1203–1211.

Hadjivasiliou, Zena, Ginger L Hunter, and Buzz Baum (Nov. 2016). “A new mechanism for spatial pattern formation via lateral and protrusion-mediated lateral signalling.” en. In: *J. R. Soc. Interface* 13.124.

Heberlein, Ulrike, Tanya Wolff, and Gerald M Rubin (Dec. 1993). “The TGFβ homolog dpp and the segment polarity gene hedgehog are required for propagation of a morphogenetic wave in the Drosophila retina.” In: *Cell* 75.5, pp. 913–926.

Hiscock, Tom W and Sean G Megason (2015). *Orientation of Turing-like Patterns by Morphogen Gradients and Tissue Anisotropies*.

Ho, William K W et al. (Feb. 2019). “Feather arrays are patterned by interacting signalling and cell density waves.” en. In: *PLoS Biol.* 17.2, e3000132.

Iron, David, Michael J Ward, and Juncheng Wei (Mar. 2001). "The stability of spike solutions to the one-dimensional Gierer–Meinhardt model." In: *Physica D* 150.1, pp. 25–62.

Itzkovitz, Shalev et al. (Feb. 2012). "Optimality in the development of intestinal crypts." en. In: *Cell* 148.3, pp. 608–619.

Kavanagh, Kathryn D, Alistair R Evans, and Jukka Jernvall (Sept. 2007). "Predicting evolutionary patterns of mammalian teeth from development." en. In: *Nature* 449.7161, pp. 427–432.

Kebrom, Tesfamichael H (Oct. 2017). "A growing stem inhibits bud outgrowth - the overlooked theory of apical dominance." en. In: *Front. Plant Sci.* 8, p. 1874.

Khalil, Ahmad S et al. (Aug. 2012). "A synthetic biology framework for programming eukaryotic transcription functions." en. In: *Cell* 150.3, pp. 647–658.

Kilfoil, Maria L, Paul Lasko, and Ehab Abouheif (Dec. 2009). "Stochastic variation: from single cells to superorganisms." en. In: *HFSP J.* 3.6, pp. 379–385.

Kondo, Shigeru and Takashi Miura (Sept. 2010). "Reaction-diffusion model as a framework for understanding biological pattern formation." en. In: *Science* 329.5999, pp. 1616–1620.

Landge, Amit N et al. (Apr. 2020). "Pattern formation mechanisms of self-organizing reaction-diffusion systems." en. In: *Dev. Biol.* 460.1, pp. 2–11.

Levine, Erel et al. (Sept. 2007). "Quantitative characteristics of gene regulation by small RNA." en. In: *PLoS Biol.* 5.9, e229.

Li, Pulin et al. (May 2018). "Morphogen gradient reconstitution reveals Hedgehog pathway design principles." en. In: *Science* 360.6388, pp. 543–548. DOI: 10.1126/science.aao0645.

Liang, Fu-Sen, Wen Qi Ho, and Gerald R Crabtree (Mar. 2011). "Engineering the ABA plant stress pathway for regulation of induced proximity." en. In: *Sci. Signal.* 4.164, rs2.

Ma, Yitong et al. (Sept. 2020). "Synthetic mammalian signaling circuits for robust cell population control." en. In: p. 39.

Marcon, Luciano et al. (Apr. 2016). "High-throughput mathematical analysis identifies Turing networks for patterning with equally diffusing signals." en. In: *Elife* 5.

Meinhardt, H and A Gierer (July 1974). "Applications of a theory of biological pattern formation based on lateral inhibition." en. In: *J. Cell Sci.* 15.2, pp. 321–346.

Milo, Ron et al. (Oct. 2009). "BioNumbers—the database of key numbers in molecular and cell biology." en. In: *Nucleic Acids Res.* 38.suppl_1, pp. D750–D753.

Mishra, Deepak et al. (July 2021). "An engineered protein-phosphorylation toggle network with implications for endogenous network discovery." en. In: *Science* 373.6550.

Moreno, Tanya A and Chris Kintner (Feb. 2004). "Regulation of segmental patterning by retinoic acid signaling during Xenopus somitogenesis." en. In: *Dev. Cell* 6.2, pp. 205–218.

Morris, Kevin V and John S Mattick (June 2014). "The rise of regulatory RNA." en. In: *Nat. Rev. Genet.* 15.6, pp. 423–437.

Morsut, Leonardo et al. (Feb. 2016). "Engineering Customized Cell Sensing and Response Behaviors Using Synthetic Notch Receptors." en. In: *Cell* 164.4, pp. 780–791.

Murray, James D (2001). *Mathematical biology II: spatial models and biomedical applications*. Vol. 3. Springer New York.

Nakajima, Keiji and Philip N Benfey (2002). "Signaling in and out: control of cell division and differentiation in the shoot and root." en. In: *Plant Cell* 14 Suppl, S265–76.

Onimaru, Koh et al. (2016). "The fin-to-limb transition as the re-organization of a Turing pattern." In: *Nat. Commun.* 7.1, pp. 1–9.

Palau-Ortin, David et al. (Mar. 2015). "Pattern selection by dynamical biochemical signals." en. In: *Biophys. J.* 108.6, pp. 1555–1565.

Pearl Mizrahi, Sivan et al. (Dec. 2016). "Persistence to anti-cancer treatments in the stationary to proliferating transition." en. In: *Cell Cycle* 15.24, pp. 3442–3453.

Phillips, Rob et al. (Oct. 2012). *Physical Biology of the Cell*. en. Garland Science.

Plahte, E (Nov. 2001). "Pattern formation in discrete cell lattices." en. In: *J. Math. Biol.* 43.5, pp. 411–445.

Potvin-Trottier, Laurent et al. (Oct. 2016). "Synchronous long-term oscillations in a synthetic gene circuit." en. In: *Nature* 538.7626, pp. 514–517.

Raser, Jonathan M and Erin K O'Shea (Sept. 2005). "Noise in Gene Expression: Origins, Consequences, and Control." en. In: *Science*.

Raspopovic, J et al. (Aug. 2014). "Modeling digits. Digit patterning is controlled by a Bmp-Sox9-Wnt Turing network modulated by morphogen gradients." en. In: *Science* 345.6196, pp. 566–570.

Rohlfs, Rori V, Patrick Harrigan, and Rasmus Nielsen (Oct. 2013). "Modeling Gene Expression Evolution with an Extended Ornstein–Uhlenbeck Process Accounting for Within-Species Variation." en. In: *Mol. Biol. Evol.* 31.1, pp. 201–211.

Ruan, Shigui (June 1998). "Diffusion-driven instability in the Gierer-Meinhardt model of morphogenesis." en. In: *Nat. Resour. Model.* 11.2, pp. 131–141.

Schnell, Santiago et al. (2002). *Models for pattern formation in somitogenesis: a marriage of cellular and molecular biology*.

Scholes, Natalie S et al. (Sept. 2019). "A Comprehensive Network Atlas Reveals That Turing Patterns Are Common but Not Robust." en. In: *Cell Syst* 9.3, 243–257.e4.

Schweisguth, François and Francis Corson (June 2019). "Self-Organization in Pattern Formation." en. In: *Dev. Cell* 49.5, pp. 659–677.

Sprinzak, David et al. (2011). *Mutual Inactivation of Notch Receptors and Ligands Facilitates Developmental Patterning*.

Sun, Gui-Quan, Cui-Hua Wang, and Ze-Yan Wu (Apr. 2017). "Pattern dynamics of a Gierer–Meinhardt model with spatial effects." In: *Nonlinear Dyn.* 88.2, pp. 1385–1396.

Thattai, Mukund and Alexander van Oudenaarden (June 2002). "Attenuation of noise in ultrasensitive signaling cascades." en. In: *Biophys. J.* 82.6, pp. 2943–2950.

Toda, Satoshi et al. (July 2018). "Programming self-organizing multicellular structures with synthetic cell-cell signaling." en. In: *Science*.

Turing, Alan Mathison (Aug. 1952). "The chemical basis of morphogenesis." In: *Philos. Trans. R. Soc. Lond. B Biol. Sci.* 237.641, pp. 37–72.

Wieschaus, Eric (Jan. 2016). "Positional Information and Cell Fate Determination in the Early Drosophila Embryo." en. In: *Curr. Top. Dev. Biol.* 117, pp. 567–579.

Woodall, Nicholas B et al. (Sept. 2021). "De novo design of tyrosine and serine kinase-driven protein switches." en. In: *Nat. Struct. Mol. Biol.* 28.9, pp. 762–770.

Zhu, Ronghui et al. (Jan. 2022). "Synthetic multistability in mammalian cells." en. In: *Science* 375.6578.

Chapter 3

RECONSTITUTION REACTION-DIFFUSION PATTERNS IN MAMMALIAN CELL CULTURE

3.1 Abstract

Alan Turing proposed diffusion-driven instability patterning in 1952 as a "simplified" mathematical explanation for periodic pattern formation in developmental biology. Since then, many studies have explained the pattern formation in various scales and species with the Turing mechanism. However, no studies have shown that the simple circuit Turing proposed is sufficient to generate the periodic spatial and temporal patterns in biology. We take advantage of synthetic biology, following a bottom-up approach to reconstitute the Turing pattern in mammalian cell culture. We build a synthetic circuit based on BMP4 and Activin signaling pathways in AD293 cells (a derived cell line from HEK293). After validating each circuit component, we test the spatial patterning of the full-circuit monoclonal cells in the cell culture plate. This versatile circuit should allow us to tune the parameter for altering the final patterns and reveals how spatial heterogeneous initial conditions affect the patterning dynamics. Finally, we will include mathematical model simulations to validate our experimental conclusions and further explore other possible circuitry based on these two signaling pathways.

3.2 Introduction

Periodic patterns are widespread and diverse in nature. They are not only for the decoration of the living creatures' appearance (Shigeru Kondo, Iwashita, and Yamaguchi, 2009) but also are found as the basis of periodic structure development, such as teeth (Kavanagh, Evans, and Jernvall, 2007), limbs (Cooper, 2015), and hairs (Jung et al., 1998). In 1952's paper, Alan Turing first explained pattern formation with reaction-diffusion theory. A homogeneous system of two diffusible components could eventually form stable periodic heterogeneity patterns with particular reaction terms and parameters (Turing, 1952).

Since then, Turing's theory has been widely used to explain the formation of natural periodic patterns. Early studies like Shigeru Kondo et al. used a classic Turing model, the diffusive activator and repressor model, to explain stripes growth and bifurcation of the marine angelfish *Pomacanthus* (Kondo and Asal, 1995). With

further understandings of the molecular basis of morphogenesis, more evidence revealed the role of signaling morphogens in natural periodic pattern formation. Han-sung Jung et al. believed BMP4 and FGF4 controlled the feather bud development in chicken embryos under the Turing mechanism. FGF4 worked as the local activator, and meanwhile, BMP4 worked as the long-range inhibitor. The perturbation studies verified the prediction from a two-morphogen Turing model of BMP4 and FGF4 (Jung et al., 1998). These studies demonstrated that the Turing mechanism is sufficient to generate periodic patterns. However, because of the complexity of cell transcriptional and signaling networks, natural development content based on in vivo studies cannot show the minimal structure and core feature of a functional Turing circuit.

Furthermore, to understand the circuit fully, a natural development system has limitations to perform perturbation studies. Rushikesh Sheth et al. tried to explain mouse digit development with the Turing mechanism by knocking out endogenous Gli and Hoxa (Sheth et al., 2012). Since there were only two components that could be tuned at three (limited) levels, respectively, the perturbation study did not provide complete evidence to model the role of these two genes under the reaction-diffusion mechanism.

Last but not least, without a clear boundary of the gene regulatory network, occasionally, the Turing mechanism could be overwhelmed in explaining natural periodic patterns. For instance, not all fish skin patterns could be explained by reaction-diffusion. Alexandria Volkening et al. claimed that the stripe formation of zebrafish is due to pigment cell migration and proliferation (Volkening and Sandstede, 2015), while the Turing mechanism is absent in this case (Watanabe and Shigeru Kondo, 2015).

Meanwhile, synthetic biology provides a new perspective on this problem. By reconstituting the Turing pattern in a blank slate cell line out of any specific developmental content, fundamentally, we could avoid some of the issues mentioned above. On the one hand, building a circuit (in parallel building a series of circuits) following the Turing pattern criteria helps us figure out the minimum requirement for the core function and the contribution from each component. On the other hand, with a reconstituted tunable system, perturbation studies help us explore a more vast parameter space in a higher dimension.

Recent attempts at building the synthetic Turing pattern are from bacteria to mammalian cells. David Karig et al. worked with *E.coli* to reconstitute periodic patterns

by using two quorum-sensing molecules as "morphogens" for the pattern formation on the growing biofilm (Karig et al., 2018). By wiring Nodal and Lefty natural signaling pathway to the Turing circuit in HEK293 cell culture, Ryoji Sekine et al. observed the dynamic of heterogeneity emerging and spatial pattern forming (Sekine, Shibata, and Ebisuya, 2018). However, the reaction-diffusion circuit in this work is based on two morphogens that have been reported working in pairs and creating Turing patterns in nature. The core reaction kinetics still hides in the natural interactions where Nodal and Lefty compete for receptors. Thus, the potential for reconstituting synthetic reaction-diffusion patterns using unconventional reaction-diffusion elements within mammalian cell cultures has been insufficiently explored, leaving a gap in our understanding of how spatial periodic patterns could be generated.

In this project, we aim to reconstitute synthetic Turing patterns from scratch in mammalian cell culture. We build a circuit for the synthetic Turing pattern based on two nearly orthogonal signaling pathways: BMP4 and Activin. BMP4, as the short-range active morphogen, induces the production of both morphogens. Meanwhile, we design to use a third component, Smad6, to mediate the inhibition from Activin to BMP4. Although involving two natural morphogens, this synthetic reaction-diffusion circuit is fully bottom-up constructed since no natural Turing pattern based on BMP4 and Activin has been reported so far. Based on this synthetic patterning circuit, we confirm the minimal requirement for reaction-diffusion patterns and provide a versatile platform to study patterning mechanisms, parameter tunability, and noise-robustness.

3.3 BMP4 and Activin signaling pathways are capable of constructing synthetic reaction-diffusion patterns

BMP and Activin all belong to the TGFβ family. They share similar signaling pathway structures but nearly two distinct sets of signaling components. BMP4 signaling transduces via the type I receptor BMPR1A/1B and type II receptor ACTR2/2B, BMPR2, further phosphorylates Smad1/5/8. The active Smad1/5/8, together with Smad4, promotes the expression of the downstream gene via binding to the BMP response element (BRE). Similarly, Activin interacts with type I receptor ACVR1B and type II receptor ACTR2/2B and further phosphorylates Smad2/3. The Smad2/3 also forms complexes with Smad4. However, they bind to the Activin response element (ARE) and activate its downstream genes (Chen, Zhao, and Mundy, 2004; Kawabata and Kohei Miyazono, 1999). Meanwhile, Smad6, classified as inhibitory

Smad, only downregulates BMP signaling by blocking phosphorylated Smad1/5/8 (Miyazono, 2000) (Figure 3.1A). On the shoulder of the TGFβ signaling pathways, we hacked the natural circuit and designed the reaction-diffusion circuit based on BMP4, Activin, and Smad6. In our circuit, BMP4 drives the expression of itself and the other morphogen Activin; Activin induces Smad6 production, further inhibiting the BMP4 self-activation.

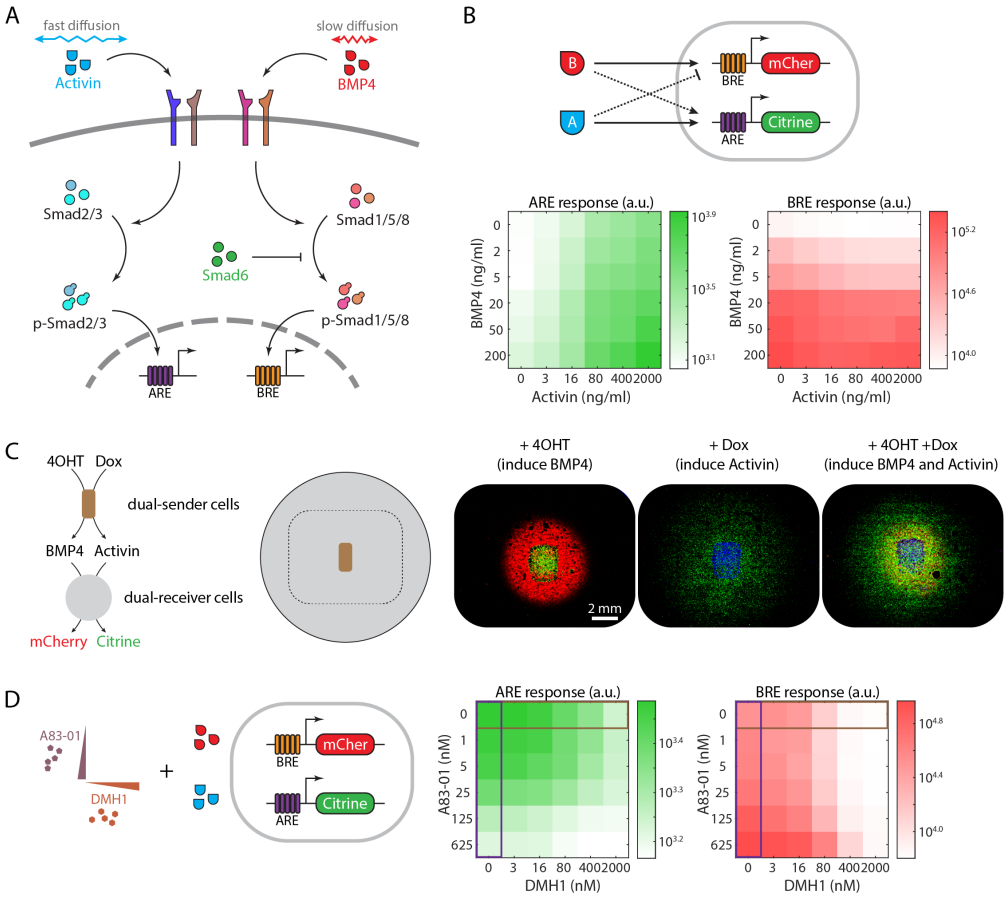

Figure 3.1: BMP4 and Activin signal pathway are capable of constructing synthetic Turing patterns.

(A) BMP and Activin signaling pathways belong to the TGFβ family but use two subsets of components mediating signal transduction. Each of the two morphogens has a combination of type I and type II receptors to receive the signal. Expect Smad4, they use two exclusive sets of Smad proteins mediating signal transducing and regulating their downstream genes. Smad6 is an inhibit smad that only blocks BMP signaling inside the cell.

(B) BMP and Activin signaling are nearly orthogonal, and the cross-interference is minor. The titration matrix of two recombinant morphogens on a dual reporter cell line indicates BMP4 mainly activates BRE response while Activin activates ARE. The data also reveals minor promotion from BMP4 to ARE reporter and slight repression from Activin to BRE reporter.

(C) BMP4 and Activin gradient formation in the same spatial sender-receiver setup shows a greater potential of Activin diffusing to a longer distance. With the iBiDi insert, the dual senders are seeded in a well-defined region at the well center. Senders produced both morphogens once induced by two different inducers. The dual reporter cells covering the rest of the well presented a gradient of fluorescent proteins in response to a morphogen gradient.

(D) Small molecule kinase inhibitors alter cell response to BMP4 and Activin. The titration test evaluates the influence on the fluorescent signals of dual reporter cells that are given an intermediate level of both two morphogens. A83-01 represses the Activin response. Meanwhile, DMH1 mainly represses the BMP4 response.

Before building the synthetic circuit for the Turing pattern, we evaluated the signaling interference between BMP4 and Activin pathways. BMP4 and Activin signaling pathways have little crosstalk. We performed a two-dimension titration on the AD293 BMP4/Activin dual receiver cells with recombinant morphogen proteins. The dual receiver is a stable cell line with BRE-mCherry and ARE-Citrine reporters. The titration matrix data confirms BMP4 and Activin are the main ligands for BRE and ARE response, respectively (Figure 3.1B). Furthermore, BMP4 can slightly lift ARE response, while Activin represses BRE signaling. However, this minor crosstalk is consistent with our circuit design, in which BMP should promote Actvin signals while Activin would inhibit BMP signals.

Then we reconstituted both morphogens' concentration gradients in the tissue culture plate to evaluate their diffusion ability. Sequential plating of senders and receivers

with iBiDi inserts creates a sender region surrounded by the receiver region—the dual-sender cells secret BMP4 and Activin via two chemically inducible promoters: 4OHT induces the UAS-Gal4 system producing BMP4, and Dox activates the TetOn system making Activin. The secreted morphogen from senders forms a concentration gradient over receiver cells. Meanwhile, receivers sense the spatial signals and interpret them as perception gradients. Activin reaches a further distance than BMP4 in the gradient formation test (Figure 3.1C), confirming that Activin diffuses faster than BMP4, which is also reported in the literature (McDowell et al., 1997; Jones, Armes, and Smith, 1996).

To further expand the tunability of our patterning system, we use commercialized small molecule kinase inhibitors to alter the morphogen signaling. A selective kinase inhibitor A83-01, which inhibits Activin receptor ALK4/7 and blocks the phosphorylation of Smad2, decreases the intracellular downstream ARE response (Tojo et al., 2005). Meanwhile, DMH1, which blocks BMP4 type I receptor ALK2, mainly dampens the response of BRE (Mohedas et al., 2013; Neely et al., 2012)(Figure 3.1D).

3.4 Stepwise evaluation with the full-circuit cell line confirms that the designed circuit works properly

Our synthetic Turing circuit contains two functional modules. The reaction-diffusion module is a three-component circuit with BMP4, Activin, and Smad6. BMP4 is the short-range active morphogen, and Activin works as the long-range inhibitive morphogen. The BRE promotor controls BMP4 production as a self-activated feedback loop. The ARE promoter regulates the Smad6 (Figure 3.2A).

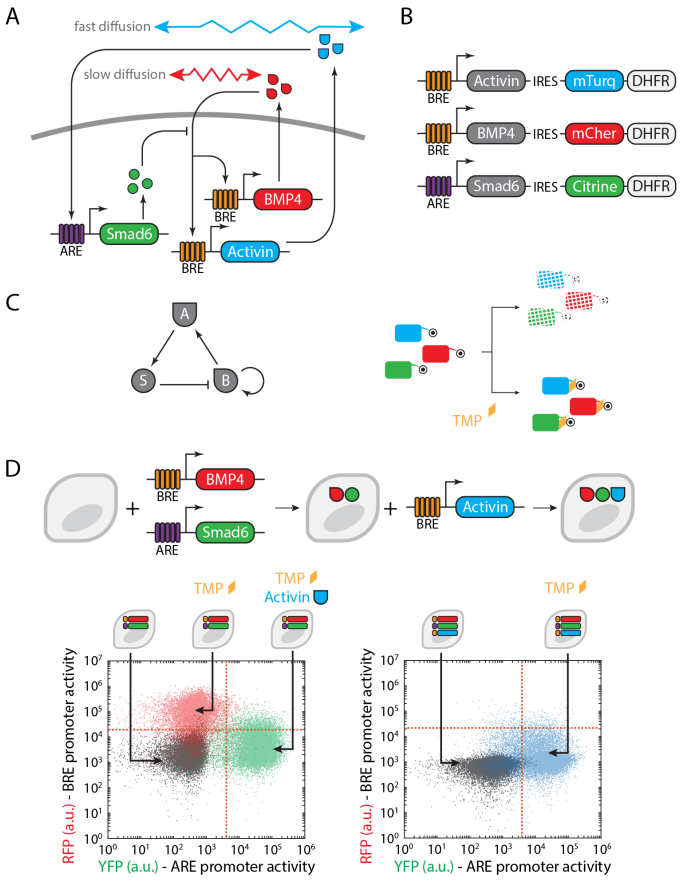

Figure 3.2: Each individual arm of the designed synthetic reaction-diffusion circuit works properly.

(A) A schematic plot presents a synthetic Turing circuit design based on BMP4 and Activin signaling pathways. BMP4 and Activin are the two morphogens in the reaction-diffusion circuit. Meanwhile, synthetically the BRE promoter regulates the production of both two morphogens, and the ARE promoter regulates the production of Smad6.

(B) Each construct has a coding sequence for a degron-tagged (DHFR) fluorescent protein downstream of the core circuit component, separated by IRES sequence. The chemical-induced degron DHFR causes fast degradation of the target protein (fluorescent proteins in this case), which can be stabilized by a small molecule ligand trimethoprim (TMP).

(C) The reaction-diffusion circuit is active all the time due to BMP4 self-activation unless actively removing extracellular BMP4. Meanwhile, the fluorescent signals are under the control of TMP. They only appear once fluorescent proteins are stabilized.

(D) Every individual arm of the synthetic reaction-diffusion circuit works properly. A monoclonal with stably integrated the first two plasmids, the BMP4 self-activation and Activin-induced Smad6-producing modules, can self-activate in the regular cell culture media, showing high mCherry signal once meet TMP. Inducing with additional recombinant BMP4 would not further increase the signal. On the other hand, adding recombinant Activin can induce Smad6 production and suppress the BMP4 self-activation. Meanwhile, further integration of the Activin-producing module in this particular monoclonal drove the cells to stay at high Citrine and low mCherry, indicating Activin was produced.

Our circuit has also equipped with a signaling readout module. Three fluorescent proteins link to each patterning component with the IRES sequence (Figure 3.2B). The mCherry and mTurquoise indicate the production dynamic of BMP4 and Activin, respectively. The third color mCitrine tracks Smad6. In practice, the reaction-diffusion module is constantly active since all three species' production is based on the self-sustained BMP positive feedback loop. (Fig 2C, left) Meanwhile, no signal readout is available without TMP induction. In our design, all fluorescent proteins have the protein degron tag DHFR attached to the C-terminal, which causes protein degradation in a TMP-dependent manner. Providing TMP to the cells blocks the degron and starts to accumulate the fluorescent protein. We could find a flu-

orescent protein half-life regime with fluorescent intensity reflecting the promoter activity dynamics by titrating the TMP level. (Fig 2C, right)

Before selecting close-loop full-circuit cell lines for patterning, we performed stepwise evaluation confirming each regulation arm of the synthetic Turing circuit works properly. We first transfected wild-type HEK293T cells with the BMP4-producing construct and Smad6-producing construct (Figure 3.2D, upper). We tested a monoclonal with various inducers, together with TMP, which is for revealing the fluorescent color. Firstly, this monoclonal shows high mCherry and low Citrine in the no-inducer condition and does not show stronger mCherry with additional recombinant BMP4, which indicates that the BMP4 self-regulation can sufficiently self-sustain in a high production state. Secondly, treated with recombinant Activin, these cells show low mCherry and high Citrine, proving that Activin induced Smad6 production and Smad6 inhibited the BMP4 self-activation (Figure 3.2D, lower-left).

Thirdly, we had another round of transfection to this monoclonal cell line with the Activin-producing construct generating the close-loop full-circuit cells (Figure 3.2D, upper). These cells show lower mCherry and higher mCitrine than the untransfected cells, indicating that BMP4 successfully induces Activin production. So that Activin can enhance Smad6 production and further represses BMP4 self-activation (Figure 3.2D, lower-right). So far, all regulation arms among the three circuit components are functional, ensured by stepwise evaluation.

3.5 Monoclonals with full circuits develop spatial patterns

With all validation above, then we evaluate the pattern formation ability of full-circuit monoclonal cell lines. The variation in monoclonals, due to random integration via the PiggyBac system, enables a broad range of sampling in parameter space. Some clones, which are situated in the appropriate parameter regime, display spatial heterogeneity during pattern formation experiments.

The pattern formation assay begins with homogeneous monoclonal cells in an off state for the reaction-diffusion circuit, and proceeds to form patterns in the tissue culture plate. Pattern formation starts with confluent cells in a homogeneous state. To achieve this, we cultured the cells in 250 ng/ml Noggin (which can neutralize BMP4 and further attenuate the BMP4 self-activation) to shut off the reaction-diffusion circuit, preventing bifurcation before the patterning experiment. Then, we suspended and loaded well-mixed cells into the culture plate and allowed 24 hours for cell settling with Noggin protection. Finally, after cells were bound to

the surface firmly, we washed away Noggin and initiated the experiment in pattern formation media, containing 0.1 uM TMP for fluorescent protein stabilization, 5 mg/ml Palbociclib for cell division inhibition, and specific levels of inducers. These procedures ensure that, in the beginning, all cells have the same circuit component profile, no morphogen production, and are localized with their clonal (Figure 3.3A).

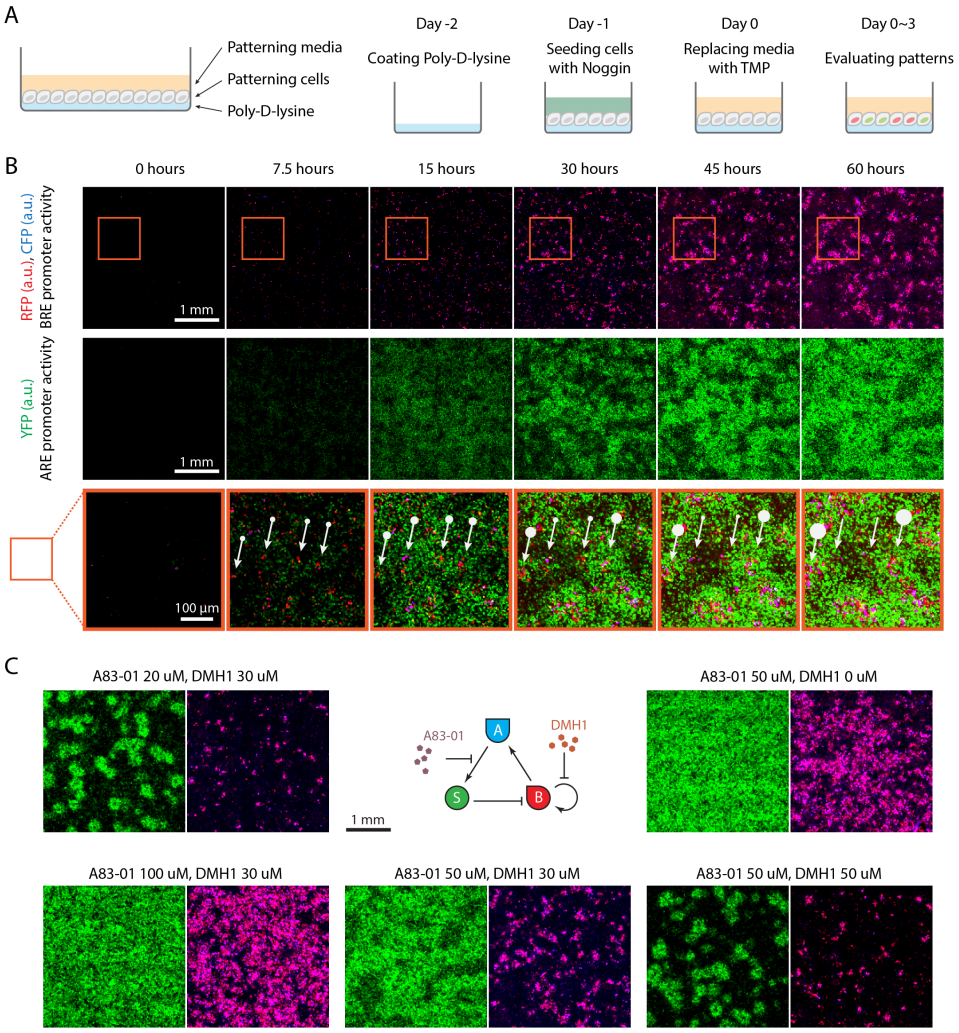

Figure 3.3: Monoclonal cells with the synthetic reaction-diffusion circuit develop spatial patterns in tissue culture plates.

(A) Monoclonals selected from AD293 cells transfected with the synthetic reaction-diffusion circuit are used for patterning experiments. Patterning cells in culture seeding confluently on the Poly-D-lysine treated surface and covered with patterning media. To keep the cells in a homogenous pre-patterning state, they were kept in the regular culture media with 250 ng/mL recombinant Noggin protein. Two days before the patterning experiment, the culture plates were treated with Poly-D-lysine for better adherence. Twenty-four hours before the experiments, patterning monoclonal cells cultured in Noggin were trypsinized and transferred to the treated patterning device. The cells were loaded at full confluency and kept in the cell seeding media containing 250 ng/mL Noggin for one day. This guarantees that the cells are well-mixed and that the synthetic circuit was off before patterning. On day 0, we replaced the cell seeding media with patterning media with no Noggin, allowing the BMP self-activation to establish. This media also contains TMP for stabilizing fluorescent signaling and Palbociclib for slowing down the cell cycle. After induction, cells were placed in the environmental chamber on top of a microscope for a three-day time-lapse movie.

(B) Spatial patterns emerge in the monoclonal cells with the synthetic reaction-diffusion circuit. The first two rows demonstrated the entire scanned field of view at various time points. The first row showed the fluorescent signal profiles from mCherry and mTurquoise. They all reveal the BRE promoter activity. Meanwhile, the second row showed the signal profiles from Citrine, which indicates the ARE promoter activity. Within 60 hours, the homogenous monoclonal cells bifurcated roughly into active and inactive populations and developed spatial patterns. Instead of being sparsely and well-separated distributed among the population, the active morphogen-producing cells (high signal in RFP and CFP channels) were clusterized into domains with a similar size. The distribution of these clusters was roughly uniform in the whole field of view. Meanwhile, the active Smad6-producing cells (high signal in the YFP channel) formed larger clusters than the RFP channel, which are almost connected into a spaghetti-shaped structure. The zoom-in view of the patterning dynamics (third row) clearly showed the “local activation with long-range inhibition”, where the morphogen-producing cell cluster is always surrounded by Smad6-producing cells, presenting a structure with a red center and green peripheral. The pattern formation dynamic of the synthetic reaction-diffusion involves the forming and competing of the LALI events. The white arrows

point to the centers of four LALI events and show their activity with the size of the arrow's nock. They grew together in the first 15 hours and then started to compete. In the later time, the middle two dampened their morphogen production and inhibition of their neighbors. Meanwhile, the other two became brighter and dominated the pattern.

(C) A83-01 and DMH1 can tune the final pattern by affecting the circuit parameters. Among the left three conditions, increasing the A83-01 level would allow more cells to become morphogen-producing cells via self-activation, resulting in larger clusters in the final patterns. Meanwhile, Smad6-producing cells are also encouraged since more Activin was produced in the system. Among the right three conditions, increasing the DMH1 level would suppress the self-activation, resulting in smaller clusters in the final patterns of both channels.

Time-lapse movies, captured with an incubator-top macroscope, reveal the following stages (Figure 3.3B). 1) Homogeneous cells randomly activate production downstream of the BRE or TRE promoter. 2) Later, morphogen-producing cells (BRE ON) contribute to local BMP4 and wide-range Activin morphogen gradients. Smad6-producing cells (TRE ON) block the BMP4 signaling pathway, preventing further morphogen production. 3) Eventually, a group of cells around the center of local morphogen production dominate signal transmission, creating a saylocal activation with long-range inhibition (LALI) zone. Fluorescent output appears as a wider green gradient (Citrine reporter) surrounding narrower red (mCherry reporter) and blue (mTurquoise reporter) gradients. 4) LALI centers adjust their positions by inhibiting each other if they are too close or allowing a third center to emerge if there is ample space in between. 5) Patterning dynamics continue until the system collapses, caused by factors such as limited nutrition, waste accumulation, signaling transduction changes in crowded cell populations, or morphogen accumulation erasing spatial heterogeneity.

The heterogeneous states in patterned cells are transient. Sorting and replating cells after three days in the patterning condition show they are able to reset their color in the new patterning test rather than committing to a certain cell state permanently. This versatility indicates the bifurcation of cell states is due to the local environment of the cell.

The parameters of the synthetic reaction-diffusion circuit are tunable. Two selective kinase inhibitors, DMH1 and A8301, can specifically dampen the BMP4 and

Activin signaling, respectively. DMH1 inhibits self-activation through BMP4 signaling, resulting in fewer Cherry and turquoise positive cells in the final pattern. Concurrently, A8301 moderates the Activin response, which weakens the repression of self-activation, leading to an increase in Cherry and turquoise positive cells in the final patterns (Figure 3.3C).

3.6 LALI events emerge during pattern formation

Next, we aim to determine if the heterogeneity in the final pattern is driven by the reaction-diffusion mechanism, in which cell state distribution has a spatial correlation. We analyzed movie data using two approaches: the spatial-temporal correlation to reveal global features and the event-based superimposition to present the self-organization of cells as local interactions.

The auto-correlation of mCherry and Citrine channels shows a "blub" size of around 400 μm (Figure 3.4A). The cross-correlation between the mCherry and Citrine channels displays a volcano-shaped spatial correlation profile. The red and green channels are roughly colocalized, but the maximum is located a short distance from the origin, indicating that strongly self-activated cells tend to repress their distant neighbors more than themselves or adjacent neighbors (Figure 3.4B).

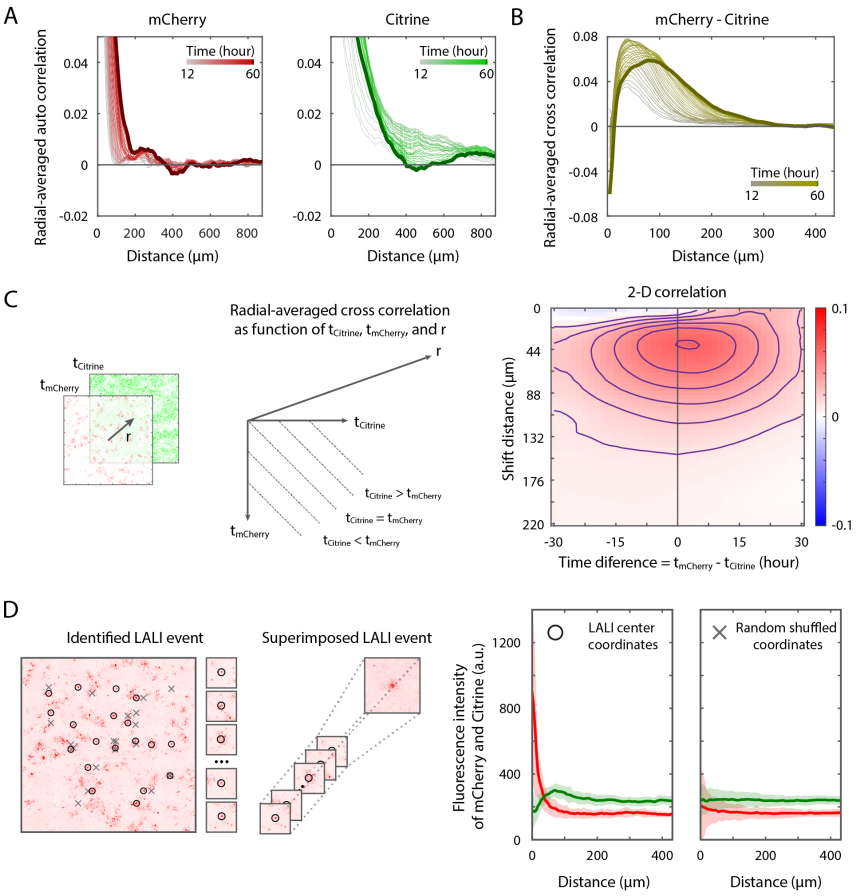

Figure 3.4: Image analysis confirms local activation with long-range inhibition in the synthetic reaction-diffusion patterning.

(A) The auto-correlation of mCherry and Citrine profiles measures the pattern wavelength. The auto-correlation matrix from the final pattern was further radially averaged. The distance where the curve passes the x-axis defines the periodic pattern wavelength. In both cases, the wavelengths measured were around 400 μm. The dynamics also showed that the auto-correlations curve gradually converged to the final stable one.

(B) The cross-correlation between mCherry and Citrine profiles indicates that the inhibition is mainly on neighbor cells. The radially averaged cross-correlation curves at each time point present the interaction dynamics between morphogen-producing and Smad6-producing cells. The distance where the maximum correlation is located is gradually increasing over time. Meanwhile, the cross-correlation is negative at zero distance. This indicates that the inhibition effect on cells is not perfectly aligned with the Activin morphogen gradient. The active morphogen-producing cells repressed their neighbor at a short distance mainly, other than themselves and their adjacent neighbors.

(C) The cross-correlation of mCherry and Citrine profiles pairwise in time series reveals the causality of morphogen-producing and Smad6-producing. For all possible combinations of mCherry and Citrine profiles as time series, the radially averaged cross-correlation was calculated. By further averaging by the time difference, the cross-correlation shows as a heatmap. The X-axis is the time difference between the two channels. The Y-axis is the shifted distance. The maximum locates where the time difference is around 3 hours and shift distance is about 40 μm.

(D) The event-based superimpose captures the "local activation with long-range inhibition" events. The event centers were identified by searching for the local maximum in the RFP channel. The neighborhood of each center was extracted as a series of sub-images. The "average" event is calculated by aligning the event centers and superimposing all these sub-images. Further radially averaged intensity profiles in both RFP and YFP channels clearly reveal the LALI feature. As a control, the same metric is applied to the randomly shuffled coordinates showing no spatial distribution of either channel.

Taking into account the time delay, we calculate the cross-correlation between the mCherry and Citrine channels pairwise between each channel's time series. For each time points combination, radial-averaged cross-correlation is a function of shift

distance discarding the directionality. We then further compress the 3-D correlation data into 2-D by averaging based on the time difference. The resulting heatmap of averaged cross-correlation has the time difference on the x-axis and the spatial shift on the y-axis. The peak position demonstrates the causality between local activation and long-range inhibition. The maximum correlation occurs when a mCherry profile pairs with a Citrine profile that is 3 hours later and 40 μm apart in the distance (Figure 3.4C).

Another way to capture LALI events is by superimposing them all. For each time frame, we identify LALI event centers by searching for peaks in the mCherry profile pre-processed with a log-LoG filter. The Laplacian of Gaussian (LoG) filter highlights peak positions in a smoothed image. The logarithm applied to the original image reduces absolute intensity differences among LALI events and presents relative changes within any LALI event. In each frame, we take all LALI events (radius 50 pixels from the center) and superimpose them, aligning by the center position. We then apply a further radial average to the averaged superimposed distributions in both mCherry and Citrine channels. This distribution profile clearly reveals "local activation with long-range inhibition", where the self-activation signal (mCherry) has a narrow distribution, while the lateral repression signal (Citrine) is widely spread. In comparison, the null model generates new coordinates by shuffling the LALI center coordinates and applies the same matrice to them. This control test only shows the uniform distribution for both channels (Figure 3.4D). This superimposing method can also apply to temporal dynamics. We track LALI center positions over time, and each trajectory records the formation and dissipation of a LALI event. Aligning all trajectories, we gain insight into the formation dynamics of an average LALI.

Both methods confirm the presence of LALI events in the patterning dynamics of our cell lines, proving that our designed synthetic reaction-diffusion circuit is the dominant mechanism guiding pattern formation in HEK cells.

3.7 Boundary conditions reshape the pattern formation

Another characteristic of reaction-diffusion patterns is their sensitivity to boundary conditions. In previous studies (Jung et al., 1998), researchers used beads soaked with morphogen proteins to perturb the local environment of patterning cells. These perturbations established new boundaries with a roughly constant morphogen influx into the reaction-diffusion system. Patterns in cells close to the boundaries deviated

from those in the rest of the field. In chicken feather bud development, BMP4 and FGF4 function as the two morphogens in the reaction-diffusion circuit, with BMP4 as the activator and FGF as the repressor. Introducing BMP4 beads induced adjacent cells to develop into feather buds, while FGF repelled feather bud formation near the beads.

We tested our synthetic reaction-diffusion circuit by sparsely co-culturing inducible morphogen senders with patterning cells. As predicted by the model, BMP4 senders caused adjacent patterning cells to become active morphogen senders, forming the center of LALI. Conversely, Noggin senders depleted BMP4 secreted by the patterning cells, inhibiting LALI formation near them. Statistical analysis of distance measurements from LALI centers to the sender cells before or after induction demonstrated a significant change in the location of LALI centers relative to senders.

3.8 Discussion

Traditional techniques employed to explore periodic patterning in nature have often hit roadblocks in definitively establishing the sufficiency of underlying patterning circuits, complicating the comprehensive understanding of spatial organization. Until the present study, the potential of reconstituting synthetic reaction-diffusion patterns using non-natural elements within mammalian cell cultures remained largely untapped, creating a knowledge gap regarding the generation of artificial spatial patterns. Here, we've established a reconstitution circuit providing compelling proof that a dual-morphogen system is sufficient for spatial pattern creation. This discovery indicates that no additional hidden factors are required to create these patterns, which paves new paths for synthetic biology research and prospective therapeutic applications.

In this research, we devised a unique synthetic reaction-diffusion circuit, showcasing pattern formation dynamics in a mammalian cell culture. The created synthetic reaction-diffusion pattern is adjustable and can adapt to a variety of boundary conditions. The circuit design incorporates two natural signaling pathways: BMP4 and Activin, which had never been identified in the same natural reaction-diffusion circuit. BMP4 serves as the short activator and Activin as the long-range inhibitor. By introducing Smad6, which only inhibits BMP4 signaling, we crafted a circuit in which BMP4 promotes itself and Activin while Activin represses both itself and BMP4. We selected monoclonals from AD293 cells stably transfected with our synthetic circuit after evaluating the circuit components and regulatory arms. The

pattern formation experiments began with a homogenous cell population seeded confluently in the culture device. Guided by reaction-diffusion mechanisms, the population started to bifurcate into active morphogen-secreting cells and inhibited cells. Interestingly, the spatial distribution of these cells was not random. Rather, the configuration of local activation with long-range inhibition domains was evenly distributed, leading to spatial periodic patterns. By modulating the signaling sensitivity with selective kinase inhibitors targeting either BMP4 or Activin pathways, we could generate variations of the original pattern.

Our study introduces a novel method for building a synthetic reaction-diffusion system that includes two morphogens not previously seen together in a natural reaction-diffusion process. This breakthrough not only propels our understanding of spatial patterning forward but also underscores the potential of alternative strategies in reconstituting synthetic reaction-diffusion circuits. In essence, any morphogen could potentially mediate cell-cell signaling within a reaction-diffusion mechanism's context, thus widening the spectrum for experimentation and application. Other morphogens with fast diffusion coefficients, or the auxin system (Liang, Ho, and Crabtree, 2011; Ma et al., 2020) as a "synthetic" morphogen, could serve as long-range morphogens. As for short-range signaling, we could employ the natural Notch-delta signaling or its synthetic counterpart: synNotch or SNIPR (Morsut et al., 2016; Toda et al., 2018; Zhu et al., 2022).

The choice of morphogens is merely one dimension of the design space. An array of possibilities exist for the "reaction" kinetics as well. Using the same morphogens, researchers can explore numerous variations in reaction kinetics, potentially unveiling new and unexpected patterns and behaviors. This extensive design space allows for the customization of synthetic reaction-diffusion systems for particular applications, such as tissue regeneration or synthetic embryogenesis, by finely adjusting the interactions between morphogens and the involved kinetics.

3.9 Methods

Plasmid construction:

The process of plasmid construction was carried out in adherence to standard molecular biology protocols. The backbone of the plasmids was linearized with the help of restriction enzymes sourced from New England Biolabs (NEB). The DNA fragments that were to be inserted into these plasmids were produced either by utilizing the PCR method or by means of gBlock synthesis, a service provided by Integrated

DNA Technologies (IDT). For the ligation process, which involves the joining of the DNA fragments to the plasmid backbones, we used Quick Ligation or Gibson Assembly methods. To confirm the successful construction of the plasmids, each was subjected to sequencing, performed by Primordium.

Cell Culture:

The cell line used in these experiments was AD293, a derivative of the standard HEK293 (Human Embryonic Kidney) cell line, chosen for its improved cell adherence and plaque formation characteristics. These parental cells were procured from Agilent. All cell lines used in subsequent experiments were derived from these parental cells. For the routine maintenance of these cell lines, cells were cultured in Dulbecco's Modified Eagle Medium (DMEM) supplemented with 10% Fetal Bovine Serum (FBS), 1x Penicillin/Streptomycin/L-glutamine, 1 mM Sodium Pyruvate, and 1 mM Non-Essential Amino Acids (NEAA). The cells were passaged every three days, with a ratio of 1:10. For the maintenance or seeding of the patterning cell line, an additional 250 ng/ml of recombinant Noggin was included in the media. When patterning was required, the regular DMEM was replaced with FluoroBrite DMEM from Gibco, and 0.1 uM TMP and 5 uM Palbociclib were added.

Transfection:

Transfection of the AD293 cells was performed when they had been plated in a 24-well plate for 24 hours, at a density of 100,000 cells per well. This transfection process followed the standard protocol associated with Lipofectamine LTX. In the transient transfection experiments, cells were transfected with the target plasmids along with a co-transfection marker. For the creation of stable cell lines, cells were co-transfected with a plasmid encoding the PiggyBac transposase and were then selected using specific antibiotics for a minimum of two passages.

Flow Cytometry:

Flow cytometry experiments were conducted using a CytoFLEX (Beckman) flow cytometer. Initially, cells were plated in a 96-well plate at a density of 30,000 cells per well. After two days of induction, the cells were dissociated using 0.05% trypsin for five minutes at room temperature and then neutralized with a flow buffer. The flow buffer contained 1x Hank's Balanced Salt Solution (HBSS) with 2.5 mg/ml Bovine Serum Albumin (BSA) and 2 mM Magnesium Chloride (MgCl2). Before being loaded into the flow cytometer, cells were passed through a 40-um cell strainer to remove clumps. The flow cytometry data were subsequently analyzed

with a Matlab-based software named EasyFlow, developed by Yaron Antebi.

Cell Sorting Procedures:

For cell sorting experiments, we utilized the MA900 cell sorter from Sony. Our protocol began by dissociating the sample cells with 0.05% trypsin for ten minutes at room temperature in their original culture vessels. This step was followed by neutralization using four times the volume of sorting buffer. After this, the cells were centrifuged, the supernatant was removed, and the cells were resuspended in 0.5 mL of fresh sorting buffer. To ensure a single-cell suspension, cells were filtered through a 40-micrometer cell strainer prior to loading into the cell sorter. The sorting buffer was specially formulated to maintain cell viability and contained 1x Hank's Balanced Salt Solution (HBSS) supplemented with 2.5 mg/ml Bovine Serum Albumin (BSA), 2 mM MgCl2, and 500 units of DNAse I to prevent cell clumping caused by extracellular DNA. Post-sorting, cells were carefully transferred to appropriately sized culture vessels and maintained in regular media to allow for recovery and further growth.

Reconstitution of Morphogen Gradients:

To recreate morphogen gradients in vitro, we employed the iBiDi 2-well silicone insert (Cat.No:80209). The insert was placed centrally in an empty well of a 24-well plate. In one of the chambers, 60,000 sender cells were seeded in 80 microliters of media. After a period of 12 hours to allow for cell attachment, the insert was carefully removed and 500,000 receiver cells were plated to cover the entire well. Once the receiver cells were firmly attached to the bottom surface of the well, the media was replaced with fresh media that contained specific inducers for the sender cells. This setup allowed the sender cells to modulate the behavior of the receiver cells via the secretion of morphogens, creating a recreated in vitro morphogen gradient. After a period of two days to allow for gradient formation and cell-cell communication, image data were acquired by scanning the cells with an EVOS imaging system. This approach allowed us to capture the effects of the morphogen gradient on receiver cell behavior in a controlled and replicable manner.

Patterning experiment preparation:

The setup for pattern formation begins with the treatment of a 96-well plate. A 50 ng/uL D-poly-lysine solution, a molecule that aids in cell adhesion, is applied to the plate for one hour at room temperature. The plate is then thoroughly washed with deionized water (ddH2O) three times to remove any residual D-poly-lysine. It's then

left to air-dry at room temperature for 24 hours, which ensures optimal adherence of cells in the subsequent steps. After the plate is prepared, patterning cells are seeded at full confluency. These cells are then cultured in a media containing 250 ng/mL Noggin for 24 hours, ensuring they are firmly attached. Following this, the Noggin media is replaced with a specific patterning media to initiate the pattern formation process. Finally, for observation and data collection, the cells are placed under an Olympus microscope equipped with an environmental chamber. This setup maintains the natural conditions required for cell behavior and capturing pattern formation process in real-time using time-lapse microscopy.

References

Chen, Di, Ming Zhao, and Gregory R Mundy (Dec. 2004). "Bone morphogenetic proteins." en. In: *Growth Factors* 22.4, pp. 233–241.

Cooper, Kimberly L (June 2015). "Self-organization in the limb: a Turing mechanism for digit development." en. In: *Curr. Opin. Genet. Dev.* 32, pp. 92–97.

Jones, C M, N Armes, and J C Smith (Nov. 1996). "Signalling by TGF-β family members: short-range effects of Xnr-2 and BMP-4 contrast with the long-range effects of activin." In: *Curr. Biol.* 6.11, pp. 1468–1475.

Jung, H S et al. (Apr. 1998). "Local inhibitory action of BMPs and their relationships with activators in feather formation: implications for periodic patterning." en. In: *Dev. Biol.* 196.1, pp. 11–23.

Karig, David et al. (June 2018). "Stochastic Turing patterns in a synthetic bacterial population." en. In: *Proc. Natl. Acad. Sci. U. S. A.* 115.26, pp. 6572–6577.

Kavanagh, Kathryn D, Alistair R Evans, and Jukka Jernvall (Sept. 2007). "Predicting evolutionary patterns of mammalian teeth from development." en. In: *Nature* 449.7161, pp. 427–432.

Kawabata, Masahiro and Kohei Miyazono (Jan. 1999). "Signal Transduction of the TGF-ß Superfamily by Smad Proteins." en. In: *J. Biochem.* 125.1, pp. 9–16.

Kondo, S and R Asal (Aug. 1995). "A reaction-diffusion wave on the skin of the marine angelfish Pomacanthus." en. In: *Nature* 376.6543, pp. 765–768.

Kondo, Shigeru, Motoko Iwashita, and Motoomi Yamaguchi (2009). "How animals get their skin patterns: fish pigment pattern as a live Turing wave." en. In: *Int. J. Dev. Biol.* 53.5-6, pp. 851–856.

Liang, Fu-Sen, Wen Qi Ho, and Gerald R Crabtree (Mar. 2011). "Engineering the ABA plant stress pathway for regulation of induced proximity." en. In: *Sci. Signal.* 4.164, rs2.

Ma, Yitong et al. (Sept. 2020). "Synthetic mammalian signaling circuits for robust cell population control." en. In: p. 39.

McDowell, N et al. (Sept. 1997). "Activin has direct long-range signalling activity and can form a concentration gradient by diffusion." en. In: *Curr. Biol.* 7.9, pp. 671–681.

Miyazono, K (2000). "TGF-beta signaling by Smad proteins." en. In: *Cytokine Growth Factor Rev.* 11.1-2, pp. 15–22.

Mohedas, Agustin H et al. (Apr. 2013). "Development of an ALK2-biased BMP type I receptor kinase inhibitor." en. In: *ACS Chem. Biol.* 8.6, pp. 1291–1302.

Morsut, Leonardo et al. (Feb. 2016). "Engineering Customized Cell Sensing and Response Behaviors Using Synthetic Notch Receptors." en. In: *Cell* 164.4, pp. 780–791.

Neely, M Diana et al. (June 2012). “DMH1, a highly selective small molecule BMP inhibitor promotes neurogenesis of hiPSCs: comparison of PAX6 and SOX1 expression during neural induction.” en. In: *ACS Chem. Neurosci.* 3.6, pp. 482–491.

Sekine, Ryoji, Tatsuo Shibata, and Miki Ebisuya (Dec. 2018). “Synthetic mammalian pattern formation driven by differential diffusivity of Nodal and Lefty.” en. In: *Nat. Commun.* 9.1, p. 5456.

Sheth, Rushikesh et al. (Dec. 2012). “Hox genes regulate digit patterning by controlling the wavelength of a Turing-type mechanism.” en. In: *Science* 338.6113, pp. 1476–1480.

Toda, Satoshi et al. (July 2018). “Programming self-organizing multicellular structures with synthetic cell-cell signaling.” en. In: *Science*.

Tojo, Masayoshi et al. (Nov. 2005). “The ALK-5 inhibitor A-83-01 inhibits Smad signaling and epithelial-to-mesenchymal transition by transforming growth factor-beta.” en. In: *Cancer Sci.* 96.11, pp. 791–800.

Turing, Alan Mathison (Aug. 1952). “The chemical basis of morphogenesis.” In: *Philos. Trans. R. Soc. Lond. B Biol. Sci.* 237.641, pp. 37–72.

Volkening, Alexandria and Björn Sandstede (Nov. 2015). “Modelling stripe formation in zebrafish: an agent-based approach.” en. In: *J. R. Soc. Interface* 12.112.

Watanabe, Masakatsu and Shigeru Kondo (Feb. 2015). “Is pigment patterning in fish skin determined by the Turing mechanism?” en. In: *Trends Genet.* 31.2, pp. 88–96.

Zhu, Iowis et al. (Apr. 2022). “Modular design of synthetic receptors for programmed gene regulation in cell therapies.” en. In: *Cell* 185.8, 1431–1443.e16.

Chapter 4

CONCLUDING REMARKS

4.1 Why show interest in this project

Multicellular circuitry is fundamental to tissue-level functions, necessitating the collaboration of numerous cells and often involving a variety of cell types. A primary challenge lies in understanding how cell populations can self-recognize, coordinate, and manipulate their spatial arrangements to achieve intricate biological functions and maintain homeostasis.

Comprehending the emergence of self-organized patterning is critical to understanding natural tissue or embryo development and ensuring their functionality through well-regulated and robust mechanisms. During the process of development, cells undergo a series of transformations, differentiating into specific cell types that eventually form the basis of tissues and organs (Shahbazi, 2020; Edelman, Chandrasekaran, and Price, 2010). This intricate process requires precise spatial organization and coordination among diverse cellular populations.

In parallel, the ability to construct artificial multicellular circuits represents a significant milestone in developing synthetic tissues with designed spatial features. Achieving this goal would enable the creation of complex, functional structures with potential applications in tissue engineering, regenerative medicine, and disease modeling. Developing synthetic tissues with spatial features would also serve as an invaluable platform for studying the fundamental principles of multicellular organization, communication, and coordination, shedding light on the underlying mechanisms that govern tissue formation and function.

Taking into account that the reconstitution of the positional information model, such as the synthetic Shh gradient pattern, still involves pre-specified sender-receiver information, we decided to focus on an alternative patterning mechanism: the reaction-diffusion model. In this approach, a pre-defined pattern is not required, offering a more dynamic and flexible means of organizing cellular structures.

4.2 Remaining questions in the field

Synthetic multicellular spatial patterning remains an area of interest in synthetic biology, with many questions still left to be addressed. The development of multi-

cellular circuitry has come a long way, but more orthogonal cell signaling modules need to be characterized and developed for further advancement in this field.

Quorum sensing modules, mediated by small molecules, have been transplanted from certain bacterial species and applied in many circuit designs (Dilanji et al., 2012; Ma et al., 2020; Karig et al., 2018). The benefits of these modules include:

1. Easy translocation across cell membranes, eliminating the need for secretion machinery and cell surface receptors.
2. Direct targeting of transcription factors, simplifying the key components of the entire signaling module.
3. Originating from bacteria, providing better orthogonality when applied in mammalian systems.

Synthetic Notch receptors, such as synNotch (Morsut et al., 2016; Toda et al., 2018) and its later version SNIPR (Zhu et al., 2022), have been used in various research and medical applications, including CAR-T therapy (Choe et al., 2021; Hyrenius-Wittsten et al., 2021). These protein-based signaling modules offer versatility in receiving and executing signals. Despite their potential, synNotch signaling modules have limitations due to their reliance on direct cell-to-cell contact, which restricts their application in certain contexts.

A synthetic orthogonal morphogen signaling system, similar to BMP or Shh, is still highly desired in many cases to address these limitations and broaden the range of possible applications.

Noise presents another challenge in multicellular circuit design. Cell-cell interactions introduce new dimensions, such as spatial location, environmental factors, and heterogeneity among cell populations. These factors can affect the extracellular signal distribution and alter the signal flow, creating new situations for noise analysis. Noise-robustness analysis in multicellular spatial patterning circuits has considered two types of extrinsic noise: temporal dynamic noise and spatial static noise (Wang, Garcia-Ojalvo, and Elowitz, 2022).

Noise control is essential, especially in self-organized spatial patterning or processes requiring precise temporal-spatial coordination. Wide distributions of circuit component levels in each cell can introduce unexpected features into the system. However, noise can also be a key factor that brings certain features to the system that

may not appear in a noise-free deterministic system. Some studies have reported how noise can lead to a bistable state in a simple circuit (Weinberger, 2015).

Synthetic biology has made significant strides in insulating circuit components from their natural biological contexts. However, there are still challenges in isolating the target process dynamics from a series of non-equilibrium transient states. For instance, reaction-diffusion theory often begins with a hypothetical uniform, homogeneous, and unsteady state for the entire cell population of interest. However, in reality, we can barely find such a case in a noisy, dynamically developing system.

In our first work, we propose two strategies. The first is to temporarily lock unpatterned cells in a ground state and unlock them to an excited "ready-for-patterning" state at the right time. This approach helps avoid unsteady unpatterned cells and ensures that the process starts from a controlled state. The second strategy is to couple patterning with tissue growth, which also helps to bypass the unsteady unpatterned cell issue while allowing for a more natural progression of development.

Interestingly, the transient transition between states may also lower the requirements for certain steps in development. In spatial patterning, regardless of what the final steady state of the circuit may be, as long as the circuit can transiently generate regular spatial patterns, these patterns can be captured and stabilized in the next step of development through other mechanisms. This allows the final steady state of the patterning circuit to be less crucial to the overall success of the developmental process.

In summary, refining and expanding our understanding of multicellular spatial patterning involves developing more orthogonal cell signaling modules, addressing the limitations of current signaling systems, and finding ways to analyze and control noise in multicellular circuits. Additionally, addressing the challenges associated with non-equilibrium transient states in synthetic biology requires innovative strategies, such as temporally controlling cell states and coupling patterning with tissue growth. By overcoming these obstacles and continuing to explore these challenges, researchers can expect to see significant advancements in the field of synthetic biology and its applications, further refining and expanding our understanding of multicellular spatial patterning.

References

Choe, Joseph H et al. (Apr. 2021). "SynNotch-CAR T cells overcome challenges of specificity, heterogeneity, and persistence in treating glioblastoma." en. In: *Sci. Transl. Med.* 13.591.

Dilanji, Gabriel E et al. (Mar. 2012). "Quorum activation at a distance: spatiotemporal patterns of gene regulation from diffusion of an autoinducer signal." en. In: *J. Am. Chem. Soc.* 134.12, pp. 5618–5626.

Edelman, Lucas B, Sriram Chandrasekaran, and Nathan D Price (2010). "Systems biology of embryogenesis." en. In: *Reprod. Fertil. Dev.* 22.1, pp. 98–105.

Hyrenius-Wittsten, Axel et al. (Apr. 2021). "SynNotch CAR circuits enhance solid tumor recognition and promote persistent antitumor activity in mouse models." en. In: *Sci. Transl. Med.* 13.591.

Karig, David et al. (June 2018). "Stochastic Turing patterns in a synthetic bacterial population." en. In: *Proc. Natl. Acad. Sci. U. S. A.* 115.26, pp. 6572–6577.

Ma, Yitong et al. (Sept. 2020). "Synthetic mammalian signaling circuits for robust cell population control." en. In: p. 39.

Morsut, Leonardo et al. (Feb. 2016). "Engineering Customized Cell Sensing and Response Behaviors Using Synthetic Notch Receptors." en. In: *Cell* 164.4, pp. 780–791.

Shahbazi, Marta N (July 2020). "Mechanisms of human embryo development: from cell fate to tissue shape and back." en. In: *Development* 147.14.

Toda, Satoshi et al. (July 2018). "Programming self-organizing multicellular structures with synthetic cell-cell signaling." en. In: *Science*.

Wang, Sheng, Jordi Garcia-Ojalvo, and Michael B Elowitz (Dec. 2022). "Periodic spatial patterning with a single morphogen." en. In: *Cell Syst* 13.12, 1033–1047.e7. DOI: 10.1016/J.CELS.2022.11.001.

Weinberger, Leor S (Dec. 2015). "A minimal fate-selection switch." en. In: *Curr. Opin. Cell Biol.* 37, pp. 111–118.

Zhu, Iowis et al. (Apr. 2022). "Modular design of synthetic receptors for programmed gene regulation in cell therapies." en. In: *Cell* 185.8, 1431–1443.e16.

Chapter 5

DATA AVAILABILITY AND DEPOSITS

Movie 1, Movie 2, and Matlab code for the mathematic model of the single-morphogen reaction-diffusion in Chapter 2 are available at CaltechDATA (Sheng, W. (2023). Synthetic Circuits for Multicellular Spatial Patterning [Data set]. CaltechDATA. https://doi.org/10.22002/sdqha-1xt88).

Further information and requests for resources and reagents should be directed to and will be fulfilled by the Elowitz lab.